Annexe A

Comparison of different gas-phase mechanisms and aerosol modules for simulating particulate matter formation

Cet appendice est constitué de

Kim, Y., Couvidat, F., Sartelet, K. et Seigneur, C. (2011). **Comparison of different gas-phase mechanisms and aerosol modules for simulating particulate matter formation**. *J. Air & Waste Manage. Assoc.*, 61 :1-9.

Sommaire

Abstract

The effects of two gas-phase chemical kinetic mechanisms, Regional Atmospheric Chemistry Mechanism version 2 (RACM2) and Carbon-Bond 05 (CB05), and two secondary organic aerosol (SOA) modules, the Secondary Organic Aerosoi Model (SORGAM) and AER/EPRI/Caltech model (AEC), on fine (aerodynamic diameter $\leq 2.5\ \mu$m) particulate matter (PM2.5) formation is studied. The major sources of uncertainty in the chemistry of SOA formation are investigated. The use of all major SOA precursors and the treatment of SOA oligomerization are found to be the most important factors for SOA formation, leading to 66% and 60% more SOA, respectively. The explicit representation of high-NOx and low-NOx gas-phase chemical regimes is also important with increases in SOA of 30–120% depending on the approach used to implement the distinct SOA yields within the gas-phase chemical kinetic mechanism; further work is needed to develop gas-phase mechanisms that are fully compatible with SOA formation algorithms. The treatment of isoprene SOA as hydrophobic or hydrophilic leads to a significant difference, with more SOA being formed in the latter case. The activity coefficients may also be a major source of uncertainty, as they may differ significantly between atmospheric particles, which contain a myriad of SOA, primary organic aerosol (POA), and inorganic aerosol species, and particles formed in a smog chamber from a single precursor under dry conditions. Significant interactions exist between the uncertainties of the gas-phase chemistry and those of the SOA module.

A.1 Introduction

Modeling air quality requires a complex system, which includes algorithms to simulate transport processes, a chemical kinetic mechanism, and an aerosol module. Various gas-phase mechanisms are currently available to simulate ozone formation and several aerosol modules are also available to simulate the evolution of particulate matter (PM) chemical composition and size distribution. A few studies have been conducted to investigate the effect of the gasphase chemical kinetic mechanism [*Luecken*, 2008; *Sarwar et al.*, 2008] or the effect of the aerosol module [*Pun et al.*, 2003; *Morris et al.*, 2006; *Bailey et al.*, 2007] on secondary PM formation. The objective of this work is to evaluate the differences in fine (aerodynamic diameter $\leq 2.5\mu$m) PM ($PM_{2.5}$) concentrations that result from the use of two different chemical mechanisms and $PM_{2.5}$ modules, with a special emphasis on identifying the major sources of uncertainties for secondary organic aerosol (SOA) formation. First, the models used in this study are briefly described and model performance evaluation against observations from routine monitoring networks is summarized. Then, $PM_{2.5}$ concentrations simulated using two different gas-phase chemical mechanisms and two secondary organic aerosol modules are compared. In particular, we investigate whether the uncertainties associated with those two distinct types of modules (gas-phase chemistry and secondary aerosol formation) are additive or whether their combination is nonlinear.

A.2 Description of the models

The air quality model used in this work is the threedimensional (3D) Eulerian chemical-transport model POLAIR3D of the Polyphemus modeling platform [*Sartelet et al.*, 2007; *Mallet et al.*, 2007].

Two recent gas-phase mechanisms are used in the following simulations: the Carbon-Bond 05 mechanism (CB05) [*Sarwar et al.*, 2008] and the Regional Atmospheric Chemistry Mechanism version 2 (RACM2) [*Goliff and Stockwell*, 2008]. The former is based on the carbon-bond formulation to represent organic chemistry, whereas the latter uses a surrogate molecule representation. Some differences also exist in the selection and kinetics of some inorganic reactions,

Table A.1: Major characteristics of the SORGAM and AEC SOA modules.

Characteristics	SORGAM	AEC
Precursors	Aromatics, long-chain alkanes, long-chain alkenes, monoterpenes	Aromatics, long-chain alkanes, long-chain alkenes, isoprene, monoterpenes, sesquiterpenes
SOA species	Two surrogates per precursor and oxidation pathway	Surrogate molecular species selected according to physicochemical properties
Gas/particle partitioning	Absorption into an hydrophobic organic phase	Absorption of hydrophobic SOA into an organic phase and absorption of hydrophilic SOA into an aqueous phase
Non-ideality of the particulate phase	Assumed constant and identical to that implicitly assumed in the gas/particle partitioning from the smog chamber experiments	Calculated via activity coefficients
Gas-phase chemistry	SOA yields for the first oxidation step with high-NO_x conditions	SOA yields from various oxidation steps with both high-NO_x and low-NO_x pathways
Particulate-phase chemistry	None	Oligomerization as a function of pH

as discussed by *Kim et al.* [2009]. For $PM_{2.5}$ formation, the ISORROPIA module [*Nenes et al.*, 1999], version 1.7, is used for inorganic species. For SOA formation, two distinct modules are used: the SORGAM module [*Schell et al.*, 2001], which uses the two-compound Odum approach [*Odum et al.*, 1996b], and the AEC module [*Pun et al.*, 2006; *Debry et al.*, 2007b], which simulates both hydrophilic and hydrophobic organic aerosols. The two-compound Odum approach consists in using two surrogate SOA compounds to represent SOA formation from a given precursor and the first step of oxidation (e.g., oxidation by the hydroxyl radical, ozone, or the nitrate radical). The stoichiometric coefficient and gas/particle partitioning coefficient of each surrogate SOA compound are estimated by fitting this empirical model to smog chamber data [*Odum et al.*, 1996b]. The treatment of gas/particle partitioning assumes that the SOA compounds absorb into a hydrophobic organic particle. This two-compound Odum approach is currently used in many air quality models such as the Community Multiscale Air Quality (CMAQ) model [*Carlton et al.*, 2010a], the Comprehensive Air quality Model with extensions (CAMx) [*Gaydos et al.*, 2007], the Weather Research & Forecast model with Chemistry (WRF/Chem) [*Zhang et al.*, 2010a], the European Monitoring and Evaluation Programme (EMEP) model [*Simpson et al.*, 2007], the European Air pollution and Dispersion (EURAD) model [*Schell et al.*, 2001], and POLAIR3D/Polyphemus [*Sartelet et al.*, 2007]. The AEC hydrophobic/hydrophilic SOA approach is used in several models such as CMAQ [*Zhang et al.*, 2004], WRF/Chem [*Zhang et al.*, 2010a], POLAIR3D/Polyphemus [*Debry et al.*, 2007b], and CHIMERE [*Bessagnet et al.*, 2008]. Thus, as for the gas-phase chemistry, two operational formulations for SOA formation are considered. SORGAM represents a standard SOA formulation with hydrophobic absorption of SOA into organic particles, whereas AEC includes a more complete set of physicochemical processes for SOA formation. In particular, AEC treats hydrophilic SOA in addition to hydrophobic SOA and it accounts for the variable nonideality of particles via the calculation of activity coefficients; in addition, the AEC version used here distinguishes between high-NO_x and low-NO_x regimes for SOA yields, it includes more SOA precursors (isoprene and sesquiterpenes) than SORGAM, and it treats pH-dependent oligomerization processes. Table A.1 summarizes the main characteristics of these two SOA modules.

Kim et al. [2009] presented a detailed discussion of the results of an application of the air

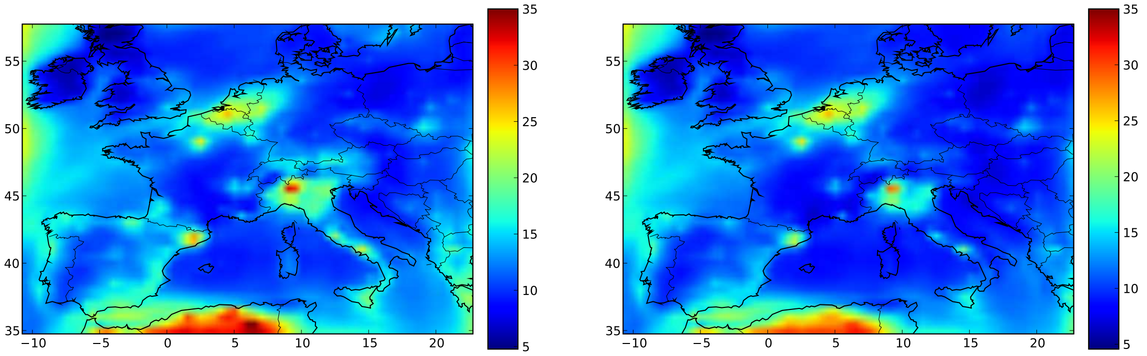

(a) **[PM$_{2.5}$]$_{AEC}$** (b) **[PM$_{2.5}$]$_{SORGAM}$**

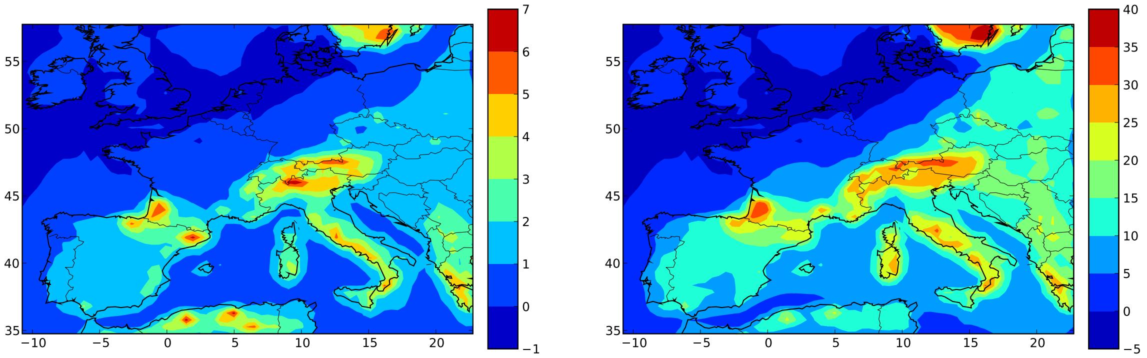

(c) **[PM$_{2.5}$]$_{AEC}$ - [PM$_{2.5}$]$_{SORGAM}$** (d) **[PM$_{2.5}$]$_{AEC}$ - [PM$_{2.5}$]$_{SORGAM}$)/[PM$_{2.5}$]$_{AEC}$**

Figure A.1: PM$_{2.5}$ concentrations (μg/m^3) over Europe simulated with AEC and SORGAM for SOA formation and RACM2 for gas-phase chemistry. Results are averaged over the 1-month simulation of 15 July to 15 August 2001: (a) [PM$_{2.5}$]$_{AEC}$ (top left); (b) [PM$_{2.5}$]$_{SORGAM}$ (top right); (c) [PM$_{2.5}$]$_{AEC}$ - [PM$_{2.5}$]$_{SORGAM}$ (bottom left); (d) ([PM$_{2.5}$]$_{AEC}$ - [PM$_{2.5}$]$_{SORGAM}$)/[PM$_{2.5}$]$_{AEC}$ (bottom right)

quality model with CB05 and RACM2 to Europe for the period 15 July to 15 August 2001. Model performance evaluation for hourly ozone (O$_3$) concentrations shows mean normalized error and bias of 23% and 9% for RACM2 and 21% and 4% for CB05, normalized mean error and bias of 43% and 30% for RACM2 and 39% and 25% for CB05, and mean fractional error and bias of 22% and 5% for RACM2 and 21% and 0% for CB05 (a threshold of 60 ppb was used for the observed hourly O$_3$ concentrations). This model performance is satisfactory compared to guidelines of mean normalized error and bias less than or equal to 35% and 15%, respectively [*Russell and Dennis*, 2000]. Average differences in O$_3$ concentrations between CB05 and RACM2 are on the order of 3 ppb, that is, about 5%. Maximum differences are 6 ppb (9%). It was concluded that both inorganic and organic chemistry contributed to differences between the mechanisms. Formation of inorganic PM is identical in those two simulations and differences are due solely to the SOA formation modules. When using RACM2, the PM$_{2.5}$ mean fractional error and bias are

41% and -4% with AEC and 45% and -16% for SORGAM, respectively; the normalized mean error and bias are 38% and 2% with AEC and 40% and -8% for SORGAM, respectively. When using CB05, the $PM_{2.5}$ mean fractional error and bias are 37% and -4% with AEC and 47% and -22% for SORGAM, respectively; the normalized mean error and bias are 36% and 1% with AEC and 44% and -15% for SORGAM, respectively. These values are within the performance goals recommended by *Boylan and Russell* [2006]. Model performance is comparable for the inorganic components and the differences in model performance are due to the particulate organic fraction (no particulate organic carbon measurements are available from the EMEP monitoring network for the period considered here). Therefore, model performance is satisfactory for $PM_{2.5}$ with both gas-phase chemical mechanisms and both SOA modules and commensurate with those of other models for atmospheric PM [*Russell*, 2008].

A.3 Sensitivity of PM concentrations to the aerosol module

The sensitivity of PM concentrations is first investigated with respect to the aerosol module. The molecule-based formulation of RACM2 is more conducive to detailed interactions between gas-phase chemistry and SOA formation than the carbon-bond formulation of CB05; therefore, RACM2 is used here for the gas-phase chemistry.

Figure A.1 presents the $PM_{2.5}$ concentrations simulated with AEC and SORGAM over Europe, as well as the differences between the two model simulations. Overall, more $PM_{2.5}$ is formed with AEC than with SORGAM. This result is due to the fact that more SOA formation processes are included in AEC (see Table A.1). Differences are significant; they reach 6-7 $\mu g/m^3$ in parts of northern Italy, southwestern France, northern Spain, and North Africa and are in the range of 3-6 $\mu g/m^3$ in southern Sweden (the European regulation is 20 $\mu g/m^3$ for annual concentrations). Relative differences follow a similar spatial pattern with differences up to 40% (with respect to the AEC simulation) in southern Sweden, southwestern France, and Austria. These results highlight that uncertainties in PM formation greatly exceed those in ozone gas-phase chemistry, which is consistent with earlier findings [*Pun et al.*, 2003; *Bailey et al.*, 2007].

Table A.2: Characteristics of SOA modules used in the sensitivity simulations.

SOA module	Precursors	NO_x regime	Hydrophobic and hydrophilic absorption	Activity coefficients	Oligomerization	Enthapies of vaporization
SORGAM	Anthropogenics, monoterpenes	High-NO_x only	Hydrophobic only	Implicit and constant	None	156 kJ/mol [*Schell et al.*, 2001]
SORGAM-ΔH	Anthropogenics, monoterpenes	High-NO_x only	Hydrophobic only	Implicit and constant	None	88 kJ/mol [*Pun et al.*, 2006]
SORGAM-NO_x	Anthropogenics, monoterpenes	High- and low-NO_x	Hydrophobic only	Implicit and constant	None	88 kJ/mol [*Pun et al.*, 2006]
SORGAM-bio	Anthropogenics, all terpenes	High- and low-NO_x	Hydrophobic only	Implicit and constant	None	42-175 kJ/mol[a]
Super-SORGAM	Anthropogenics, all terpenes	High- and low-NO_x	Hydrophobic, parametrization for hydrophilic isoprene SOA	Implicit and constant	None	42-175 kJ/mol[a]
Mini-AEC	Anthropogenics, all terpenes	High- and low-NO_x	Hydrophobic and hydrophilic	Constant (unity)	None	25-175 kJ/mol[b]
AEC-no-oligo	Anthropogenics, all terpenes	High- and low-NO_x	Hydrophobic and hydrophilic	Calculated and variable	None	25-175 kJ/mol[b]
AEC	Anthropogenics, all terpenes	High- and low-NO_x	Hydrophobic and hydrophilic	Calculated and variable	Parametrization for aldehyde SOA	25-175 kJ/mol[b]

Notes: [a] 42 kJ/mol for isoprene SOA [*Zhang et al.*, 2007b], 88 kJ/mol for anthropogenic and monoterpene SOA [*Pun et al.*, 2006], 175 kJ/mol for sesquiterpene SOA [*Pun et al.*, 2006].

[b] 25 kJ/mol for glyoxal [*Debry et al.*, 2007b], 38 kJ/mol for methylglyoxal [*Debry et al.*, 2007b], 42 kJ/mol for isoprene SOA [*Zhang et al.*, 2007b], 88 kJ/mol for biogenic hydrophilic aldehyde and monocarboxylic SOA and for anthropogenic SOA [*Pun et al.*, 2006], 109 kJ/mol for biogenic dicarboxylic acids [*Pun et al.*, 2006], 175 kJ/mol for biogenic hydrophobic SOA [*Pun et al.*, 2006].

Because SORGAM and AEC represent two ends of a spectrum of SOA models, it is of particular interest to investigate which of the structural differences that distinguish SORGAM from AEC contribute the most to the differences in simulated SOA concentrations: number of SOA precursors, treatment of high- versus low-NO_x regimes, treatment of hydrophilic SOA, treatment of the variability of activity coefficients, or treatment of oligomerization. To that end, we conducted a series of simulations with SORGAM and AEC that involve modifications to the SOA modules to represent these various structural modifications. In addition to these structural changes, the influence of the enthalpies of vaporization on SOA concentrations was also investigated. Table A.2 presents the characteristics of the SOA modules used in those sensitivity simulations.

Figures A.2 and A.3 present the SOA concentrations averaged over the 1-month simulation period for each of the eight simulations. Differences between a model simulation and the simulation of the nearest model in terms of formulation are also presented. Overall, SOA concentrations increase as the SOA module evolves from SORGAM (the simplest mechanistic representation of SOA formation) to AEC (the most complete representation of SOA formation processes). The results are discussed in detail below.

The values of the enthalpies of vaporization for the equilibrium calculations of SOA have been shown to have some effects on average SOA concentrations [*Zhang et al.*, 2007b] as well as on their diurnal patterns [*Pun and Seigneur*, 2008]. Accordingly, we replaced the original enthalpies of vaporization of SORGAM (156 kJ/mol for all SOA) by a value of 88 kJ/mol, which better reflects the more recent values used in AEC, as shown in Table A.2 (SORGAM-ΔH). The difference in SOA concentrations averaged over the entire domain is low (0.01 $\mu g/m^3$) because there are both positive and negative differences in various parts of the domain depending on temperature. In areas with the lower temperatures (the Alps, the Pyrenean Mountains, and Sweden), the decrease in the enthalpies of vaporization leads to a decrease in SOA concentrations by as much as 0.5 $\mu g/m^3$ because the experimental data used in the SOA model were obtained at greater temperatures than those modeled in those areas and the temperature correction, which leads to greater SOA concentrations as the temperature decreases, is less for a smaller value of the enthalpy of vaporization. For the other areas where the temperatures are higher, the opposite effect is obtained. The lower enthalpy of vaporization used in SORGAM-ΔH leads to less displacement of the gas/particle equilibrium toward the gas phase and the SOA concentrations are consequently greater than in SORGAM by up to 0.2 $\mu g/m^3$.

Adding some representation of the NO_x regime for SOA formation (SORGAM-NO_x) has some effects because SOA formation is more important for aromatics and monoterpenes (which are major SOA precursors in SORGAM) under low-NO_x conditions than under high-NO_x conditions according to the smog chamber results of *Ng et al.* [2007a,b]. Here the stoichiometric coefficients and partitioning coefficients of *Ng et al.* [2007a,b] were used for the low-NO_x regime. Because most SOA formation at the regional scale occurs under low-NO_x conditions, SOA yields increase when one allows the mechanism to treat both high- and low-NO_x regimes. The effect depends, however, on how the low-NO_x versus high-NO_x regimes are implemented in the gas-phase chemical kinetic mechanism. On one hand, if one simply uses the low-NO_x regime SOA yields in the first oxidation step of the precursor species (for both aromatics and monoterpenes), thereby neglecting the occurrence of the high-NO_x regime for SOA formation, the differences in SOA concentrations are significant: they reach 2 $\mu g/m^3$ in northern Italy and are about 0.35 $\mu g/m^3$ on average over the entire domain (not shown). On the other hand, if one implements the high-NO_x and low-NO_x SOA yields in later oxidation steps corresponding to reactions of precursor oxidation products with nitrogenous species and peroxyl radicals, respectively, but for aromatics only (because of insufficient information for monoterpenes), the differences are smaller, because the overall SOA yields include a combination of all oxidation routes and the

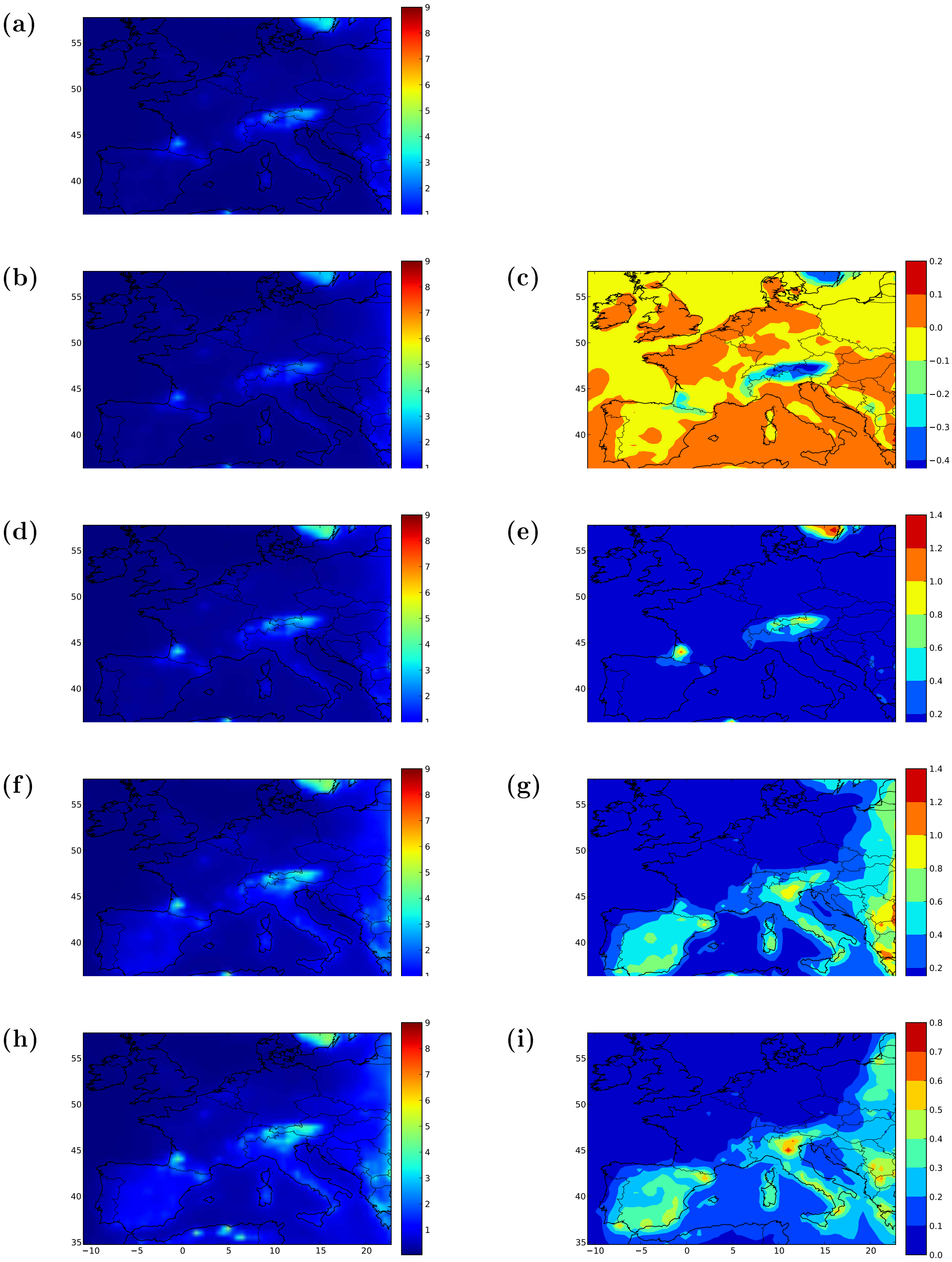

Figure A.2: Simulations of PM$_{2.5}$ SOA (μg/m^3) over Europe with RACM2 for gas-phase chemistry and distinct SORGAM modules for SOA formation: (a) SORGAM (first row); (b) SORGAM-ΔH (second row left); (c) [SORGAM-Δ - SORGAM] (second row right); (d) SORGAM-NO$_x$ (third row left); (e) [SORGAM-NO$_x$ - SORGAM-ΔH] (third row right); (f) SORGAM-bio (fourth row left); (g) [SORGAM-bio - SORGAM-NO$_x$] (fourth row right); (h) Super-SORGAM (fifth row left); (i) [Super-SORGAM - SORGAM-bio] (fifth row right).

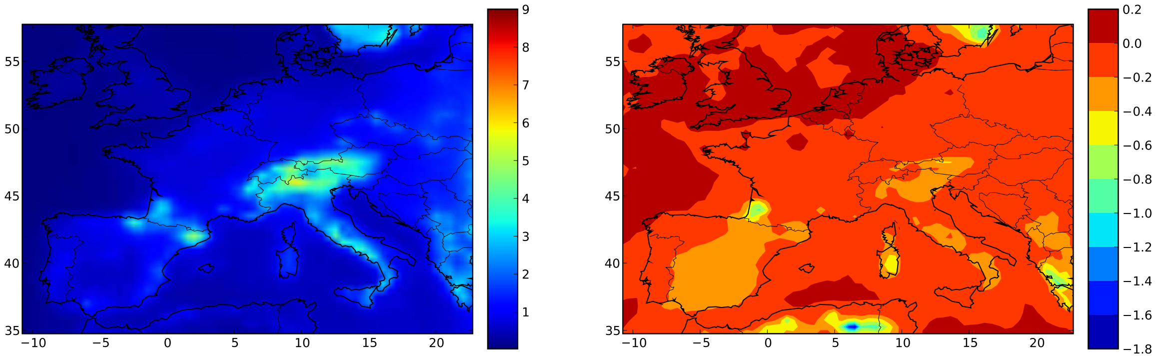

(a) **Mini-AEC**

(b) **Mini-AEC - AEC-no-oligo**

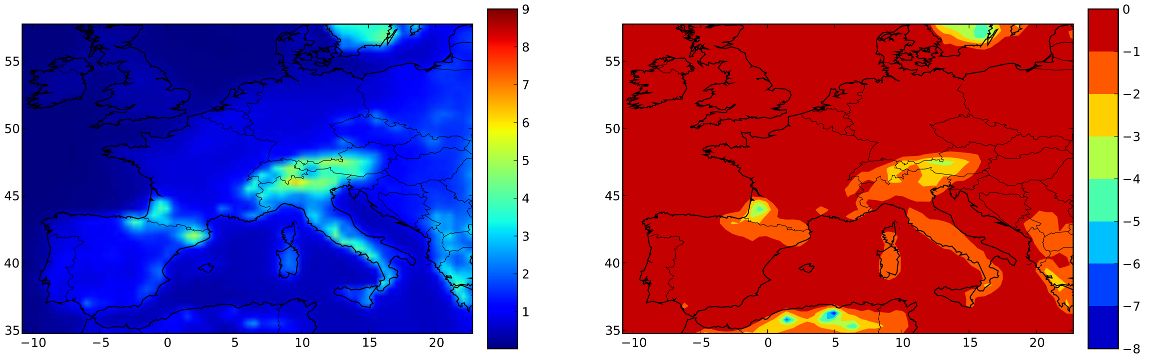

(c) **AEC-no-oligo**

(d) **AEC-no-oligo - AEC**

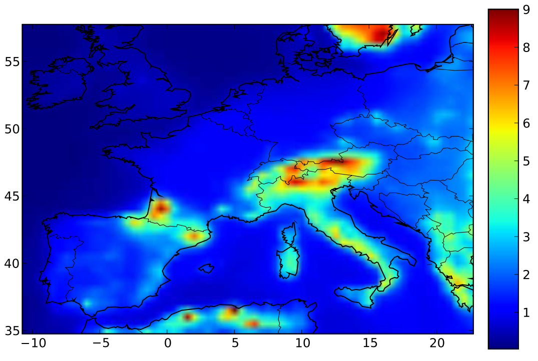

(e) **AEC**

Figure A.3: Simulations of $PM_{2.5}$ SOA ($\mu g/m^3$) over Europe with RACM2 for gas-phase chemistry and distinct AEC modules for SOA formation: (a) Mini-AEC (first row left); (b) [Mini-AEC - AEC-no-oligo] (first row right); (c) AEC-no-oligo (second row left); (d) [AEC-no-oligo - AEC] (second row right); and (e) AEC (third row).

low-NO_x regime is not treated for monoterpenes. Then, as shown in Figure A.2, the differences in SOA concentrations reach 1.4 μg/m^3 in Sweden, southwestern France, and North Africa and approach 1 μg/m^3 in northern Italy; they are, however, only 0.08 μg/m^3 on average. These two results underscore the importance of treating the effect of the NO_x regime with sufficient detail in the gas-phase mechanism and further work is needed to develop gas-phase chemical kinetic mechanisms that can better integrate the dependency of SOA yields on NO_x regimes.

Adding isoprene and sesquiterpenes as precursors of SOA also increases the SOA concentrations (SORGAM-bio). The effect of NO_x regimes is also included in this simulation. However, SOA formation from sesquiterpenes is assumed to be lower under low-NO_x conditions than under high-NO_x conditions following *Ng et al.* [2007a]. For isoprene, no NO_x dependency is considered here, following *Zhang et al.* [2007b]. The enthalpy of vaporization used by *Zhang et al.* [2007b] was used for isoprene SOA; this value is in good agreement with the more recent experimental values of *Kleindienst et al.* [2009]. The enthalpy of vaporization used by *Pun et al.* [2006] was used for sesquiterpene SOA. Most of the increase in SOA concentrations is due to isoprene oxidation rather than sesquiterpene oxidation [*Debry et al.*, 2007b]. The largest increases occur in the lower latitudes where temperature and solar radiation are greater and, therefore, where isoprene emissions are higher. The SOA concentration increase reaches 1.4 μg/m^3 in the eastern part of the domain and is 0.25 μg/m^3 on average over the entire domain.

SOA formed from isoprene oxidation are believed to be hydrophilic and, therefore, may absorb into aqueous particles rather than into hydrophobic organic particles [*Pun*, 2008]. The affinity of those SOA compounds for aqueous particles is significantly larger than for organic particles, which could lead to greater SOA formation under humid conditions; for example, *Pun* [2008] calculated that SOA concentrations due to isoprene oxidation could be up to 5 times greater under humid conditions than under dry conditions. To account for this process, a simple parameterization is incorporated in the version of SORGAM, which already includes NO_x regimes and all terpene precursors. This parameterization accounts for a linear increase in isoprene SOA formation as a function of relative humidity (RH) (Super-SORGAM): $K_i(\mathrm{RH}) = K_i(\mathrm{RH} = 0)\ (1 + 4\ \mathrm{RH})$, where K_i, $i = 1, 2$, are the partitioning constants of the two isoprene SOA species and RH is expressed as a fraction (i.e., RH = 1 at 100% relative humidity). This parameterization leads to about 5 times more isoprene formation at 100% relative humidity than at 0% relative humidity, following the simulation results of *Pun* [2008]. The result shows an increase in SOA concentrations in regions where SOA formation from isoprene is significant, that is, mostly near the Mediterranean Sea. They reach 0.5-0.8 μg/m^3 in northern Italy and northern Spain, where SOA concentrations are in the 2-3 μg/m^3 range. They are less than 0.1 μg/m^3 in northern Europe, where SORGAM-NO_x SOA concentrations are mostly less than 2 μg/m^3.

AEC was simplified to obtain a version that closely resembles the formulation of Super-SORGAM, hereafter referred to as Mini-AEC. In that version, the activity coefficients are set to one (i.e., assuming ideal solutions) and oligomerization of SOA in the particulate phase is not simulated. The effect of activity coefficients set to one (ideal organic and aqueous solutions) for particulate SOA leads to a decrease in SOA concentrations of about 10% on average (0.08 μg/m^3). This relatively small effect, for example, compared to the difference reported by *Pun* [2008] is due in part to compensating effects for hydrophobic particles and aqueous particles. In some areas, the effect can be significant with the largest differences ($>$ 0.5 μg/m^3) occurring in southern Sweden, southwestern France, Corsica, and North Africa.

The two other versions of AEC used here include one where only oligomerization [*Pun and Seigneur*, 2007] is not taken into account but the activity coefficients are calculated (referred to as AEC-no-oligo), and the base AEC configuration where all processes are simulated (see Table A.1).

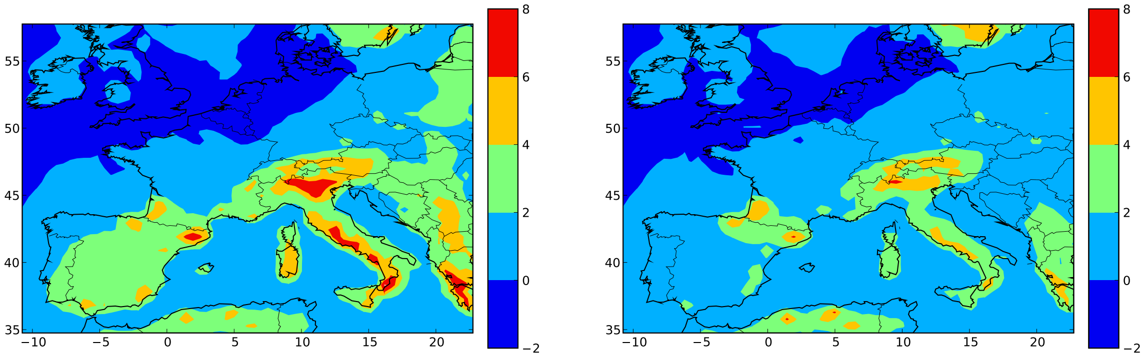

(a) $\mathbf{[PM_{2.5}]}_{CB05,AEC}$ **-** $\mathbf{[PM_{2.5}]}_{CB05,SORGAM}$ (b) $\mathbf{[PM_{2.5}]}_{RACM2,AEC}$ **-** $\mathbf{[PM_{2.5}]}_{RACM2,SORGAM}$

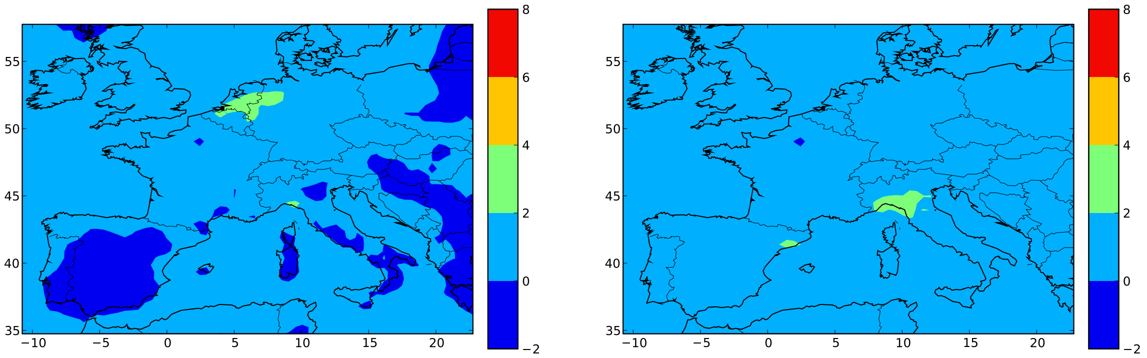

(c) $\mathbf{[PM_{2.5}]}_{RACM2,AEC}$ **-** $\mathbf{[PM_{2.5}]}_{CB05,AEC}$ (d) $\mathbf{[PM_{2.5}]}_{RACM2,SORGAM}$ **-** $\mathbf{[PM_{2.5}]}_{CB05,SORGAM}$

Figure A.4: Differences in $PM_{2.5}$ concentrations (µg/m^3) over Europe simulated with RACM2 and CB05 for gas-phase chemistry and with AEC and SORGAM for SOA formation. Results are averaged over the one-month simulation of 15 July to 15 August 2001: (a) $[PM_{2.5}]_{CB05,AEC}$ - $[PM_{2.5}]_{CB05,SORGAM}$ (top left); (b) $[PM_{2.5}]_{RACM2,AEC}$ - $[PM_{2.5}]_{RACM2,SORGAM}$ (top right); (c) $[PM_{2.5}]_{RACM2,AEC}$ - $[PM_{2.5}]_{CB05,AEC}$ (bottom left); (d) $[PM_{2.5}]_{RACM2,SORGAM}$ - $[PM_{2.5}]_{CB05,SORGAM}$ (bottom right).

Neglecting oligomerization has a significant effect with an average decrease of 0.57 µg/m^3 in SOA concentrations over the entire domain. The largest decrease occurs in North Africa (up to 8 µg/m^3). Decreases in southwestern France and Austria are up to 5 µg/m^3. Significant increases are also obtained over southern Sweden. These regions have significant emissions of monoterpenes, which are precursors of the aldehyde SOA surrogate species that is subject to oligomerization in AEC.

A.4 Joint sensitivity of PM concentrations to the gas-phase chemistry and aerosol module

The joint sensitivity of PM concentrations to different treatments of both gas-phase chemistry and SOA formation is investigated. In particular, we evaluate whether the effects of gas-phase chemistry and SOA formation are simply additive or whether synergistic or antagonistic effects are significant. Figure A.4 presents the differences in $PM_{2.5}$ concentrations averaged over the 1-month simulation obtained with the four possible combinations of gasphase chemistry (RACM2 and CB05) and SOA modules (SORGAM and AEC).

The effect of the gas-phase chemical mechanism differs depending on which aerosol module is used. With both aerosol modules, the average $PM_{2.5}$ concentration is greater with RACM2 than with CB05: when SORGAM is used, the difference in $PM_{2.5}$ concentrations is 6% on average; it is 3% on average when AEC is used. These differences are commensurate with the 5% difference obtained for ozone concentrations between CB05 and RACM2 [*Kim et al.*, 2009]; however, the $PM_{2.5}$ differences result from compensating differences in inorganic and organic $PM_{2.5}$ concentrations. Secondary inorganic aerosol concentrations are greater on average with RACM2 than with CB05 by about 14%. On the other hand, SOA concentrations are greater with CB05 than with RACM2. The difference is only 3% with SORGAM, but it is 20% on average with AEC. This larger difference obtained with AEC is due in part to the fact that AEC takes into account the influence of the NO_x regime on SOA formation explicitly. At low NO_x concentrations, the formation of organic peroxide SOA is favored, whereas at high NO_x concentrations, the formation of other condensable products such as organic nitrates is favored. Because the SOA yields differ for those distinct SOA species, the gas-phase chemical mechanism has a strong influence on the SOA formation rate, particularly in the transition regime between high-NO_x and low-NO_x regimes (i.e., as the air mass is transported, for example, from an urban area to a remote location). CB05 switches more rapidly from a high-NO_x regime to a low-NO_x regime than RACM2, as documented by a map of HO_2/NO concentration ratios (not shown), which are greater with CB05 than with RACM2. As a result, CB05 is more conducive to SOA formation than RACM2.

This result demonstrates that the formation of SOA is very closely tied to the gas-phase chemical kinetic mechanism because the types of SOA formed and, therefore, the SOA yields differ in low-NO_x versus high-NO_x regimes. Consequently, uncertainties in the gas-phase chemistry and the aerosol module should not be treated separately but jointly.

A.5 Conclusion

The gas-phase chemical mechanism and aerosol module used in air quality models are shown to influence the simulated ozone and PM concentrations. Differences in SOA formation resulting from the use of different modules are more significant than those due to gas-phase chemistry and can be up to about 65%. The major sources of those differences include the following: the list of VOC included as VOC precursors (+66%, particularly isoprene, +44%), the explicit treatment of high-NO_x and low-NO_x regimes in the gas-phase chemistry leading to SOA (+32% to +122% depending on the implementation within the gas-phase chemical mechanism), and the treatment of oligomerization (+60%). Further work is needed to develop gas-phase chemical kinetic mechanisms that can explicitly account for different SOA yields depending on the oxidation pathways for high-NO_x (e.g., organonitrate formation) and low-NO_x (e.g., peroxide formation) regimes.

The enthalpies of vaporization have a small effect on average (4%) but may have an important effect locally with lower values leading to less SOA in regions with low temperature and more SOA in regions with high temperature.

The treatment of activity coefficients in the particulate phase has a small effect on average (+9%); however, the effect can be significant in some areas. Furthermore, the values of the activity coefficients may differ significantly between their implicit value in SORGAM and their calculated values in AEC because the activity coefficients of an SOA compound may differ significantly between their values in a smog chamber experiment with only one precursor and ammonium sulfate seed particles under dry conditions and the atmosphere where a myriad of SOA and POA species interact with inorganic salts and water.

The treatment of isoprene SOA (hydrophobic in SORGAM and hydrophilic in AEC) has a significant effect on SOA concentrations: 0.15 $\mu g/m^3$ of isoprene SOA is formed with SORGAM, whereas 0.34 $\mu g/m^3$ is formed with AEC. This result is consistent with that obtained by *Pun* [2008], who found a large increase in SOA concentration when hydrophilic SOA condensed in an aqueous phase. However, the two models differ because AEC includes interactions among SOA and inorganic salts in the aqueous phase, whereas the model of *Pun* [2008] only considered SOA in the aqueous phase. Further investigations appear warranted to better characterize the effect of an atmospheric aqueous particulate phase on isoprene SOA. Aqueous-phase formation of SOA species was not considered here; it could be a significant factor [*Pun et al.*, 2000; *Lim et al.*, 2005; *Carlton et al.*, 2008; *Ervens et al.*, 2008; *El Haddad et al.*, 2009; *Deguillaume et al.*, 2009] and should be investigated in future work.

The uncertainties due to the gas-phase chemistry and to the aerosol module are not additive and some strong nonlinearities occur for PM concentrations. In this study, one gas-phase chemical mechanism led to greater secondary inorganic aerosol formation, but to less secondary organic aerosol formation due to the intricate interactions between the gas-phase mechanism and secondary aerosol formation processes. These results have implications for air quality modeling in general, as they highlight which processes appear to be the most important for SOA modeling and the uncertainties associated with neglecting or parameterizing those processes.

Appendix B

Impact of biogenic emissions on air quality over Europe and North America

Cet appendice est constitué de

Sartelet, K., Couvidat, F., Seigneur, C. et Roustan, Y. (2012). **Impact of biogenic emissions on air quality over Europe and North America**. *Atmos. Environ.*, 53:131-141.

Sommaire

Abstract

This study aims to compare the relative impact of biogenic emissions on ozone (O_3) and particulate matter (PM) concentrations between North America (NA) and Europe. The simulations are conducted with the Polyphemus air quality modeling system over July and August 2006. Prior to the sensitivity study on the impact of biogenic emissions on air quality, the modeling results are compared to observational data, as well as to the concentrations obtained by other modeling teams of the Air Quality Model Evaluation International Initiative (AQMEII) study.

Over Europe, three distinct emission inventories are used. Model performance is satisfactory for O_3, PM_{10} and $PM_{2.5}$ with all inventories with respect to the criteria described in the literature. Furthermore, the rmse and errors are lower than the average rmse and errors of the AQMEII simulations. Over North America, the model performance satisfies the criteria described in the literature for O_3, PM_{10} and $PM_{2.5}$. Polyphemus results are within the range of the AQMEII model results. Although the rmse and errors are higher than the average of the AQMEII simulations for O_3, they are lower for PM_{10} and $PM_{2.5}$.

The impact of biogenic and anthropogenic emissions on O_3 and PM concentrations is studied by removing alternatively biogenic and anthropogenic emissions in distinct simulations. Because biogenic species interact strongly with NO_x, the impact of biogenic emissions on O_3 concentrations varies with variations of the Volatile Organic Compound (VOC)/NO_x ratio. This impact is larger over NA than Europe. O_3 decreases by 10-11% in average over Europe and 20% over NA. Locally, the relative impact is also higher in NA (60% maximum) than in Europe (35% maximum). O_3 decreases near large urban centers where biogenic emissions are large (e.g., Los Angeles, Chicago, Houston in NA, Milan in Europe).

Most of secondary organic aerosols (SOA) formed at the continental scale over Europe and NA are biogenic aerosols. Eliminating biogenic emissions reduces SOA by 72% to 88% over Europe and by 90% over NA. However, biogenic SOA are not only impacted by biogenic but also by anthropogenic emissions: eliminating all anthropogenic emissions affects oxidant levels and the absorbing carbon mass, reducing the formation of SOA by 15 to 16% over Europe and by about 10% over NA; Furthermore, locally, the reduction may be as large as 50%, especially over large urban centers in Europe and NA.

B.1 Introduction

Ozone (O_3) and particulate matter (PM) concentrations are believed to contribute to adverse health effects [*Ostro and Chestnut*, 1998] and climate change [*Yu et al.*, 2006]. Emissions of volatile organic compounds (VOC) and nitrogen oxides (NO_x) affect both O_3 and PM concentrations. Emissions are from different origins: anthropogenic, biogenic, marine, natural and re-suspended dust and biomass burning. Biogenic VOC (BVOC) emissions are highest in summer [e.g. *Guenther et al.*, 1995; *Steinbrecher et al.*, 2009]. During the summer heat wave of 2006, O_3 concentrations frequently exceeded air quality standards over Europe [*Struzewska and Kaminski*, 2008]. The year 2006 was also the second-hottest year in North America (NA) since the mid 1900s. As BVOC emissions depend on light and temperature, their impact on air quality during the summer 2006 may be high. Because precursor emission regulations can only target anthropogenic emissions, high biogenic emissions are not controllable and it is essential to understand how they may increase difficulties in meeting air quality standards via their interactions with anthropogenic species.

Over Europe, *Curci et al.* [2009] showed that for the years 1997, 2000, 2001 and 2003, BVOC emissions increased summer daily O_3 maxima by 5% on average. They also found that the average impact is higher during the hot summer of 2003 than during the other cooler summers.

Over the northeastern United States, *Pun et al.* [2002b] estimated the contribution of biogenic emissions to O_3 and $PM_{2.5}$ for a few days in July 1995. They showed that the contribution to O_3 was lower than 23%. The contribution to $PM_{2.5}$ was low (4 to 13%). *Pun et al.* [2002b] argued that it is because of the long life-time of $PM_{2.5}$, and the relatively short time period and small spatial domain of the simulations. In their simulations, biogenic secondary organic aerosols (SOA) only contributed to a small fraction of $PM_{2.5}$ and isoprene SOA was not modeled. *Mueller and Mallard* [2011] studied the relative contributions of natural to total emissions over the United States. They found that biogenic emissions were the primary source of fine particles in all parts of the country. For the eastern United States, *Hogrefe et al.* [2011] found that the impact of uncertainties in biogenic estimates from two models on O_3 and $PM_{2.5}$ is significant. *Koo et al.* [2011] studied the impact of natural emissions on anthropogenic emission control strategies, and found substantial uncertainties in current representation of natural sources, such as lightning NO emissions, which affect O_3 concentrations in the southeastern US where biogenic VOC emissions are large.

Anthropogenic NO_x concentrations may increase the oxidation of BVOC and the formation of O_3 and PM. *Curci et al.* [2009] and *Pun et al.* [2002b] found that O_3 production is more impacted by BVOC emissions in metropolitan regions than in rural areas. O_3 production depends on the initial amounts of VOC (non-methane VOC)/NO_x ratio (in ppbC/ppb, see the ozone isopleth diagram of *Seinfeld and Pandis* [1998] for example). The variations of this VOC/NO_x ratio is used in this paper to understand the variation of the O_3 production regime. *Hoyle et al.* [2011] detailed the mechanisms through which the anthropogenic emissions enhance the formation of biogenic SOA: anthropogenic emissions impact the concentration of oxidants (O_3, OH, NO_3), which oxidize BVOC to form semi-volatile species, and anthropogenic primary organic aerosols may serve as an absorbing medium favoring their condensation. *Carlton et al.* [2010b] estimated that more than 50% of biogenic SOA in the eastern U.S. can be controlled via the influence of anthropogenic emissions on biogenic SOA.

For the Air Quality Model Evaluation International Initiative (AQMEII) study, several air quality models were compared over North America (NA) and Europe [*Rao et al.*, 2011]. One of these models (Polyphemus) is used here to investigate the effect of biogenic emissions on air quality. The model is described in the first section. Then, its performance is evaluated by comparisons to available observations in the Ensemble system [*Bianconi et al.*, 2004] as well as by comparisons with other models of the AQMEII study. Over Europe, four simulations are conducted with and without biomass burning emissions and with different anthropogenic emission inventories and biogenic emission schemes. Over North America (NA), the simulation is conducted using the default data provided for the AQMEII study. Finally, the relative impacts of biogenic and anthropogenic emissions on air quality over Europe and NA are estimated and compared for the different Polyphemus simulations.

B.2 Model Description

The Polyphemus air-quality modeling platform (http://cerea.enpc.f/polyphemus) is used here with the chemistry transport model Polair3D. Polyphemus/Polair3D has already been used for many applications at the continental scale over Europe and East Asia [e.g. *Sartelet et al.*, 2007; *Kim et al.*, 2009; *Roustan et al.*, 2010; *Kim et al.*, 2011b; *Sartelet et al.*, 2008].

For gas-phase chemistry, the Regional Atmospheric Chemistry Mechanism [RACM, *Stockwell et al.*, 1997] is used over Europe and the Carbon-Bond Mechanism [CB05, *Yarwood et al.*, 2005] over NA. Over NA, photolysis rates are computed online, that is the influence of particles on photolysis rates is taken into account [*Real and Sartelet*, 2011]. The aerosol model used is SIREAM-SuperSorgam [*Debry et al.*, 2007a; *Kim et al.*, 2011a]. It models coagulation and condensation/evaporation. It uses a standard SOA formulation with hydrophobic absorption of SOA into organic particles. The SOA precursors are aromatics, long-chain alkanes, long-chain alkenes, isoprene, monoterpenes and sesquiterpenes. The biogenic SOA formation varies depending on the NO_x regime.

Simulations are performed from 1 July 2006 to 31 August 2006. In all simulations, 9 vertical levels are considered from the ground to 12 km (40m, 120m, 300m, 800m, 1500m, 2400m, 3500m, 6000m, 12000m). The Global Land Cover Facility (GLCF2000) map with 23 categories is used for land use coverage. Initial and boundary conditions are the default AQMEII conditions provided by ECMWF-GEMS. Sea-salt emissions are parameterized following *Monahan et al.* [1986]. The emitted mass of sea salt is assumed to be made of 30.61% of sodium, 55.025% of chloride and 7.68% of sulfate [*Seinfeld and Pandis*, 1998]. Over Europe, the horizontal domain is (35°N-70°N ; 15°W-35°E) with a resolution of 0.25° x 0.25°. The meteorological data correspond to the default MM5 data provided for the AQMEII inter-comparison with 32 vertical levels [*Vautard et al.*, 2012]. In the first of the four simulations conducted over Europe, and labelled Pol 1, anthropogenic emissions are the default AQMEII emissions data provided by TNO [*Pouliot et al.*, 2012]. They are referred to as the TNO anthropogenic emission inventory. Biogenic emissions are computed as in *Simpson et al.* [1999], and referred to as the Simpson biogenic emission scheme. Biogenic (terpene) emissions are distributed among pinene (62.54%), limonene (37.03%) and sesquiterpene (humulene, 0.43%), following *Johnson et al.* [2006] and *Helmig et al.* [1999a,b]. Biomass burning emissions provided by Finnish Meteorological Institute (FMI) for AQMEII are also used in one simulation. Following Mikhail Sofief (communication on AQMEII web site), 50% is emitted between the surface and 200 m, and the remaining 50% is emitted between 200 m and 1000 m. The fire PM emissions are assumed to consist of 70% of $PM_{2.5}$ and 30% of PM_{10}-$PM_{2.5}$. For gaseous species emissions from biomass burning, the PM emission rate is multiplied by 7.88 and then split amongst CO, HCHO, NO_x, NH_3 and SO_2 according to the following fractions: 0.94, 0.013, 0.029, 0.014 and 0.004, respectively. In the other three simulations conducted over Europe, biomass burning is ignored, because $PM_{2.5}$ are strongly over-estimated over Portugal when biomass burning emissions are used. The second simulation labelled "Pol 2" uses the TNO emission inventory for anthropogenic emissions and Simpson for biogenic emissions, as Pol 1. The third simulation, labelled "Pol 3", uses the European Monitoring and Evaluation Program (EMEP, http://www.emep.int/) expert inventory for 2006 and Simpson for biogenic emissions. The time distribution of EMEP emissions, as well as the speciation are detailed in *Sartelet et al.* [2007]. The fourth simulation, labelled "Pol 4", uses the EMEP emission inventory for anthropogenic emissions and the Model of Emissions of Gases and Aerosols from Nature with the EFv2.1 dataset [MEGAN, *Guenther et al.*, 2006]. Differences between the MEGAN and Simpson emission schemes are discussed elsewhere [*Steinbrecher et al.*, 2009]. The two biogenic emission schemes use different methodologies: MEGAN uses canopy-scale emission factors based on leaf area index obtained from the standard MEGAN LAIv database [MEGAN-L, *Guenther et al.*, 2006] whereas Simpson uses leaf-scale emission factors based on GLC2000 land-use categories. Furthermore, although terpene emissions are distributed amongst pinene, limonene and sesquiterpenes with constant factors, different emission factors are used for several species in MEGAN. Table B.1 compares the domain-mean Simpson and MEGAN biogenic emissions. Except for sesquiterpenes, MEGAN emissions are lower than Simpson emissions, especially over the northeastern part of the domain, such as over Finland. Differences in the spatial distribution are also observed, such as in Poland, Croatia or central France. Table B.2 summarizes the emission inventories used in the four simulations.

Over North America, the horizontal domain is (24°N-53.75°N; 125.5°W-64°W) with a resolution of 0.25° x 0.25°. The meteorological data correspond to the default WRF data provided for the AQMEII inter-comparison [*Vautard et al.*, 2012]. As Polyphemus uses a Lat-Lon projection

	Simpson	MEGAN
Isoprene	0.0799	0.0312
Terpenes	0.0436	0.01792
Sesquiterpenes	0.000188	0.00129
NO	0.00118	0.00108

Table B.1: Domain-mean Simpson and MEGAN biogenic emissions (in μg m^{-2} s^{-1}).

	Pol 1	Pol 2	Pol 3	Pol 4
Anthropogenic emissions	TNO	TNO	TNO	Emep
Biogenic emissions	Simpson	Simpson	Simpson	MEGAN
Biomass burning emissions	Yes	No	No	No

Table B.2: Emission inventories used in the four simulations conducted over Europe with Polyphemus.

versus Lambert for WRF, the meteorological data do not cover the whole computational domain. Therefore, the Polyphemus domain (24°N-53.75°N; 125.5°W-64°W) is slightly smaller than the AQMEII domain (23.5°N-58.5°N; 130°W-59.5°W). For the remaining few grid cells missing in the southwestern and southeastern parts of the domain over the ocean, the same meteorological fields as those along the boundary are used. Anthropogenic, biogenic from BEIS3.14 and biomass burning emissions are those provided by US-EPA for AQMEII [*Pouliot et al.*, 2012].

B.3 Base simulations over Europe and North America

B.3.1 Model performance evaluation

The following statistics are computed for comparing the surface levels from the base case simulation with observations between 7 July 2006 and 31 August 2006: root mean square error (rmse), mean fractional error (mfe), mean fractional bias (mfb), and correlation coefficient (r). For O_3, the mean normalized gross error (mnge) and mean normalized gross bias (mngb) are also computed with a cutoff of 80 μg m^{-3} (i.e. about 40 ppb). *Russell and Dennis* [2000] recommend performance criteria for hourly O_3 to be mngb $\leq \pm$ 15% and mnge $\leq$ 30%. For PM, *Boylan and Russell* [2006] propose that a model performance goal is met when both the mfe is less than or equal to $+50\%$ and the mfb is within $\pm 30\%$ respectively, and a model performance criterion is met when both mfe $\leq +75\%$ and $-60\% \leq$ mfb $\leq$ 60%. The first week is excluded when computing statistics to allow for model initialization and spin-up. Observational data at rural and suburban stations were obtained from the ensemble system. The results of simulations provided by other modeling teams at these stations were also obtained and compared with the results of this modeling study. Over Europe, the observational data include stations from Airbase (http://air-climate.eionet.europa.eu/databases/airbase) and EMEP (http://tarantula.nilu.no/projects/ccc/emepdata.html) databases. Over NA, these data include stations from Interagency Monitoring of Protected Visual Environments (IMPROVE, http://vista.cira.colostate.edu/improve/), the U.S. Environmental Protection Agency (EPA) Aerometric Information Retrieval System (AIRS, http://www.epa.gov/air/data/index.html), and the Environment Canada National Air Pollution Surveillance network (Cast and Naps) databases. Hourly concentration data are used for gaseous species and daily data are used for particulate matter (PM).

Over Europe

Over Europe, the 4 different Polyphemus simulations are compared to observations for O_3, PM_{10} and $PM_{2.5}$ in Tables B.3, B.4 and B.5 respectively. Comparisons for NO_2 and SO_2, PM_{10} sulfate, PM_{10} nitrate and PM_{10} ammonium are presented in the supplementary electronic materials. The comparison of model results with observations is also conducted for 9 different models that participated to the AQMEII inter-comparisons, not including Polyphemus, in order to compare the performances. The mean of the statistics of the AQMEII models is computed as well as the minimum and maximum values.

For all pollutants, the different simulations using Polyphemus perform well according to the performance criteria detailed above and they are within the range of results obtained by other AQMEII models.

For hourly O_3, the average simulated concentration is close to the average measured concentration, although it is slightly lower (73.0 μg m^{-3} measured against between 67.0 and 69.3 μg m^{-3} simulated with rmse between 28.6 and 29.9 μg m^{-3}). The mngb is slightly higher than the range of the model performance criterion of *Russell and Dennis* [2000] ($\leq \pm$ 15%). However, the mnge is well within the range of the model performance criterion of *Russell and Dennis* [2000] ($\leq$ 30%). The different Polyphemus simulations compare well to other AQMEII simulations: the highest rmse of the Polyphemus simulations is lower than the lowest rmse of the AQMEII simulations, while the correlation of Polyphemus are close to the highest correlation of the AQMEII simulations or higher for Pol 4. Other errors and bias are close to the average of the AQMEII simulations. The differences between the different Polyphemus simulations are much lower than differences between the different AQMEII simulations.

O_3 - Europe	Pol 1	Pol 2	Pol 3	Pol 4	AQMEII models		
					Min	Mean	Max
Number of stations	796	796	796	796	790	795.4	796
Mean obs	73.0	73.0	73.0	73.0	73.0	73.0	73.1
Mean sim	68.7	67.0	69.3	67.5	60.9	72.4	97.0
rmse	29.8	29.9	29.2	28.6	30.0	32.8	38.8
correlation	65.8%	66.4%	67.3%	69.8%	56.6%	62.8%	68.6%
mfb	-24.5%	-27.3%	-23.2%	-25.2%	-39.0%	-21.7%	5.7%
mfe	28.3%	30.0%	27.1%	28.1%	17.1%	29.5%	41.8%
mngb	-19.6%	-22.1%	-18.7%	-20.6%	-29.4%	-15.8%	8.3%
mnge	24.0%	25.1%	23.1%	23.8%	18.3%	24.9%	32.6%

Table B.3: Comparisons to observations for surface O_3 over Europe (concentrations and rmse are in μg m^{-3}).

The average PM_{10} concentration is well simulated, although it is slightly under-estimated for Pol 2, Pol 3 and Pol 4 (23.2 μg m^{-3} measured against between 18.5 and 21.1 μg m^{-3} simulated, and rmse between 28.6 and 29.9 μg m^{-3}). The model performance goal of *Boylan and Russell* [2006] is met for all Polyphemus simulations as the mfb is within ±30%, and the mfe is lower than 50%. The different Polyphemus simulations compare well to other AQMEII simulations: the highest rmse is lower than the lowest rmse of the AQMEII simulations. The correlation of Polyphemus are above the average of the correlations of the AQMEII simulations. As for O_3, the differences between the different Polyphemus simulations are much lower than the differences between the different AQMEII simulations.

The average simulated $PM_{2.5}$ concentration is higher than the average measured $PM_{2.5}$ con-

PM_{10} - Europe	Pol 1	Pol 2	Pol 3	Pol 4	AQMEII models		
					Min	Mean	Max
Number of stations	235	235	235	235	235	235	235
Mean obs	23.2	23.2	23.2	23.2	23.2	23.2	23.2
Mean sim	21.1	19.3	19.9	18.5	6.2	12.9	23.4
rmse	15.9	14.7	14.7	15.1	16.2	23.2	24.6
correlation	18.6%	19.1%	19.6%	18.9%	8.2%	17.3%	25.0%
mfb	-5.2%	-11.4%	-9.0%	-16.3%	-111.0%	-64.3%	3.9%
mfe	46.9%	46.6%	46.3%	48.7%	44.5%	80.8%	112.7%

Table B.4: Comparisons to observations for surface PM_{10} over Europe (concentrations and rmse are in μg m^{-3}).

centration (13.3 μg m^{-3} measured against between 17.4 and 19.2 μg m^{-3} simulated, with rmse between 12.0 and 14.0 μg m^{-3}). The model performance goal of *Boylan and Russell* [2006] is met for the mfb for Pol 4, but it is not met for Pol 1 to Pol 3. The model performance goal is not met for the mfe. However the model performance criteria are met for both the mfb and the mfe for all Polyphemus simulations, as the mfb and mfe are within ±60% and lower than 75% respectively. The different Polyphemus simulations compare well to other AQMEII simulations: the mfe and the rmse are in the low range of the AQMEII models, while correlation is in the high range. As for O_3 and PM_{10}, the differences between the different Polyphemus simulations are lower than differences between the different AQMEII simulations.

$PM_{2.5}$ - Europe	Pol 1	Pol 2	Pol 3	Pol 4	AQMEII models		
					Min	Mean	Max
Number of stations	39	39	39	39	39	39	39
Mean obs	13.3	13.3	13.3	13.3	13.3	13.3	13.3
Mean sim	19.2	17.7	18.6	17.4	5.0	12.3	21.4
rmse	14.0	12.0	12.7	12.2	11.4	24.1	69.2
correlation	14.1%	10.6%	9.2%	9.1%	3.2%	11.8%	21.1%
mfb	36.8%	31.7%	35.7%	28.9%	-85.7%	-30.5%	44.9%
mfe	59.6%	57.0%	59.0%	57.4%	55.1%	72.3%	94.2%

Table B.5: Comparisons to observations for surface $PM_{2.5}$ over Europe (concentrations and rmse are in μg m^{-3}).

Over Portugal, where high-intensity biomass burning occurred, taking biomass burning into account (Pol 1) leads to a large over-estimation of $PM_{2.5}$. The mean measured concentration at the 6 rural Airbase stations over Portugal is equal to 14.3 μg m^{-3}. The simulated concentration is equal to 34.1 μg m^{-3} for Pol 1, 15.2 for Pol 2, 17.1 for Pol 3 and 14.0 μg m^{-3} for Pol 3. One of the reason for this large over-estimation of $PM_{2.5}$ at the ground over Portugal for Pol 1 is related to the emission height of biomass burning. For example, *Hodzic et al.* [2007] relates the emission height to the intensity of fire. They estimate that 95% of emissions of the largest fires over Portugal is emitted above the boundary layer, whereas in Pol 1 all the pollutants are emitted in the boundary layer. Therefore, Pol 1 is not considered in the impact study conducted below.

Over North America

Over NA, only one Polyphemus simulation is performed using the default AQMEII emission inputs. It is compared to observations for O_3, PM_{10} and $PM_{2.5}$ in Tables B.6, B.7 and B.8, respectively. The comparison to observations is also conducted for 6 different models that participated to the AQMEII inter-comparisons. Performance evaluation for NO_2 and SO_2 is presented in the supplementary electronic materials, as well as for elemental carbon of $PM_{2.5}$, organic matter of $PM_{2.5}$, sulfate of $PM_{2.5}$, nitrate of $PM_{2.5}$ and ammonium of $PM_{2.5}$.

For O_3, PM_{10} and $PM_{2.5}$, the Polyphemus simulation performs well according to the performance criteria detailed above and it is within the range of results obtained by other AQMEII models.

Although O_3 is over-estimated by Polyphemus (34.0 ppb measured and 43.6 ppb simulated with a rmse of 20.1 ppb), the Polyphemus simulation satisfies the model performance criterion of *Russell and Dennis* [2000]: the mngb and mnge are within ±15% and lower than 30%. Compared to the other AQMEII models, the rmse of the Polyphemus simulation is slightly higher than the higher rmse of all models, but the mfe and mnge corresponds to the average of all models.

For PM_{10}, the average simulated PM_{10} concentration is under-estimated (28.0 μg m^{-3} measured and 15.1 μg m^{-3} simulated with a rmse of 27.5 μg m^{-3}). The model performance goal of *Boylan and Russell* [2006] is not met, but the model performance criterion of *Boylan and Russell* [2006] is met as the mfb is within ±60% and the mfe is less than 75%. Compared to the other AQMEII models, the rmse and mfe of the Polyphemus simulation are lower than the average of all models.

For $PM_{2.5}$, the average simulated $PM_{2.5}$ concentration is over-estimated (12.9 μg m^{-3} measured and 16.1 simulated with a rmse of 9.3 μg m^{-3}). However, the model performance goal of *Boylan and Russell* [2006] is met as the mfb is within ±30% and the mfe is less than 50%. As for PM_{10}, the correlation is lower than the average of all models, but the rmse and the mfe are also lower.

O_3 - NA	Polyphemus	AQMEII models		
		Min	Mean	Max
Number of stations	634	634	634	634
Mean obs	34.0	34.0	34.0	34.0
Mean sim	43.6	33.8	39.4	44.6
rmse	20.2	15.3	17.5	19.9
correlation	60.4%	61.9%	66.0%	69.5%
mfb	-1.3%	-19.2%	-7.4%	1.7%
mfe	24.7%	18.7%	25.3%	39.9%
mngb	3.8%	-12.3%	-2.2%	5.5%
mnge	25.6%	18.5%	23.7%	34.5%

Table B.6: Comparisons to observations for surface O_3 over NA (concentrations and rmse are in ppb).

B.3.2 Spatial distribution

Over Europe

Over Europe, Figure B.1 shows the O_3 concentrations averaged over July and August for Pol 2. The spatial distribution of O_3 shows similar patterns to previously computed distributions [e.g.

PM_{10} - NA	Polyphemus	AQMEII models		
		Min	Mean	Max
Number of stations	638	638	638	638
Mean obs	28.0	28.0	28.0	28.0
Mean sim	15.1	5.4	13.8	30.7
rmse	27.5	24.5	28.4	32.6
correlation	15.1%	11.4%	20.4%	29.3%
mfb	-49.4%	-122.4%	-65.8%	19.1%
mfe	67.5%	49.7%	81.6%	123.7%

Table B.7: Comparisons to observations for surface PM_{10} over NA (concentrations and rmse are in μg m^{-3}).

$PM_{2.5}$ - NA	Polyphemus	AQMEII models		
		Min	Mean	Max
Number of stations	733	733	733	733
Mean obs	12.9	12.9	12.9	12.9
Mean sim	16.1	6.7	12.6	28.2
rmse	9.3	7.0	9.6	20.0
correlation	50.4%	47.5%	60.3%	67.0%
mfb	23.1%	-59.6%	-11.6%	75.4%
mfe	47.7%	33.1%	52.5%	79.6%

Table B.8: Comparisons to observations for surface $PM_{2.5}$ over NA (concentrations and rmse are in μg m^{-3}).

Curci et al., 2009]. O_3 is high in southern Europe, especially over the Black Sea, the Mediterranean Sea and the Baltic Sea. O_3 is low in northern Europe (Finland and northern Sweden). Over land, the highest concentrations are observed over Greece, Italy, Portugal, southern Spain and central Europe. O_3 concentrations lower than the surrounding values are observed over large cities, such as Paris and Milan, because of NO titration. The NO titration is also observed along the sea traffic lines. Maps of O_3 concentrations for simulations other than Pol 2 are not shown, as they are similar despite local differences. Taking into account biomass burning emissions (Pol 1 rather than Pol 2) only slightly increases O_3 locally where biomass burning occurs, such as over Portugal. Using the EMEP rather than the TNO anthropogenic emission inventory, i.e. Pol 3 rather than Pol 2, leads to lower NO titration along the sea traffic lines and therefore higher O_3. Using the MEGAN biogenic emission scheme rather than Simpson, i.e. Pol 4 rather than Pol 3, leads to higher O_3 over the northeastern part of the domain such as over Finland, where MEGAN biogenic emissions are much lower than Simpson's. This O_3 increase with lower biogenic emissions is explained by the very high VOC/NO_x ratio over this part of the domain (see Figure B.7 and section B.4.1).

Figure B.2 shows PM_{10} concentrations averaged over July and August for Pol 2. The spatial distribution of PM_{10} shows similar patterns to previously computed distributions [e.g. *Sartelet et al.*, 2007] with high concentrations over cities, and areas such as northern Italy, the northeastern Spain, and the Netherlands. Although the map of PM_{10} shows high concentrations around cities, the highest concentrations appear to be generated by maritime traffic and by sea-salt emissions. Maps of PM_{10} concentrations for simulations other than Pol 2 are not shown, as they

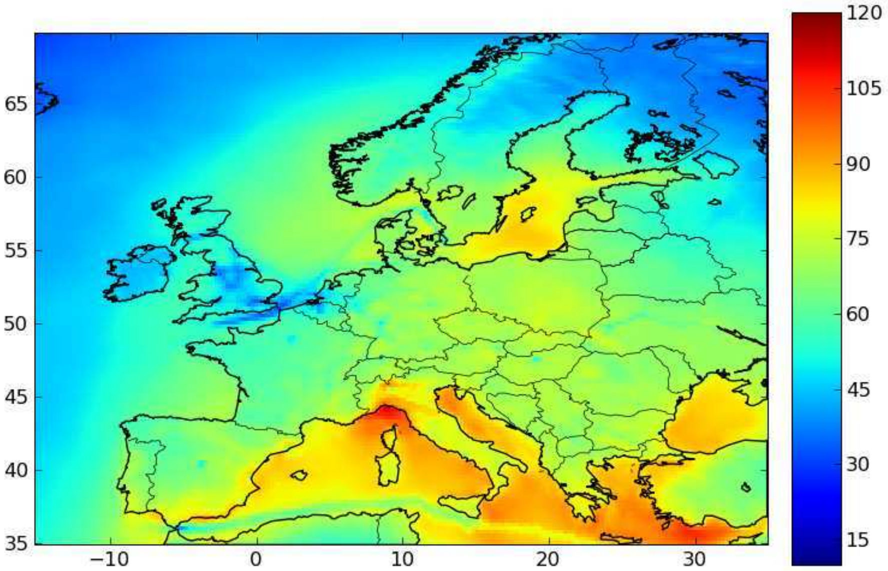

Figure B.1: Surface O_3 concentrations (in μg m^{-3}) over Europe averaged over July and August for Pol 2.

are similar despite local differences. As for O_3, the impact of maritime traffic on the formation of PM_{10} is slightly higher using the TNO rather than the EMEP anthropogenic emission inventory, i.e. Pol 3 rather than Pol 2. Furthermore, the variations of PM_{10} around cities are more sharply defined using TNO than EMEP. Using the MEGAN biogenic emission scheme rather than Simpson, i.e. Pol 4 rather than Pol 3, leads to lower PM_{10} over the northeastern part of the domain such as over Finland (see below).

Figure B.3 shows secondary organic aerosol (SOA) concentrations averaged over July and August using the Simpson (Pol 3, left panel) and MEGAN (Pol 4, right panel) biogenic emission schemes. The spatial distribution is very similar between Pol 2 and Pol 3, i.e. when changing the anthropogenic emission inventory. The overall spatial distribution agrees with previously published distributions [*Kim et al.*, 2011a], and similarities in spatial distributions are found between Pol 3 and Pol 4: high SOA concentrations are observed in Portugal, southwestern France, northeastern Spain, southeastern France, northern Italy, Greece, western Russia, Finland and southern Sweden. However, the spatial distribution locally differs in areas such as in Poland, Croatia and central France. The amplitude of SOA concentrations is very different in Sweden and Finland when using Simpson and MEGAN: the concentrations are locally reduced by a factor 5 when using MEGAN, because of lower biogenic emissions in MEGAN. On average over Europe, the SOA concentrations are reduced by a factor of 2 with MEGAN.

Over North America

O_3 concentrations (see Figure B.4) are higher in the eastern United States than in the western U.S., except in California where high O_3 is simulated. High O_3 concentrations are also simulated along the east coast in the region of New York, as well as near Alabama in the southern U.S., and near the Michigan and Erie Great Lakes. The spatial distribution corresponds well to those simulated by others such as *Luecken et al.* [2008].

The map of $PM_{2.5}$ concentrations averaged over July and August (Figure B.5) shows high concentrations especially around cities. The spatial distribution corresponds well to the ones

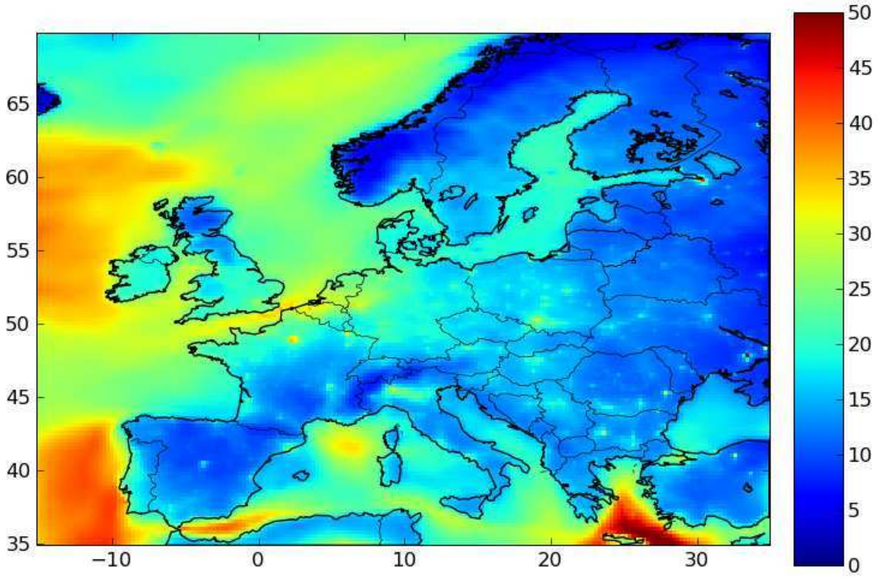

Figure B.2: Surface PM_{10} concentrations (in μg m^{-3}) over Europe averaged over July and August for Pol 2.

simulated in *Bailey et al.* [2007], with high concentrations in California as well as in the eastern U.S. along the coast.

For SOA, the spatial distribution (see Figure B.6) corresponds to that obtained by *Carlton et al.* [2010b]: high concentrations are observed in the southeastern U.S., in California near Los Angeles as well as in the western U.S. However, the concentrations are much higher here with a maximum SOA concentration of 11 μg m^{-3}, against about 1 μg m^{-3} in *Carlton et al.* [2010b] for controllable biogenic SOA. However, the simulated SOA compare relatively well to observations, as shown in the supplementary electronic materials: the average simulated concentration is equal to 3.6 μg m^{-3} against 2.8 μg m^{-3} estimated from measurements, with a mfb of 35.5%. In the southeast where high concentrations are simulated, measurements from the database “AIRS” at the station AIRSUSGA1MCN (-83.65, 32.78) report an average concentration of 7.7 μg m^{-3} over July and August, whereas the simulated concentration is 9.3 μg m^{-3}.

B.4 Impact of biogenic emissions

To estimate the contribution of biogenic emissions to O_3 and PM under current conditions, the methodology of *Pun et al.* [2002b] and *Curci et al.* [2009] is used. The simulation with all emissions is considered as the base case, and a simulation is performed without biogenic emissions (BVOC and NO) to calculate their contribution. As biogenic emissions interact with anthropogenic emissions to form O_3 and secondary PM, a simulation is also performed without anthropogenic emissions to compare the impact.

B.4.1 Over Europe

Over Europe, the sensitivity simulations are performed for the three simulations Pol 2, Pol 3 and Pol 4.

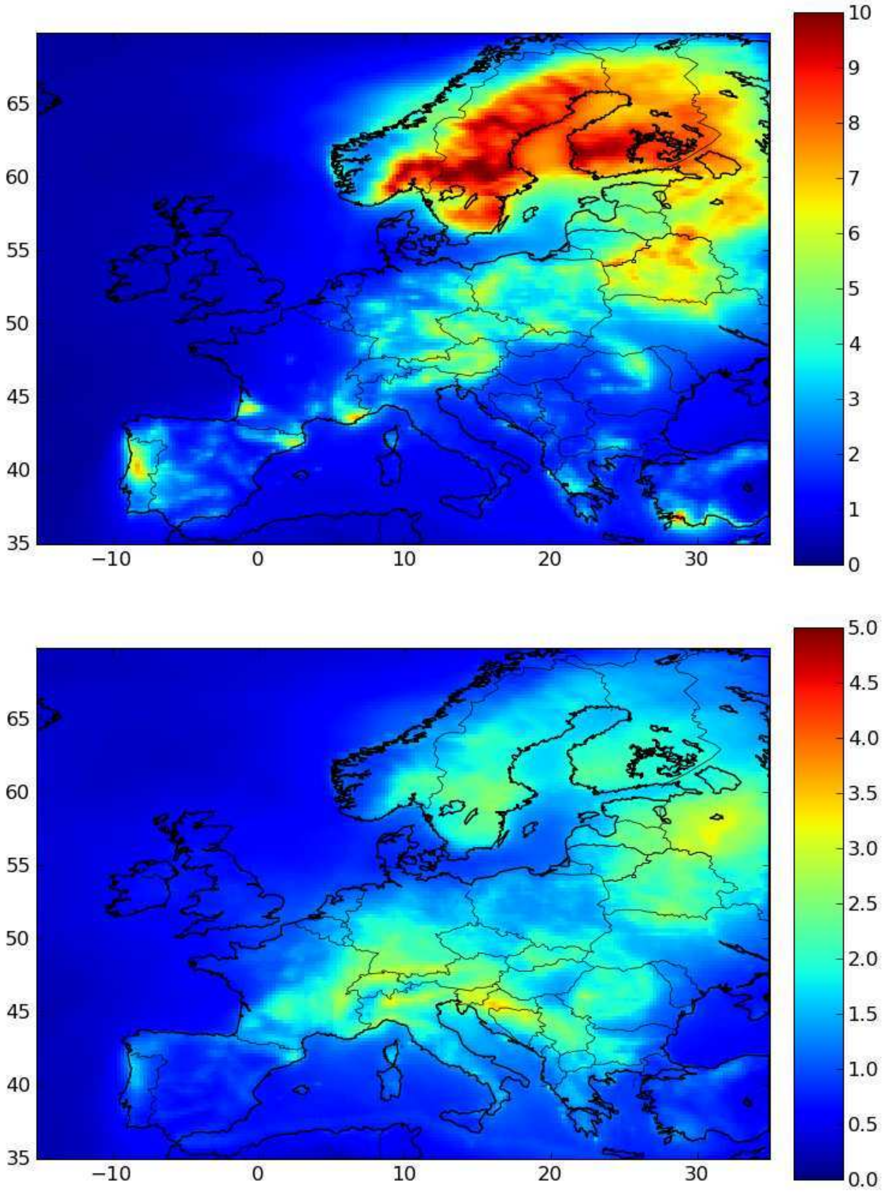

Figure B.3: Surface SOA concentrations (in μg m^{-3}) over Europe averaged over July and August using Simpson (Pol 3, upper panel) and MEGAN (Pol 4, lower panel) biogenic emission schemes.

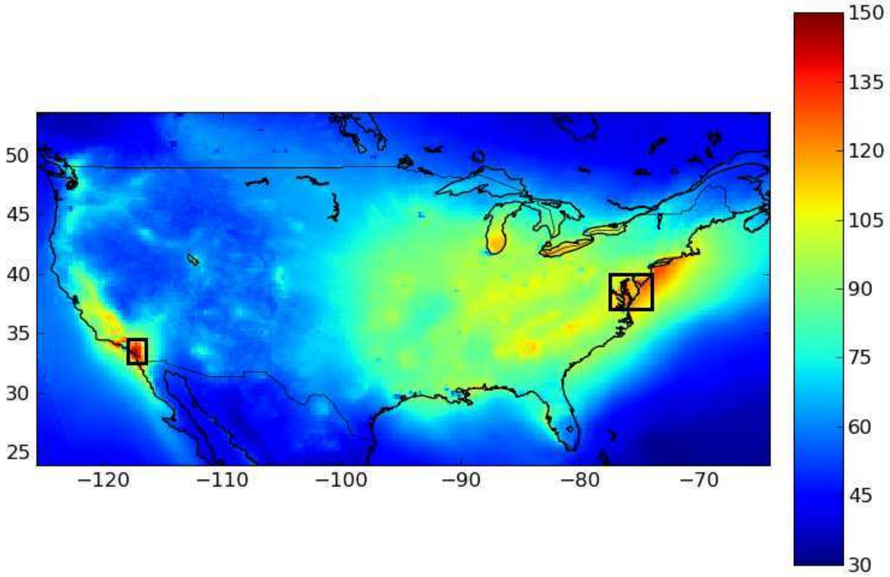

Figure B.4: Surface O_3 concentrations (in μg m^{-3}) over North America averaged over July and August.

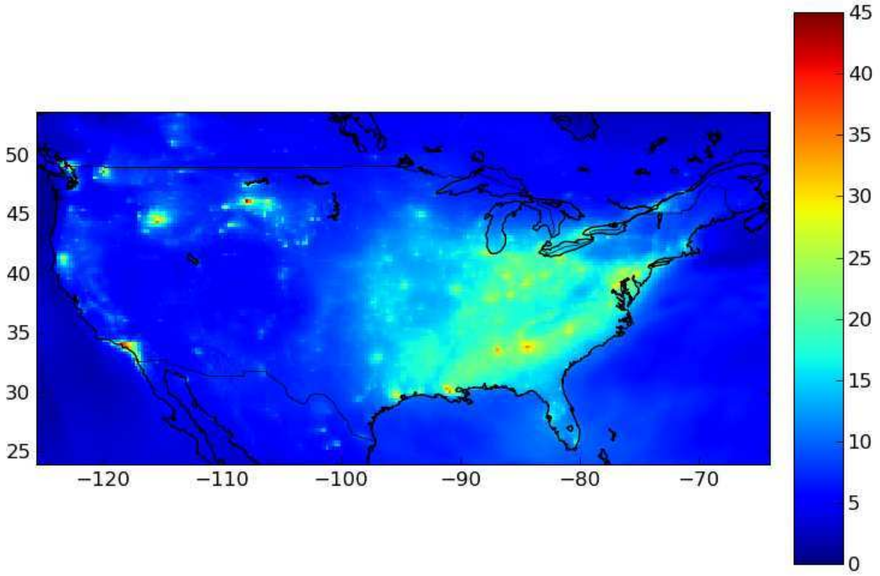

Figure B.5: Surface $PM_{2.5}$ concentrations (in μg m^{-3}) over North America averaged over July and August.

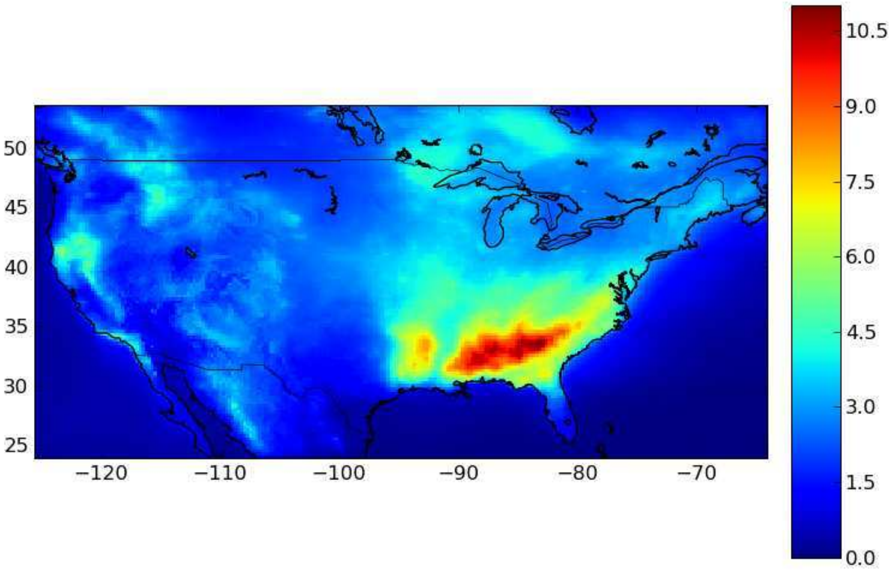

Figure B.6: Surface SOA concentrations (in μg m^{-3}) over North America averaged over July and August.

Table B.9 shows the mean concentrations of O_3, PM_{10} (without Na and Cl), SOA, isoprene SOA and terpene SOA averaged over Europe for July and August.

The impact of biogenic emissions on O_3 concentrations is lower than the impact of anthropogenic emissions. Removing biogenic emissions reduces O_3 concentrations by 10 to 11%, whereas removing anthropogenic emissions reduces O_3 concentration by 38% to 42%. The impact of removing biogenic emissions is lower when MEGAN biogenic emission scheme is used instead of Simpson (10% instead of 11%). This slightly lower impact is a consequence of the lower VOC emissions in MEGAN than in Simpson. Removing anthropogenic emissions also has a lower impact with Pol 4 (-38%) than with Pol 2 or Pol 3 (-41 to -42%), that is when MEGAN biogenic emission scheme is used rather than Simpson. Differences in the impacts of emission computed using the two different anthropogenic emission inventories are small, as EMEP and TNO emissions are commensurate.

To understand the local variations of O_3 concentrations when BVOC emissions are removed, the relative difference in O_3 computed with all emissions and without BVOC emission is shown in Figure B.8 for Pol 2, Pol 3 and Pol 4. Figure B.7 shows the VOC/NO_x concentration ratio for Pol 3 and Pol 4. The regions where the impact of biogenic emissions is high in Figure B.8 are strongly correlated to those where the VOC/NO_x ratio is low compared to surroundings in Figure B.7 (e.g. Milan, northeastern Spain, central Europe). The decrease in O_3 concentration is as high as 30% near cities, which are surrounded by biogenic emissions, such as Milan in Italy, Porto in Portugal or Warsaw in Poland. Around these cities, although BVOC emissions are high, the O_3 regime is probably VOC limited, leading to a strong decrease in O_3 concentrations when BVOC are removed. On the opposite, O_3 increases by as much as 10 to 20% in northern Sweden, Finland and part of Russia, where the VOC/NO_x ratio becomes higher than 200. This increase is removed when using MEGAN. Because BVOC emissions over Sweden and Finland are lower in MEGAN, the VOC/NO_x ratio is lower and O_3 concentrations are not modified by removing BVOC emissions. Although the impact of BVOC emissions on O_3 is almost the same for the two different anthropogenic emission inventories, local differences are important in central Europe near cities such as in Ukraine and Lithuania. Sea-traffic also has a larger impact using Pol 2 (TNO) than Pol 3 (EMEP).

PM_{10} is much more impacted by anthropogenic than biogenic emissions: the concentration decreases by 8 to 21% on average when biogenic emissions are removed, whereas it decreases by as much as 54 to 62% when anthropogenic emissions are removed. As for O_3, differences in the impacts of emission computed using the two different anthropogenic emission inventories are small. The impact of removing biogenic emissions is lower when using MEGAN rather than the Simpson biogenic emission scheme (8% for MEGAN and 21% for Simpson).

As SOA is mostly formed from isoprene (20% to 23%) and terpenes (62% to 67%) in our simulations, it is strongly impacted by biogenic emissions. SOA is very low when biogenic emissions are ignored: the concentrations are reduced by 87% to 88% on average in Pol 2 and Pol 3 and by 72% in Pol 4 where MEGAN is used. However, removing anthropogenic emissions only reduces SOA by 15 to 16%.

Locally, removing anthropogenic emissions may lead to a large decrease in SOA as shown in Figure B.9. SOA is reduced by as much as 40% to 50% along the maritime traffic lines, as well as around large cities such as Milan or Paris. The map of the relative difference of SOA when all emissions are taken into account and when biogenic emissions are removed is strongly correlated to the map of NO_x emissions, with emphasis where biogenic emissions are high (such as Portugal, southern Spain and Poland). In Figure B.9, the impact of anthropogenic emissions on SOA is shown only for Pol 3 and Pol 4, as the impact is very similar for Pol 2 and Pol 3, as suggested by the average numbers of Table B.9. Differences between Pol 3 and Pol 4 arise mostly in Germany, Poland, Estonia and Belarus, southwestern Spain and southwestern France, which are places where the two biogenic emission schemes lead to different patterns of SOA concentrations, and where significant anthropogenic emissions are present. In contrast, despite large differences in SOA concentrations simulated in Pol 3 and Pol 4 over northern Sweden and northern Finland, the impact of anthropogenic emissions is low over these countries because anthropogenic emissions are low.

Removing biogenic emissions does not only affect the biogenic compounds of SOA, but also the anthropogenic ones. By providing an absorbing organic mass, the biogenic compounds of particles facilitate the condensation of anthropogenic compounds. The absolute impact is low as the concentration of anthropogenic SOA is low compared to biogenic SOA at the continental scale. However, the relative impact of biogenic SOA on anthropogenic SOA may be as high as 40%, as shown in Figure B.10, which shows the relative difference of anthropogenic SOA when all emissions are taken into account and when biogenic emissions are ignored for Pol 3 and Pol 4. The map describing the impact of biogenic SOA on anthropogenic SOA is strongly correlated with the map of biogenic SOA concentrations. The relative impact is higher in Pol 3 than in Pol 4 as biogenic emissions are higher.

B.4.2 Over North America

The contributions of biogenic and anthropogenic emissions to domain-wide averaged concentrations of O_3, PM_{10}, SOA, isoprene SOA and terpene SOA over North America are shown in Table B.10.

Removing biogenic emissions reduces O_3 concentrations by about 20% on average, whereas removing anthropogenic emissions reduces O_3 concentrations by 49%. This result is consistent with the seminal work of *Pun et al.* [2002b] who estimated the contribution of biogenic emissions to O_3 to be less than 23% in Nashville/TN and the northeastern U.S., with a contribution between 22% and 34% in urban areas. The contribution of biogenic emissions to O_3 is also observed to be regionally more important around urban areas, especially in the northeastern U.S. and in California near Los Angeles, as shown in Figure B.12, which depicts the relative

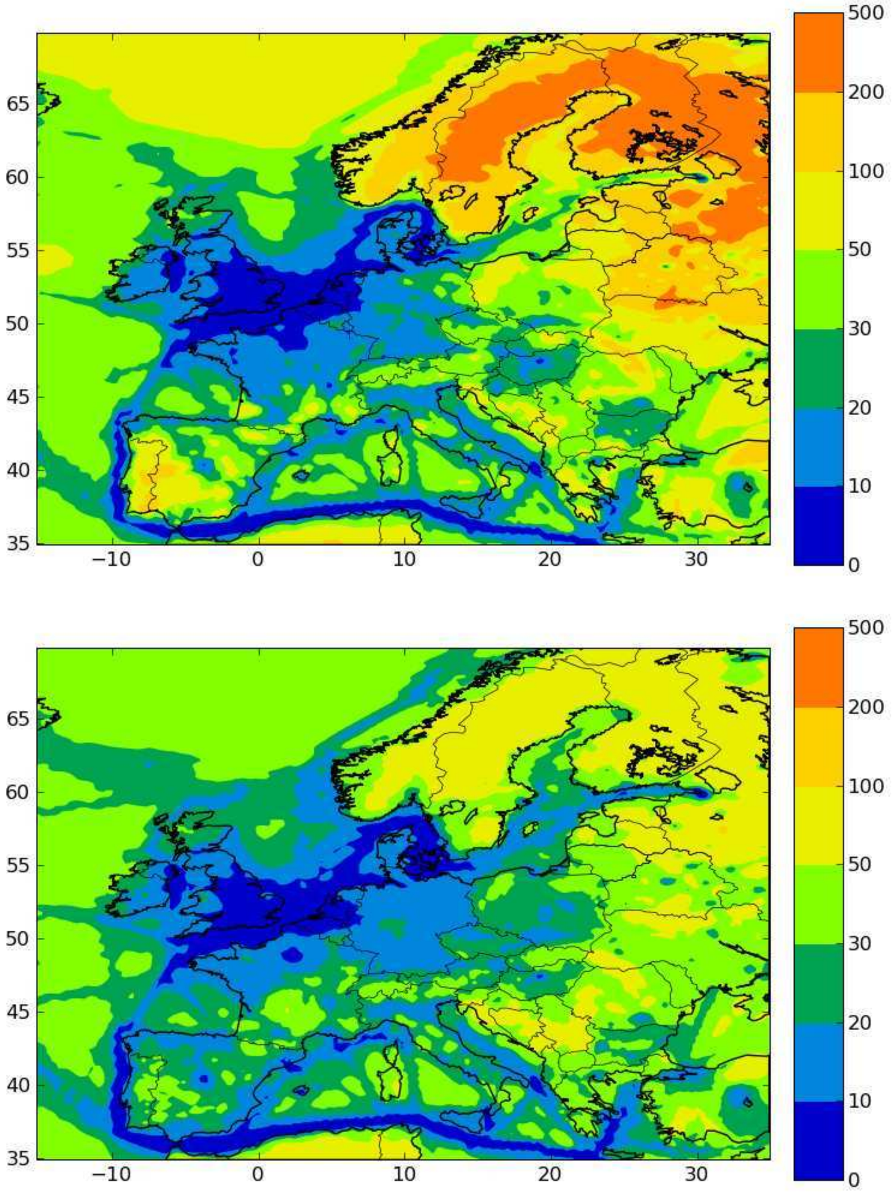

Figure B.7: Ratio of surface VOC over NO_x concentrations averaged over July and August computed using Pol 3 (Simpson biogenic emission scheme, upper panel) and Pol 4 (MEGAN biogenic emission scheme, lower panel).

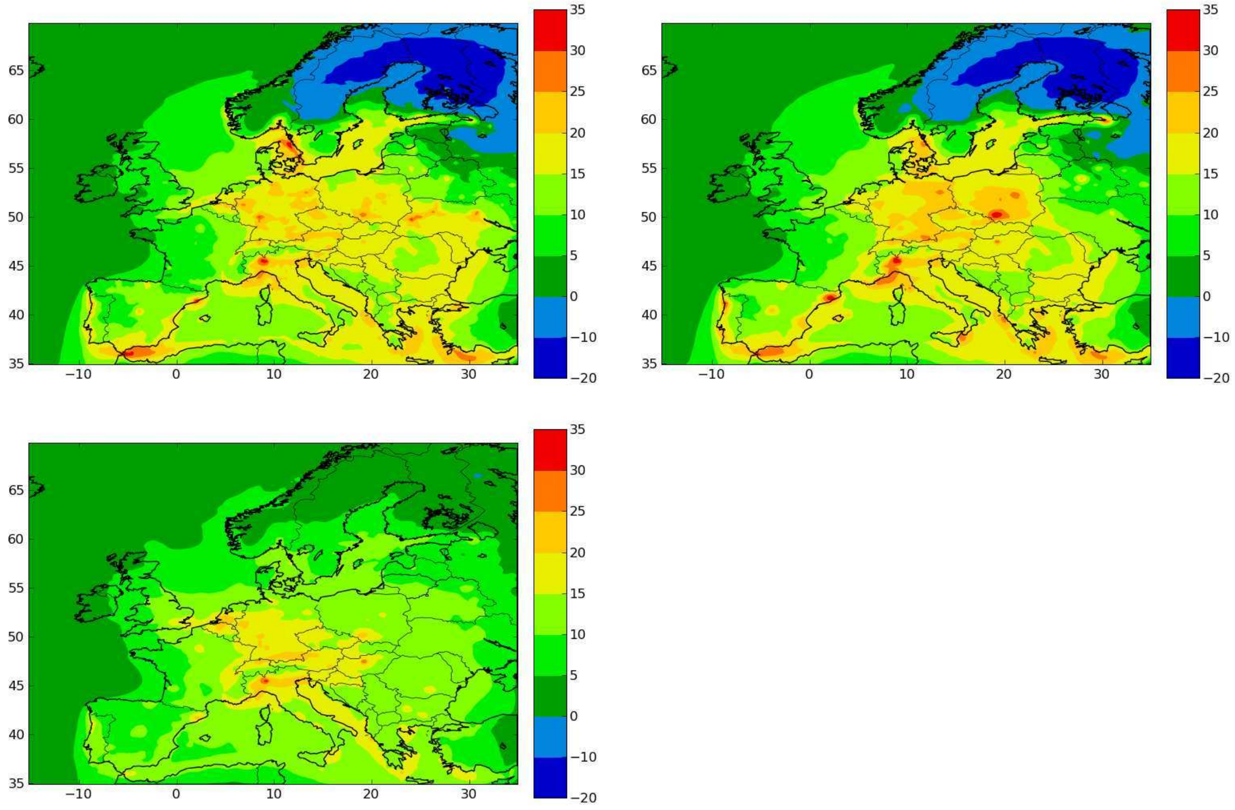

Figure B.8: Relative difference between surface O_3 concentrations (in %) averaged over July and August computed with and without biogenic emissions, using Pol 2 (upper panel), Pol 3 (middle panel) and Pol 4 (lower panel).

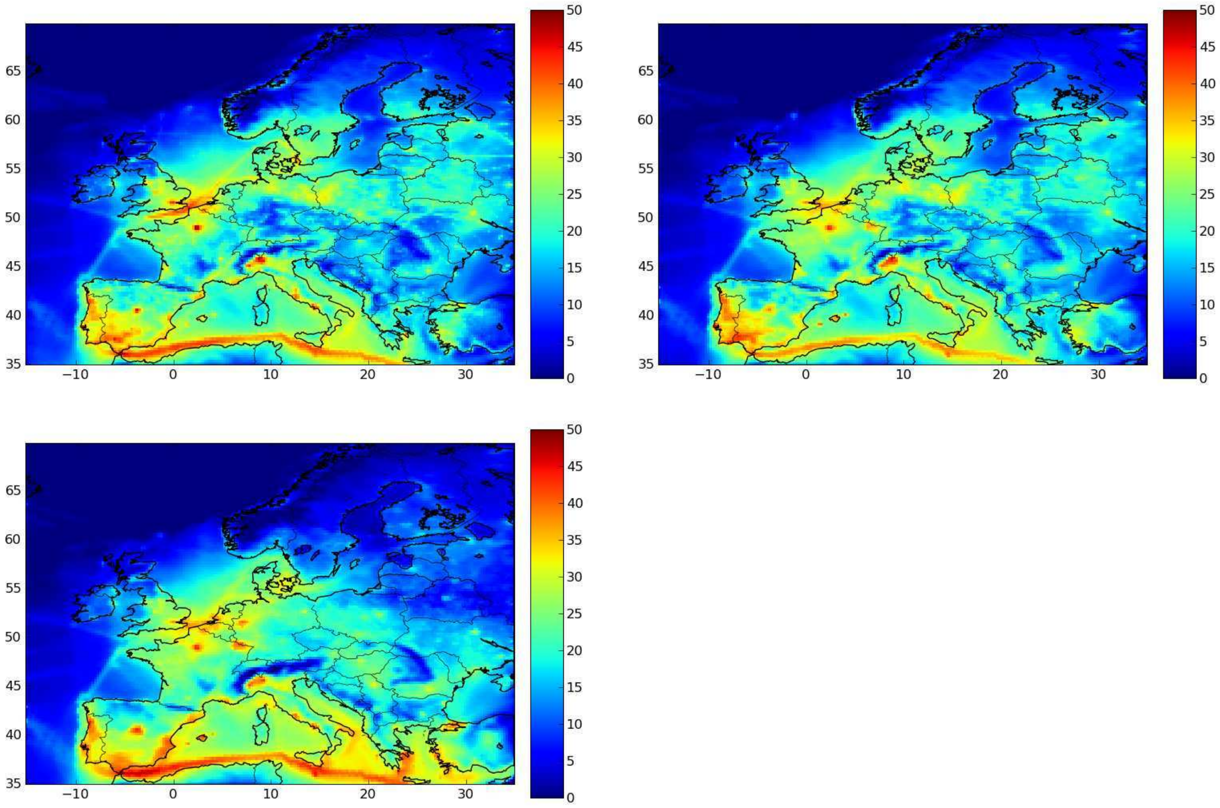

Figure B.9: Relative difference between surface SOA concentrations (in %) averaged over July and August computed with and without anthropogenic emissions, using Pol 2 (upper panel), Pol 3 (middle panel) and Pol 4 (lower panel).

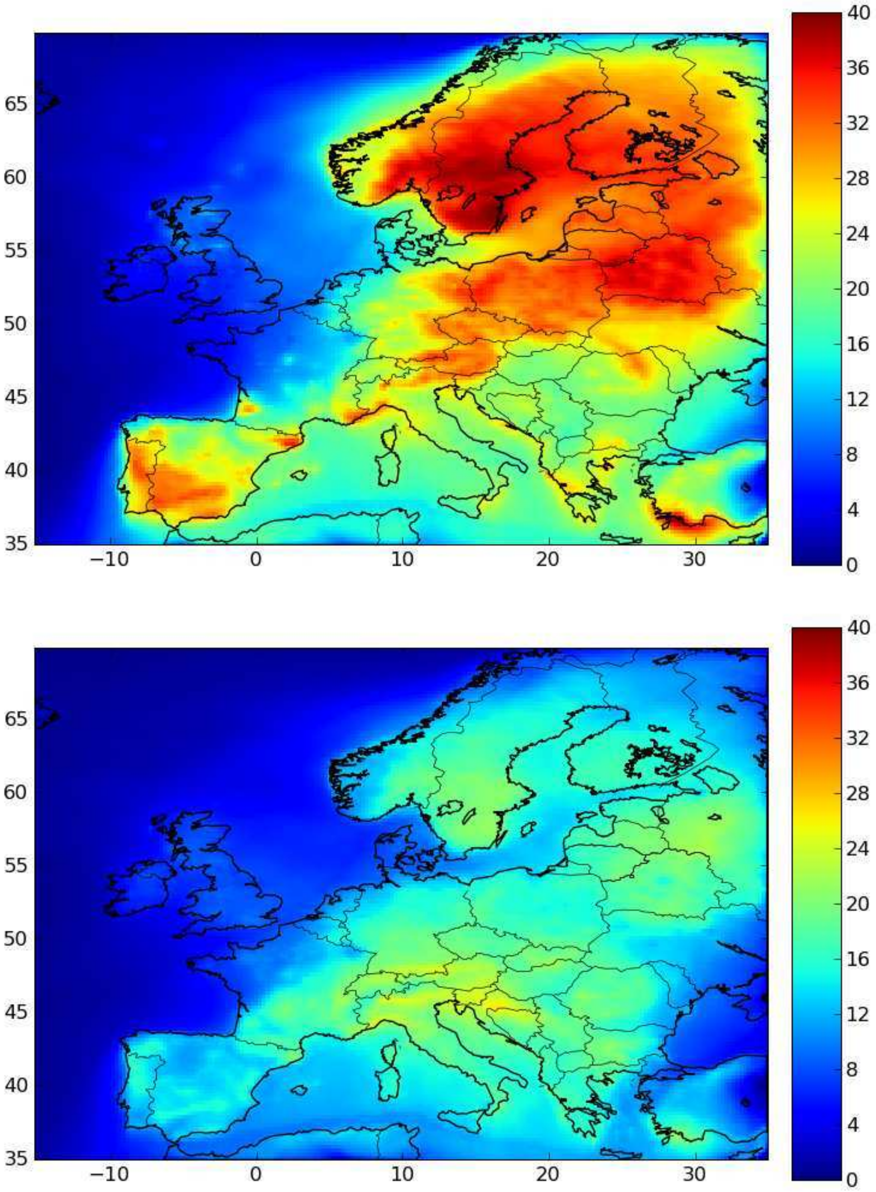

Figure B.10: Relative difference averaged over July and August between surface anthropogenic SOA concentrations (in %) computed with and without biogenic emissions, using Pol 3 (upper panel) and Pol 4 (lower panel).

		Base case	No biogenic emissions	No anthropogenic emissions
O_3	Pol 2	61.9	55.2 (-11%)	36.6 (-41%)
	Pol 3	63.0	56.0 (-11%)	36.6 (-42%)
	Pol 4	61.9	56.0 (-10%)	38.2 (-38%)
PM_{10}	Pol 2	9.4	7.4 (-21%)	4.4 (-54%)
	Pol 3	9.7	7.6 (-21%)	4.4 (-55%)
	Pol 4	8.3	7.6 (-8%)	3.2 (-62%)
SOA	Pol 2	2.6	0.3 (-87%)	2.1 (-16%)
	Pol 3	2.6	0.3 (-88%)	2.1 (-16%)
	Pol 4	1.1	0.3 (-72%)	1.0 (-15%)
Isoprene SOA	Pol 2	0.6	0.0 (-94%)	0.4 (-24%)
	Pol 3	0.6	0.0 (-94%)	0.4 (-24%)
	Pol 4	0.2	0.0 (-84%)	0.2 (-22%)
Terpene SOA	Pol 2	1.7	0.1 (-93%)	1.5 (-10%)
	Pol 3	1.7	0.1 (-93%)	1.5 (-10%)
	Pol 4	0.7	0.1 (-84%)	0.7 (-6%)

Table B.9: Contribution of biogenic emissions to concentration of surface O_3, PM_{10}, SOA, isoprene SOA and terpene SOA averaged over Europe and over July and August (concentrations are in μg m^{-3}). Sea-salt (sodium and chloride) are not included in PM_{10}.

difference of hourly O_3 concentrations averaged over July and August when all emissions are taken into account and when biogenic emissions are removed. O_3 is found to be 26% and 38% lower in the northeastern U.S. (near Washington DC and New Jersey) and California near Los Angeles, respectively (see rectangles in Figure B.12). A high decrease in O_3 concentration is observed over large cities close to high-VOC emission areas when biogenic emissions are removed. As for Europe, the regions where the impact of biogenic emissions is high correspond to those where the VOC/NO_x concentration ratio is low compared to surroundings (large urban centers), as seen by comparing Figures B.11 and B.12.

PM_{10} is not much impacted by biogenic emissions: the concentration decreases by 14% on average when biogenic emissions are removed, whereas it decreases by as much as 50% when anthropogenic emissions are removed. However, biogenic emissions largely contribute to secondary organic aerosols (SOA). If they are not considered, SOA decrease by 90% on average over the domain. In comparison, removing anthropogenic emissions only reduces SOA by 10% on average. SOA are composed mostly of isoprene (23%) and terpene (67%) oxidation products. Isoprene and terpene SOA are reduced by 16% and 7%, respectively, on average over the domain when anthropogenic emissions are removed. However, locally, the reduction may be larger. Large cities, such as Los Angeles, Atlanta, Birmingham, Saint Louis, Washington DC, Chicago and Minneapolis may clearly be identified by looking at the map of the relative difference of SOA concentrations when all emissions are considered and when anthropogenic emissions are removed (Figure B.13). Removing anthropogenic emissions leads to a large decrease of biogenic SOA near these large cities. A decrease as large as 60% is observed locally around cities such as Los Angeles and Houston. A decrease on the order of 60% around cities is consistent with the results of *Carlton et al.* [2010b].

As for the European study, removing biogenic emissions does not only affect the biogenic compounds of SOA, but also the anthropogenic ones. The relative impact of biogenic SOA on anthropogenic SOA may be as high as 60%, as shown in Figure B.14, which shows the relative difference of anthropogenic SOA when all emissions are taken into account and when biogenic

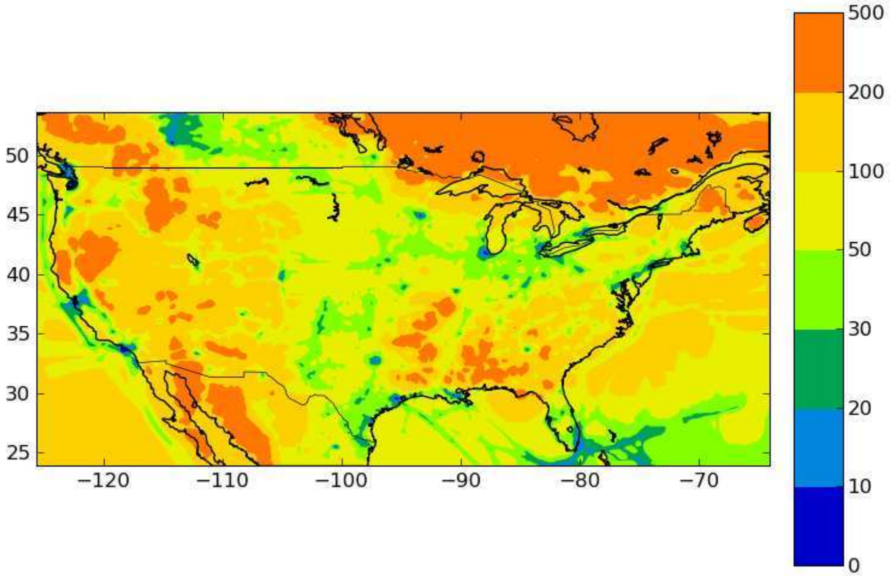

Figure B.11: Ratio of surface VOC over NO_x concentrations averaged over July and August.

emissions are ignored.

	Base case	No biogenic emissions	No anthropogenic emissions
O_3	64.5	51.5 (-20%)	33.2 (-49%)
PM_{10}	9.3	8.1 (-14%)	4.6 (-50%)
SOA	2.3	0.2 (-90%)	2.1 (-10%)
Isoprene SOA	0.5	0.0 (-93%)	0.4 (-16%)
Terpene SOA	1.6	0.1 (-94%)	1.5 (-7%)

Table B.10: Contribution of biogenic emissions to concentration of surface O_3, PM_{10}, SOA, isoprene SOA and terpene SOA averaged over North America and over July and August (concentrations are in μg m^{-3}). Sea-salt (sodium and chloride) are not included in PM_{10}.

B.5 Conclusion

Over both Europe and NA, Polyphemus performances are satisfactory for O_3 and PM with respect to criteria used in the literature, as well as in comparison to other AQMEII models. Over Europe, the simulation with biomass burning emissions over-estimate $PM_{2.5}$ over Portugal, probably because the fire emission height is not accurately modeled.

The impact of biogenic emissions is higher on average over NA than over Europe for O_3, and it is commensurate for SOA. Locally, the impacts of biogenic emissions tends to be higher in NA than in Europe because of the presence in NA of large urban centers surrounded by regions of high biogenic emissions.

Both over Europe and NA, the impact of biogenic emissions on O_3 (-10% to -20%) is lower than the impact of anthropogenic emissions (-38% to -49%). The regions where the impact of biogenic emissions is high correspond to those where the VOC/NO_x ratio is low compared

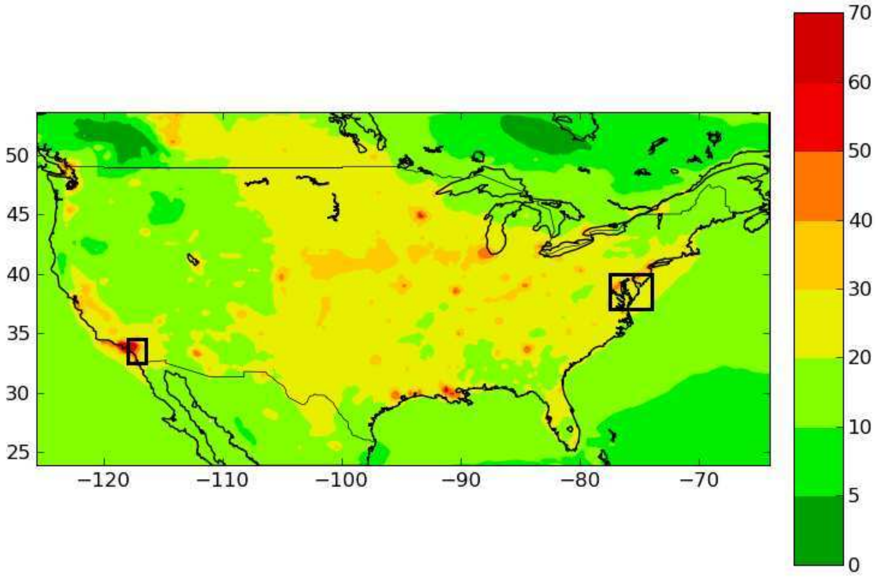

Figure B.12: Relative difference between surface O_3 concentrations (in %) averaged over July and August computed with and without biogenic emissions.

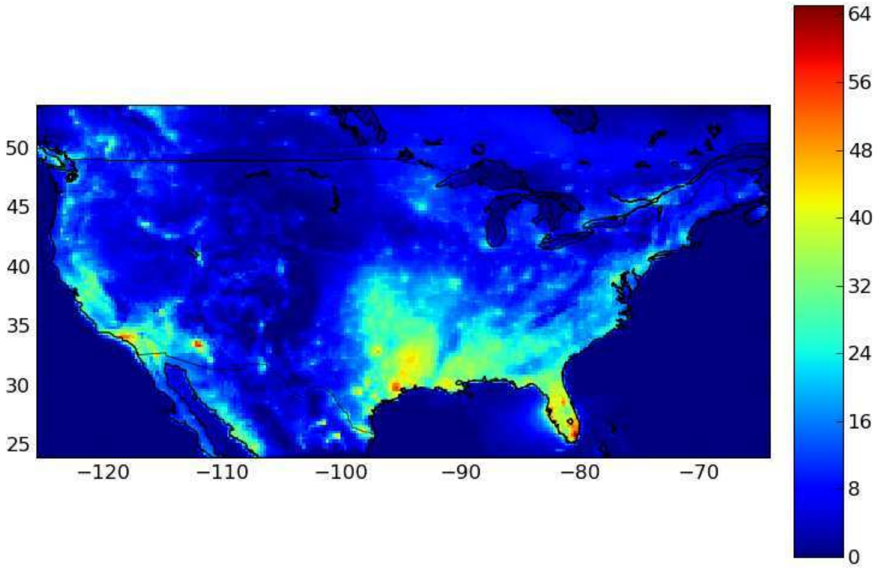

Figure B.13: Relative difference between surface SOA concentrations (in %) averaged over July and August computed with and without anthropogenic emissions.

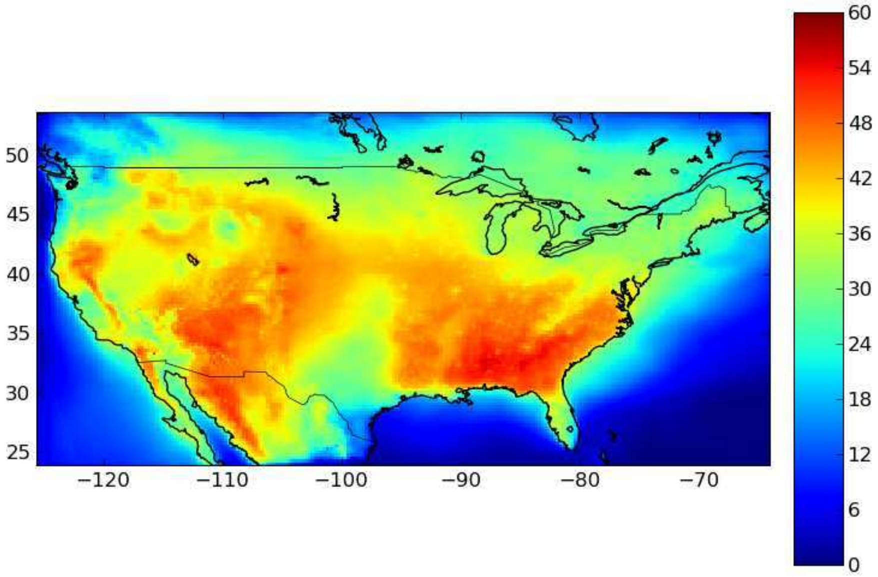

Figure B.14: Relative difference between surface anthropogenic SOA concentrations (in %) averaged over July and August computed with and without biogenic emissions.

to surroundings. For SOA, which are mostly biogenics, the impact of biogenic emissions (72% to 90%) is much greater than the impact of anthropogenic emissions (10% to 16%). However, locally, the impact of anthropogenic emissions may be high (up to 50%, both in NA and Europe), stressing the fact that even biogenic SOA may be controlled for a large part by controlling anthropogenic emissions. The biogenic SOA reduction when all anthropogenic emissions are eliminated varies depending on the chemical precursors: isoprene SOA is more reduced than terpene SOA because of differences in their volatility. Anthropogenic SOA are also impacted by biogenic emissions (absorbing organic mass for SOA), with a relative impact that can be as high as 40% locally. To accurately model SOA, it is, therefore, necessary to accurately model both biogenic and anthropogenic SOA.

Over Europe, for O_3 and SOA, the impact of biogenic emissions is lower in Pol 4 (which uses the MEGAN biogenic emission scheme) than in Pol 2 or Pol 3 (which use the Simpson biogenic emission scheme). The largest differences between the impacts simulated with Pol 4 compared to those simulated with Pol 2 and Pol 3 show that uncertainties in the biogenic emission schemes used here are larger than uncertainties in the two anthropogenic emission inventories.

B.6 Supplementary electronic materials

B.6.1 Model performance evaluation over Europe

The Polyphemus simulations are compared to observations for NO_2, SO_2, sulfate, ammonium and nitrate in Tables B.11, B.12, B.13, B.14 and B.15, respectively. Observational data at rural and suburban stations were extracted from the Ensemble system, except for sulfate, ammonium and nitrate, which are obtained from the EMEP databases.

NO_2 - Europe	Pol 1	Pol 2	Pol 3	Pol 4	AQMEII models		
					Min	Mean	Max
Number of stations	684	684	684	684	681	683.7	684
Mean obs	12.8	12.8	12.8	12.8	12.8	12.8	12.8
Mean sim	8.8	8.3	8.7	8.8	5.6	9.3	15.1
rmse	13.8	13.1	13.2	13.1	12.5	14.1	15.9
correlation	38.0%	41.3%	40.1%	40.4	20.7%	33.2%	42.4%
mfb	-40.9%	-44.3%	-38.4%	-36.2	-66.7%	-32.3%	-2.7%
mfe	77.7%	78.6%	77.1%	76.2%	67.6%	77.8%	90.9%

Table B.11: Comparisons to observations for surface NO_2 over Europe (concentrations and rmse are in μg m^{-3}).

SO_2 - Europe	Pol 1	Pol 2	Pol 3	Pol 4	AQMEII models		
					Min	Mean	Max
Number of stations	501	501	501	501	498	500.7	501
Mean obs	3.7	3.7	3.7	3.7	3.7	3.7	3.8
Mean sim	4.3	4.2	3.5	3.6	1.1	2.5	4.2
rmse	9.5	9.4	9.3	9.3	9.0	9.3	10.2
correlation	14.5%	14.0%	12.9%	12.9%	7.6%	16.0%	20.8%
mfb	19.6%	17.5%	1.7%	2.3%	-110.0%	-46.6%	-0.7%
mfe	79.2%	79.0%	78.5%	78.4%	74.3%	95.0%	127.4%

Table B.12: Comparisons to observations for surface SO_2 over Europe (concentrations and rmse are in μg m^{-3}).

PM_{10} sulfate - Europe	Pol 1	Pol 2	Pol 3	Pol 4
Number of stations	25	25	25	25
Mean obs	2.2	2.2	2.2	2.2
Mean sim	3.1	3.1	3.0	3.0
rmse	1.8	1.8	1.7	1.7
correlation	65.7%	65.4%	69.0%	68.6%
mfb	32.5%	31.6%	31.7%	32.9%
mfe	54.5%	54.3%	53.7%	53.8%

Table B.13: Comparisons to observations for surface $PM_{2.5}NO_3$ sulfate over Europe (concentrations and rmse are in μg m^{-3}).

$PM_{2.5}NO_3$ ammonium - Europe	Pol 1	Pol 2	Pol 3	Pol 4
Number of stations	7	7	7	7
Mean obs	0.8	0.8	0.8	0.8
Mean sim	1.7	1.7	1.9	1.9
rmse	1.4	1.3	1.6	1.6
correlation	42.7%	39.9%	40.1%	39.2%
mfb	79.1%	75.7%	83.7%	86.3%
mfe	92.9%	91.2%	97.9%	99.5%

Table B.14: Comparisons to observations for surface $PM_{2.5}NO_3$ ammonium over Europe (concentrations and rmse are in μg m^{-3}).

$PM_{2.5}NO_3$ nitrate - Europe	Pol 1	Pol 2	Pol 3	Pol 4
Number of stations	11	11	11	11
Mean obs	1.3	1.3	1.3	1.3
Mean sim	1.9	1.7	2.3	2.4
rmse	2.6	2.5	3.1	3.2
correlation	14.3%	13.9%	14.2%	12.6%
mfb	-13.1%	-25.2%	-3.0%	2.2%
mfe	108.2%	112.7%	113.2%	112.7%

Table B.15: Comparisons to observations for surface $PM_{2.5}NO_3$ nitrate over Europe (concentrations and rmse are in μg m^{-3}).

B.6.2 Model performance evaluation over NA

The Polyphemus simulation is compared to observations for NO_2, SO_2, elemental carbon of $PM_{2.5}$, organic mass of $PM_{2.5}$, sulfate of $PM_{2.5}$, ammonium of $PM_{2.5}$ and nitrate of $PM_{2.5}$ in Tables B.16, B.17, B.18, B.19, B.20, B.21 and B.22, respectively. Observational data at rural and suburban stations were extracted from the Ensemble system.

NO_2 - NA	Polyphemus	AQMEII models		
		Min	Mean	Max
Number of stations	315	315	315	315
Mean obs	8.2	8.2	8.2	8.2
Mean sim	8.4	3.0	9.7	17.8
rmse	10.0	8.3	11.6	19.0
correlation	43.1%	41.5%	46.9%	53.5%
mfb	-16.6%	-79.7%	-11.2%	53.2%
mfe	74.4%	67.7%	78.2%	93.4%

Table B.16: Comparisons to observations for surface NO_2 over NA (concentrations and rmse are in ppb). Six models are included in the AQMEII models used for the comparison.

SO_2 - NA	Polyphemus	AQMEII models		
		Min	Mean	Max
Number of stations	379	379	379	379
Mean obs	2.7	2.7	2.7	2.7
Mean sim	3.8	0.7	4.0	8.1
rmse	6.8	6.7	8.0	10.7
correlation	21.0%	12.5%	16.8%	22.3%
mfb	26.6%	-108.8%	0.2%	71.0%
mfe	81.9%	86.6%	94.1%	119.3%

Table B.17: Comparisons to observations for surface SO_2 over NA (concentrations and rmse are in ppb). Six models are included in the AQMEII models used for the comparison.

$PM_{2.5}EC$ - NA	Polyphemus	AQMEII models		
		Min	Mean	Max
Number of stations	262	262	262	262
Mean obs	0.4	0.4	0.4	0.4
Mean sim	0.5	0.2	0.5	1.1
rmse	0.5	0.5	0.7	1.3
correlation	51.5%	39.5%	46.5%	56.3%
mfb	23.6%	-70.5%	1.5%	80.6%
mfe	56.5%	50.4%	70.7%	90.4%

Table B.18: Comparisons to observations for surface $PM_{2.5}$ elemental carbon ($PM_{2.5}EC$) over NA (concentrations and rmse are in $\mu g\ m^{-3}$). Five models are included in the AQMEII models used for the comparison.

$PM_{2.5}OM$ - NA	Polyphemus	AQMEII models		
		Min	Mean	Max
Number of stations	265	265	265	265
Mean obs	2.6	2.6	2.6	2.6
Mean sim	3.5	0.4	4.7	11.5
rmse	3.1	2.4	5.6	12.7
correlation	24.6%	19.7%	37.1%	50.0%
mfb	41.5%	-132.4%	15.7%	120.3%
mfe	72.1%	56.2%	97.2%	136.7%

Table B.19: Comparisons to observations for surface $PM_{2.5}$ organic mass ($PM_{2.5}OM$) over NA (concentrations and rmse are in $\mu g\ m^{-3}$). Four models are included in the AQMEII models used for the comparison.

$PM_{2.5}SO_4$ - NA	Polyphemus	AQMEII models		
		Min	Mean	Max
Number of stations	113	113	113	113
Mean obs	4.2	4.2	4.2	4.2
Mean sim	4.0	3.4	4.1	4.8
rmse	3.2	1.9	2.5	2.9
correlation	55.7%	63.9%	75.3%	85.8%
mfb	-8.1%	-28.9%	-2.5%	14.6%
mfe	54.8%	32.7%	43.8%	53.0%

Table B.20: Comparisons to observations for surface $PM_{2.5}$ sulfate ($PM_{2.5}SO_4$) over NA (concentrations and rmse are in μg m^{-3}). Four models are included in the AQMEII models used for the comparison.

$PM_{2.5}NH_4$ - NA	Polyphemus	AQMEII models		
		Min	Mean	Max
Number of stations	112	112	112	112
Mean obs	1.4	1.4	1.4	1.4
Mean sim	1.9	1.2	1.4	1.5
rmse	1.4	0.8	1.0	1.2
correlation	50.4%	27.3%	61.5%	78.5%
mfb	28.8%	-4.9%	8.1%	16.7%
mfe	62.9%	41.0%	54.3%	77.7%

Table B.21: Comparisons to observations for surface $PM_{2.5}$ ammonium ($PM_{2.5}NH_4$) over NA (concentrations and rmse are in μg m^{-3}). Four models are included in the AQMEII models used for the comparison.

$PM_{2.5}NO_3$ - NA	Polyphemus	AQMEII models		
		Min	Mean	Max
Number of stations	264	264	264	264
Mean obs	0.4	0.4	0.4	0.4
Mean sim	0.9	0.3	0.4	0.7
rmse	1.8	0.7	0.8	0.8
correlation	35.3%	36.0%	38.0%	40.0%
mfb	-32.6%	-96.7%	-50.3%	60.9%
mfe	129.3%	90.5%	115.7%	129.9%

Table B.22: Comparisons to observations for surface $PM_{2.5}$ nitrate ($PM_{2.5}NO_3$) over NA (concentrations and rmse are in μg m^{-3}). Four models are included in the AQMEII models used for the comparison.

Appendix C

Modeling air pollution in Lebanon: evaluation at a suburban site in Beirut.

Cet appendice est constitué de

Waked, A., Seigneur, C., Couvidat, F., Kim, Y., Sartelet, K., Afif, C., Borbon, A., Formenti, P. and Sauvage, S. (2012). **Modeling air pollution in Lebanon : evaluation at a suburban site in Beirut.**. Soumis à *Atmos. Chem. Phys.*.

Sommaire

Abstract

Beirut, the capital city of Lebanon, which is located on the eastern shore of the Mediterranean basin, experiences high air pollution episodes. Annual average concentrations of coarse and fine particulate matter ($PM_{2.5}$) as well as nitrogen oxides (NO_x) often exceed the World Health Organization (WHO) guidelines. Therefore, improving air quality in this region is essential. The Polyphemus/Polair3D modeling system is used here to investigate air pollution episodes in Beirut during 2-18 July 2011. The modeling domain covers two nested grids of 1 and 5 km horizontal resolution over the greater Beirut and Lebanon, respectively. The anthropogenic emission inventory was developed earlier [*Waked et al.*, 2012b]. The Weather and Research Forecasting (WRF) model is used to generate the meteorological fields and the Model of Emissions of Gases and Aerosols from Nature (MEGAN) is used for biogenic emissions. The results of the study are compared to measurements from a field campaign conducted in the suburb of Beirut during 2-18 July 2011. The model reproduces satisfactorily the concentrations of most gaseous pollutants, the total mass of PM2.5 as well as PM2.5 elemental carbon (EC), organic carbon (OC), and sulfate.

C.1 Introduction

The Middle East region is characterized by a diverse landscape including elevated terrain, semi-arid and Saharan deserts, sea shores and vast plains. Covering fourteen Arab countries as well as Turkey and Iran, the region stretches from Egypt in the West to Iran in the East, Turkey in the North and the Arabian Peninsula in the South. Being an enclosed region, it experiences high pollution episodes, elevated particulate matter (PM) concentrations and major acid deposition problems [*Saliba et al.*, 2006]. Moreover, anthropogenic emissions are increasing rapidly over this region due to large industrialized areas, the absence of any efficient public transport system, dense traffic areas and high population densities [*ESCWA*, 2010; *Lelieveld et al.*, 2009]. In addition, steady winds originating from eastern Europe as well as intense solar radiation contribute to the formation of high levels of secondary pollutants and other reactive species [*Lelieveld et al.*, 2002; *Kouvarakis et al.*, 2000]. To date, few studies have been conducted to investigate air pollution in this region. *Lelieveld et al.* [2002, 2009]; *Smoydzin et al.* [2012] investigated ozone (O_3) pollution over the Middle East region and the Arabian Peninsula. The results showed that in the Arabian Peninsula, high levels of O_3 concentrations were observed especially in summer [*Liu et al.*, 2009a] due to the highly favorable weather conditions and high local air pollutant emissions [*Lelieveld et al.*, 2009]. In particular, nitrogen oxides (NO_x) concentrations in this area are exceptionally high [*Stavrakou et al.*, 2008]. As a result, air pollution in this region needs to be investigated, monitored, and reduced. Lebanon, a small developing country in the Middle East region, located on the eastern shore of the Mediterranean Sea, experiences high pollution episodes due to local emissions because of a growing population, especially in urban areas, the absence of any public transport system [*MoE*, 2005], steady winds from eastern Europe and Saharan dust storms from the desert [*Saliba et al.*, 2007]. Therefore, the country represents a good case study for investigating air pollution in the region. The few measurements conducted in Beirut, the capital city of Lebanon, revealed high levels of nitrogen dioxide (NO_2) with an annual average concentration of 66 $\mu g/m^3$ [*Afif et al.*, 2009] and high levels of particulate matter, PM_{10} and $PM_{2.5}$, with annual concentrations of 64 and 20 mug/m^3, respectively [*Massoud et al.*, 2011]. The levels exceed World Health Organization (WHO) guideline values of 40 mug/m^3 for NO_2 and 20 and 10 mug/m^3 for PM_{10} and $PM_{2.5}$, respectively. Although these measurements provide valuable information on air pollution, they are scarce and limited to a few areas. Therefore, the use of chemical-transport models (CTM) is essential for understanding the spatio-temporal distribution of gaseous and particulate pollutants in the region. Previous studies have focused on simulating the distribution of O_3 over this region using regional CTM. The EMAC chemistry general circulation model [*Roeckner et al.*, 2006] was used to investigate O_3 levels in the Persian gulf region [*Lelieveld et al.*, 2009] and a fully coupled on-line model (WRF-Chem version 3.3.1) [*Grell et al.*, 2005] was used for the Arabian Peninsula [*Smoydzin et al.*, 2012]. However, no modeling study has yet been conducted for Lebanon or its capital city Beirut. In this study, the WRF-ARW version 3.3 meteorological model [*Skamarock et al.*, 2008b] is used with the Polyphemus/Polair3D CTM [*Mallet et al.*, 2007; *Sartelet et al.*, 2007] to investigate air pollution in Beirut as well as in Lebanon from July 2 till July 18, 2011. WRF has been evaluated against observations in many regions [*Borge et al.*, 2008; *Carvalho et al.*, 2012; *Molders*, 2008] but, to our knowledge, has never been applied to Lebanon. The Polyphemus/Polair3D CTM has been evaluated over Europe [*Sartelet et al.*, 2007, 2012; *Couvidat et al.*, 2012a], Asia [*Sartelet et al.*, 2008], and North America [*Sartelet et al.*, 2012], but not in the Middle East region. This study aims to investigate air pollution in Beirut in July 2011 via meteorological and air quality modeling. The evaluation of WRF and Polyphemus/Polair3D in this region is essential prior to the use of such models for future air quality studies.

The methodology and the model configurations for WRF and Polyphemus/Polair3D are described in Section C.2. The evaluation results for the meteorological and chemical simulations against observations are presented and discussed in Sections C.3 and C.4, respectively. Conclusions are provided in Section C.5.

C.2 Method

C.2.1 Modeling domains

For meteorological modeling, three modeling domains were set on a latitude-longitude projection. A mother domain (D3) with 25 km horizontal resolution covering the Middle East region, as well as some parts of eastern Europe, northern Africa and the Mediterranean Sea, and two nested domains with 5 km resolution for Lebanon (D2) and 1 km resolution for Beirut and its suburbs (D1) were adopted. The two nested domains D1 and D2 are used for the air quality model simulations. A map of the modelind domain is shown in Figure C.1.

C.2.2 Episode selection and observational data set

The modeling study was conducted from July 2 till July 18, 2011. During this period, meteorological and air quality measurements were conducted at the Faculty of Sciences of the Saint Joseph University campus (USJ site) in the region of Mansourieh (33.86 N ; 35.56 E) distant by 6 km from the center of Beirut. Meteorological measurements included wind speed (anemometer), wind direction (weather vane), surface temperature (thermometer), relative humidity (hygrometer) and atmospheric pressure (barometer). Average temperatures in Beirut exceeded 28 °C and clear skies were dominant. No precipitation was recorded during this period. These weather conditions, as well as westerly and easterly winds coming from eastern Europe and Asia, respectively, favored oxidant and secondary organic aerosol (SOA) formation. Trace gases including carbon monoxide (CO), NO_x and O_3 were measured on-line on a 1-min basis using trace gas analyzers [*Michoud et al.*, 2012] while VOC were measured on a 1-hour basis using an on-line Thermal Desorption Gas Chromatography with a Flame Ionization Detector (TD-GC-FID) and on a 5-min basis using a Proton Transfer Reaction Mass Spectrometry (PTRMS). However only, the results obtained from the TD-GC-FID are used for the evaluation of modeled VOC. $PM_{2.5}$ samples were collected using a high-volume sampler (30 m3/h) on a 12-h basis. They were analyzed for OC and EC using the EUSAAR2 protocol [*Cavalli et al.*, 2010], for organic aerosols

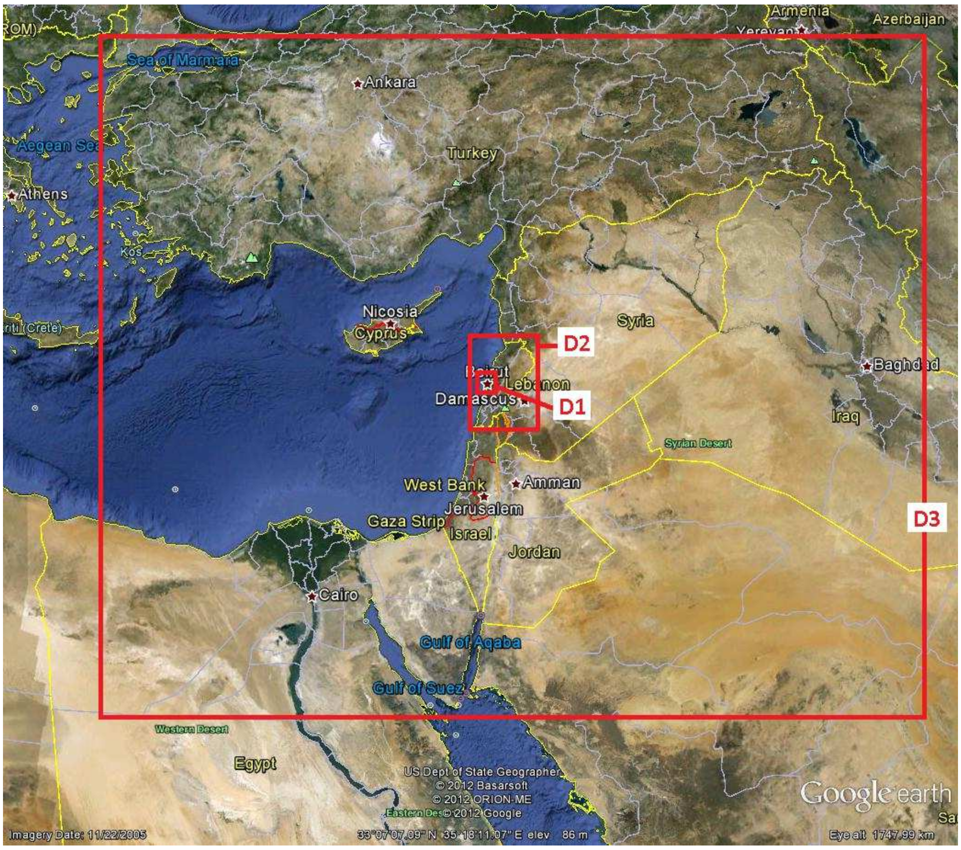

Figure C.1: The modeling domains D1, D2 and D3 used in this study.

using a gas chromatography coupled to a mass spectrometry (GC/MS) technique and for inorganic aerosols using an ion chromatography (IC) technique. The model simulation results are compared with those measurements to evaluate the ability of the model to reproduce major chemical components of photochemical air pollution in Beirut.

C.2.3 Meteorological modeling

WRF-ARW was used to generate the meteorological fields using a two-way nesting approach with a vertical structure of 24 layers covering the whole troposphere. Initial and boundary conditions were driven by the National Centers for Environmental Prediction (NCEP) global tropospheric analyses with 1°x 1°spatial resolution and 6 h temporal resolution. Topography and land use were interpolated from the United States Geological Survey (USGS) global land covers with the appropriate spatial resolution for each domain.

Physical parameterizations used in the model include the Kessler microphysics scheme [*Kessler*, 1969], the RRTM long-wave radiation scheme [*Mlawer et al.*, 1997], the Goddard NASA shortwave scheme [*Chou and Suarez*, 1994], the Grell-Devenyi ensemble cumulus parameterization scheme [*Grell and Devenyi*, 2002] and the Noah land surface model [*Chen et al.*, 2001]. Several physical options such as planetary boundary layer (PBL) dynamics, land surface model as well as several numerical options are available in WRF. A series of model experiments changing one option at a time was conducted to identify the simulation which provides the lowest biases and errors when compared to the observations. Because meteorological models tend to diverge after some integration time (typically two or three days), segmented simulations were also performed. Thus, several two-day restarted simulations were performed to complete an 18 day long simulation. For each simulation, the first 12-hour period was considered as a spin-up period for the model. Because the PBL has an important impact on the near surface wind field, two PBL schemes were tested: the Yunsai University (YSU) PBL scheme [*Hong et al.*, 2006], which is a non-local closure scheme [*Stull*, 1988] and the Mellor-Yamada-Nakanishi and Niino (MYNN) level 2.5 scheme [*Nakanishi and Niino*, 2004], which is a local TKE-based scheme. The MYNN scheme was developed to improve performance of its original Mellor-Yamada model [*Mellor and Yamada*, 1974]. Major differences between the two schemes (MYNN and MY) are the formulations of the mixing length scale and the method to determine unknown parameters. In addition, because the inner domain (D1) includes large urban areas, an urban surface model was used. WRF includes three urban surface models: the urban canopy model (UCM) [*Kusaka et al.*, 2001], which is a single layer model, and two multi-layer models, the Building Environmental Parameterization (BEP) [*Martilli et al.*, 2002] and the Building Energy Model (BEM) [*Salamanca et al.*, 2010]. In this study, UCM was used because it includes the anthropogenic heat release, which is not included in the multi-layer models [*Kim*, 2011]. Using UCM, several influential parameters such as the anthropogenic heat flux, road width, and building width and height values typical for Beirut were chosen, whereas for other parameters (urban ratio for a grid, surface albedo of roof, road and wall, thermal conductivity of roof, road and wall, etc.), the values provided by the WRF configuration file were adopted because of a lack of data. Therefore, a reference building width of 11 m [*CBDE*, 2004] and a road width of 8.5 m were adopted [*Chélala*, 2008]. A building height of 17.9 m was chosen [*Chélala*, 2008] while the mean annual anthropogenic heat flux for Beirut was estimated to be 17 W/m^2 [*IIASA*, 2012].

C.2.4 Air quality modeling

The Polyphemus/Polair3D CTM was used. Aerosol modeling was performed using SIREAM (Size Resolved Aerosol Model) [*Debry et al.*, 2007a] coupled to the Hydrophilic/Hydrophobic Organic (H^{2}O) model for SOA formation [*Couvidat et al.*, 2012a], ISORROPIA [*Nenes et al.*, 1998] for inorganic aerosols thermodynamics, and the CB05 chemical kinetic mechanism for gas-phase chemistry [*Yarwood et al.*, 2005; *Kim et al.*, 2009, 2011a]. SIREAM segregates the particle size distribution into sections and solves the general dynamic equation by splitting coagulation and condensation/evaporation-nucleation [*Debry et al.*, 2007a]. In H^{2}O, two anthropogenic and five biogenic SOA precursors species are used as surrogate precursors. In order to account for the fact that primary organic aerosols (POA) are semi-volatile organic compounds (SVOC), an SVOC/EI-POA (Emissions Inventory based POA) value of 5 was adopted following *Couvidat et al.* [2012a] to estimate SVOC emissions.

The USGS land cover was used. Initial and boundary conditions for the outer domain (D2) were extracted from the output of the Model for Ozone And Related chemical Tracers version 4 (MOZART-4; http://www.acd.ucar.edu/wrf-chem/mozart.shtml), which is an off-line global tropospheric CTM [*Emmons et al.*, 2010]. It is driven by NCEP/NCAR reanalysis meteorology and uses emissions based on a database of surface emissions of ozone precursors (POET), Regional Emission Inventory in Asia (REAS) and Global Fire Emissions Database (GEFD2). The results are at 2.8°x 2.8°horizontal resolution for 28 vertical levels. It should be noted that a pre-simulation was performed for the D1 (June 24 till July 2) and D2 (June 15 till July 2) domains to eliminate the effect of initial conditions. Outputs from the meteorological model (WRF-ARW) were used to compute vertical diffusion with the *Troen and Mahrt* [1986] and *Louis* [1979] parameterizations within the PBL. For horizontal diffusion, the CMAQ parameterization was used [*Byun and Schere*, 2009]. Gas and particle deposition as well as sea-salt emissions were pre-processed using relevant meteorological variables. Biogenic emissions were calculated using the Model of Emissions of Gases and Aerosols from Nature [*Guenther et al.*, 2006]. This model, which is designed for global and regional emission modeling, has a global

Table C.1: Numerical options and physical parameterizations considered.

Options	M1	M2	M3	M4	M5
UCM	no	yes	yes	no	no
PBL	YSU	YSU	MYNN	MYNN	YSU
Continuous simulations	yes	yes	yes	yes	no*

*Restarts every two days.

coverage with a 1 km x 1 km resolution.

For anthropogenic emissions, a spatially-resolved and temporally-allocated emission inventory was developed for Lebanon as well as for Beirut and its suburbs in a previous study [*Waked et al.*, 2012b]. This emission inventory is used here. Emissions were spatially allocated using a resolution of 5 km over Lebanon and a resolution of 1 km over Beirut. The inventory includes the emissions of CO, NO_x, sulfur dioxide (SO_2), VOC, ammonia (NH_3), PM_{10}, and $PM_{2.5}$. A wide variety of emission sources including road transport, maritime shipping, aviation, energy production, residential and commercial activities, industrial processes, agriculture, and solvent use are included in this inventory. A bottom-up methodology was used for the major contributing sources such as road transport, cement industries and power plant energy production. For other sources, a top-down approach was adopted. Spatial allocation was performed using population density maps, land cover and road network as well as traffic count data and surveys in many regions [*Waked and Afif*, 2012]. Temporal profiles were allocated with monthly, daily, and diurnal resolutions for all sources. The inventory was developed for a base year of 2010.

C.3 Meteorological simulations

C.3.1 Model simulation configurations

The results obtained from WRF were evaluated with meteorological data collected at the USJ site. Reliable meteorological data at other locations were not available within the D1 and D2 domains, thereby preventing a more complete model performance evaluation. Different simulations from M1 to M5 (Table C.1) were performed in order to select the meteorological simulation which has the lowest biases and errors when compared to observations.

For physical parameterizations, the YSU PBL scheme (simulation M2) and the MYNN scheme (simulation M3) were tested with the use of UCM. In addition, two simulations (M1 and M4) with the YSU and MYNN schemes, respectively, were performed without the use of UCM. To test numerical options, a simulation (M5) was performed using segmented simulations with two-day restarts to assess whether the model tends to diverge significantly after 2 days of simulation.

C.3.2 Results

To evaluate a model, several approaches can be used [*Gilliam et al.*, 2006]. Here, we compare model simulation results to measurements at one site using model performance statistical indicators that include the root mean square error (RMSE), mean fractional bias (MFB), mean fractional error (MFE), normalized mean bias (NMB), normalized mean error (NME), and the correlation coefficient (see Appendix C.6). The results of the statistical evaluation for wind speed and wind direction at 10 m above ground level (agl), surface temperature, relative humidity, and pressure at 2 m agl are presented in Table C.2 for the five simulations tested. Overall, the model is able to reproduce local wind speed, surface air temperature, and pressure with correlations greater than 0.74 (simulation M1). For wind direction and relative humidity, lower correlations (0.2 - 0.4) are obtained. Wind speed and wind direction have values of MFB and NMB in the range of 20 to 60 %. For surface temperature, relative humidity, and pressure, the statistical biases indicate a low over-prediction of 1 to 10 %. Accordingly, RMSE reported values for surface temperature (1.54 °C) and wind speed (1.34 m/s) are low, those of relative humidity (13 %) and pressure (14 hPa) are moderate, and that of wind direction is high (92°, simulation M1). Thus, model predictions of wind direction are the worst among the five variables. Other studies have shown RMSE values for surface temperature of 2.8 °C in Alaska [*Molders*, 2008], 3.46 °C in the southern U.S. [*Zhang et al.*, 2006], and 2.82 °C in Paris [*Kim*, 2011]. For wind speed, these values were 3 m/s in Portugal [*Carvalho et al.*, 2012], 1.62 m/s in the southern U.S. [*Zhang et al.*, 2006], and 1.93 m/s in Paris [*Kim*, 2011]. For wind direction, RMSE values of 92°are comparable to the value obtained in the southern U.S. (97°, *Zhang et al.* [2006]), but greater than the value obtained in Portugal (52°, *Carvalho et al.* [2012]). Therefore, this meteorological simulation shows satisfactory performance when compared to other similar studies.

C.3.3 Numerical options

The evaluation of segmented simulations is reported in this section because grid nudging of the NCEP initial and boundary conditions was used in all simulations. Comparison between simulation M5 (segmented simulations with two-day restarts) and the other simulations (M1-M4) showed better correlations for all the variables for the long simulations without segmentation, especially for wind components where M5 gives correlations of 0.55 and 0.23 for wind speed and wind direction respectively, compared to values of 0.74 and 0.38 obtained from a long simulation without segmentation such as M1. For other variables, differences between simulations are not significant. RMSE and other statistical indicator values are comparable between M5 and the continuous simulations. This leads to the conclusion that the model does not diverge significantly after some integration time, which results in part from the small size of the D1 domain and its two-way nesting to greater domains. On the other hand, there is considerable uncertainty in the initial conditions, which are generated every two days in the non-continuous simulations because these initial conditions are provided with a spatial resolution of 100 km to be used in a simulation for Beirut with a spatial resolution of 1 km, thereby leading to biases and errors that are higher than those of a continuous simulation.

C.3.4 Physical parameterizations

The MYNN PBL scheme used with UCM (simulation M3) was found to produce the best statistical results for all the variables. Accordingly, this physical option influences wind speed, surface temperature, relative humidity, and pressure. Using this option leads to the best correlations among all the simulations for all variables except for wind speed. The correlations are 0.63, 0.39, 0.91, 0.31, and 0.97 for wind speed, wind direction, surface temperature, relative humidity, and pressure. For MFB, MFE, NMB and NME, no significant differences are observed among these simulations (M1-M4). In summary, M1 with the YSU scheme gives the best results for wind speed and M3 with the MYNN scheme and UCM gives the best results for wind direction and relative humidity.

C.3.5 Best configuration

Temporal variations for wind speed, wind direction, surface temperature, and relative humidity of the two best selected simulations (M1 and M3) are shown from July 2 0h00 till July 17 0h00, 2011 in Figure C.2 because after July 17 0h00, no observations were recorded. The model reproduces wind direction better from July 6 till July 10 in both simulations while from July 2 till July 6 and from July 12 till July 16, the model is not able to reproduce winds originating from the East. The model reproduces satisfactorily relative humidity for the selected period in simulations except on July 4, 5, 15 and 16 when the model over-predicts relative humidity. Surface temperature is better reproduced in simulation M3 than in simulation M1 which over-predicts surface temperature. Lastly, a comparable pattern is observed with lower values for wind speed in simulation M3 due to the use of UCM, which has an effect of decreasing wind speeds due to urbanization. In summary, the model performs better from July 6 till July 10 for all the variables.

Clearly, the PBL scheme influences wind speed, wind direction, and surface temperature [*Borge et al.*, 2008]. Temperature is best modeled with the MYNN scheme using UCM. This result agrees with that obtained by *Kim* [2011] in a simulation over Paris, France. Outside the center of the city, the effect of UCM on temperature is not significant and is compensated by the effect of the PBL scheme. For wind speed and wind direction, no significant variation is observed between M1 and M3. For relative humidity, a better correlation is obtained using the MYNN PBL scheme, and a lower non-significant correlation is obtained for wind speed. Overall, simulation M3 performs slightly better for most variables than simulation M1 particularly for temperature and humidity and we may consider that the correlation of 0.63 obtained for wind speed in simulation M3 is close to the correlation of 0.74 (systematic error of 18 %) obtained in simulation M1 while the correlation for relative humidity of 0.31 obtained in simulation M3 is significantly different from the value of 0.2 (systematic error of 43 %) obtained in simulation M1. In addition, surface air temperature and wind direction were slightly better modeled in simulation M3 in terms of temporal variation (Figure C.2) and NMB (Table C.2). Based on these considerations, the results obtained from simulation M3 are used for air quality modeling.

C.4 Air quality simulations

The results obtained from Polyphemus/Polair3D were evaluated against measurements of gaseous species (O_3, NO_2, VOC and CO) and $PM_{2.5}$ (total mass and major components) collected at the USJ site. Statistical indicators used for model evaluation include MFB, MFE, mean normalized bias (MNB), and mean normalized error (MNE) (see Appendix C.6).

C.4.1 Gaseous species

The base simulation conducted with the MOZART-4 boundary conditions (A1) led to O_3 concentrations within the D1 domain that were too high compared to the observations by nearly a factor of two (see Table C.3). Sensitivity simulations were conducted where emissions of NO_x (A2) and VOC (A3) were reduced by a factor of two; these simulations did not lead to satisfactory O_3 concentrations, in part because of the strong influence of the boundary conditions. A decrease of NO_x emissions leads to an increase in O_3 concentrations (A2) because the study area is saturated in NO_x. Moreover, NO_x concentrations are well reproduced by the model in the base simulation A1. VOC reductions are effective in reducing O_3 concentrations (A3) due to the fact that the area of the study is considered to be VOC-limited, having a VOC to NO_x ratio in the range of 3 to 5. However, the decrease in O_3 concentrations is insufficient to

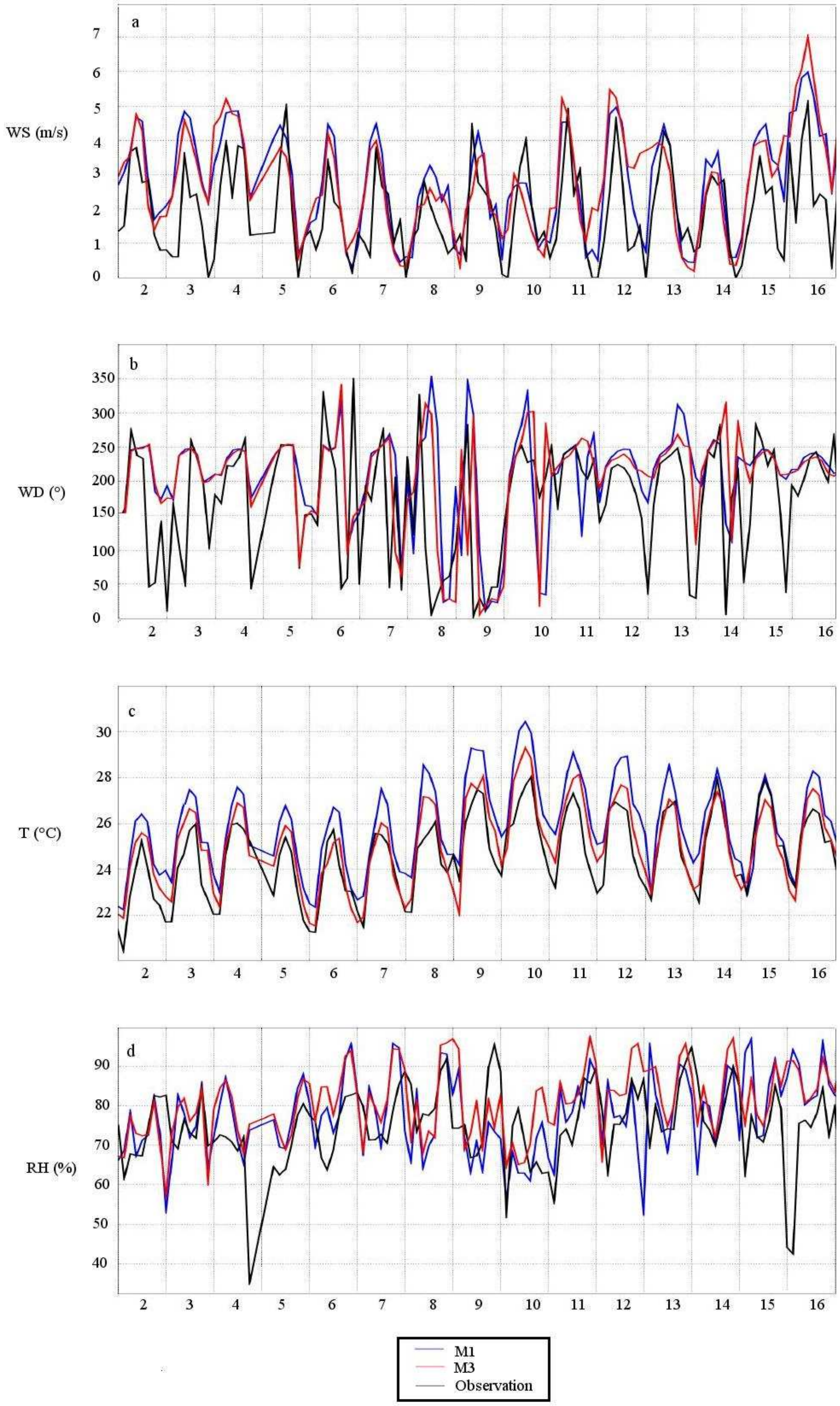

Figure C.2: Temporal variation of meteorological variables (observations and model simulations M1 and M3) from July 2 till July 17, 2011; (a) : wind speed (m/s); (b) : wind direction (°); (c) : air temperature (°C); (d) : relative humidity (%)).

Table C.2: Statistical performance evaluation of the meteorological variables for the WRF simulations.

Wind speed:

Simulation	RMSE (m/s)	MFB (%)	MFE (%)	NMB (%)	NME (%)	Correlation
M1	1.34	34	50	43	55	0.74
M2	1.63	39	55	56	66	0.72
M3	1.54	32	56	45	62	0.63
M4	1.33	26	50	33	53	0.63
M5	1.43	35	54	45	60	0.55

Wind direction:

Simulation	RMSE (°)	MFB (%)	MFE (%)	NMB (%)	NME (%)	Correlation
M1	92.06	23	41	21	35	0.38
M2	93.5	24	41	21	35	0.36
M3	94.23	20	41	19	34	0.39
M4	94.6	20	42	20	35	0.35
M5	132.48	35	62	44	61	0.23

Surface air temperature:

Simulation	RMSE (°C)	MFB (%)	MFE (%)	NMB (%)	NME (%)	Correlation
M1	1.54	5	5	5	5	0.9
M2	1.19	4	4	4	4	0.91
M3	0.88	2	3	2	3	0.91
M4	1.18	4	4	4	4	0.91
M5	1.47	3	5	3	5	0.84

Relative humidity:

Simulation	RMSE (%)	MFB (%)	MFE (%)	NMB (%)	NME (%)	Correlation
M1	12.78	4	12	4	12	0.20
M2	13.46	5	13	5	13	0.14
M3	12.65	8	13	8	13	0.31
M4	12.17	7	12	7	12	0.33
M5	11.62	5	11	5	11	0.21

Atmospheric pressure:

Simulation	RMSE (hPa)	MFB (%)	MFE (%)	NMB (%)	NME (%)	Correlation
M1	13.83	1	1	1	1	0.98
M2	13.85	1	1	1	1	0.98
M3	14.01	1	1	1	1	0.97
M4	14	1	1	1	1	0.97
M5	13.96	1	1	1	1	0.88

Table C.3: Results from simulations A1 to A4 from July 2 to July 18, 2011 at USJ..

	O_3 Mean concentration (μg/m^3)	CO Mean concentration (μg/m^3)	NO_x Mean concentration (μg/m^3)	$PM_{2.5}$ Mean concentration (μg/m^3)
Obs*	51	519	65	22
A1	95	703	69	21
A2	136	702	31	23
A3	82	702	72	20
A4	50	703	68	21

*Observations at USJ.

match the observed concentrations and VOC concentrations are already underestimated by the model in A1 by a factor of 2 to 3 (Table C.4). An increase of NO_x emissions and a decrease of VOC emissions could lead to satisfactory O_3 concentrations, but would lead to non-satisfactory results for VOC and NO_x modeled concentrations. Therefore, a sensitivity simulation was also conducted with the boundary O_3 concentrations halved (A4). That simulation led to reasonable agreement with the observations for all gaseous species. A comparison between simulation A1 and simulation A4 shows that modifying the O_3 boundary concentrations has negligible effect on CO, NO_x and $PM_{2.5}$ modeled concentrations. Although a recent evaluation of MOZART-4 with ozone study led to satisfactory results [*Emmons et al.*, 2010], a detailed evaluation with PBL O_3 data in the Middle East region has not been conducted because of a lack of data. Better characterization of PBL air pollution concentrations in that region is needed to obtain realistic O_3 boundary concentrations.

This strong influence of boundary conditions which leads to a significant overestimation of O_3 concentrations may be due to the fact that the MOZART-4 data used during this study have a horizontal resolution of 280 km and are used as boundary conditions for a domain D2 with a horizontal resolution of 5 km. It is possible that the use of an intermediate domain of 25 or 50 km horizontal resolution may decrease the uncertainties generated by the MOZART-4 data. However, an emission inventory for the Middle East region is not currently available and the use of an intermediate domain D3 for air quality simulation is therefore not feasible. In addition, we compared the results of this simulation to O_3 concentrations measured in the summer of 2004 in Beirut at an urban site [*Saliba et al.*, 2006] in order to assess the accuracy of the simulation at a different location than the one where the measurements are performed. Such comparisons are not true evaluations of the model because the years of the simulation and observations differ. Nevertheless, such comparisons may point to some possible biases in the air quality simulation if the differences cannot be justified. The results show a modeled value of 1585 μg/m^3 for CO in both simulations A1 and A4 compared to a measured value of 1213 μg/m^3. For PM_{10}, a value of 47 μg/m^3 was modeled in both simulations compared to a measured value of 44 μg/m^3. The modeled O_3 concentrations are 54 μg/m^3 in simulation A1 and 32 μg/m^3 in simulation A4, compared to a measured value of 34 μg/m^3. Clearly, the results obtained from this evaluation show that simulation A4 with modified O_3 boundary conditions leads to better results for O_3 concentrations and has negligible effect on other pollutants. Therefore, simulation A4 is used below.

Average modeled surface concentrations (over both land and sea) of O_3, NO_2, and CO from July 2 to 18 are 50, 49 and 700 μg/m^3 in the inner domain (D1) and 72, 10 and 240 μg/m^3 in the outer domain (D2), respectively. The modeled surface spatial distributions of O_3 and

Table C.4: Statistical performance evaluation for O_3, NO_2, NO_x, CO and some VOC at USJ..

Species	Obs[a]	Mod[b]	MFB	MFE	MNB	MNE
O_3 [c]	51	50	-17 %	33 %	-9 %	33 %
NO_x	65	69	27 %	118 %	74 %	108 %
NO_2	54	54	16 %	105 %	42 %	76 %
CO	519	703	20 %	41 %	55 %	73 %
TOL	19[d]	7[e]	-96 %	97 %	-61 %	62 %
XYL	17[f]	8[g]	-87 %	89 %	-55 %	58 %
α-Pinene	0.05	0.1[h]	37 %	97 %	261 %	301 %
Isoprene	0.62	0.4	-94 %	122 %	-14 %	109 %

a) Observed mean concentrations ($\mu g/m^3$).

b) Modeled mean concentrations ($\mu g/m^3$).

c) A threshold value of 80 $\mu g/m^3$ was used for observations.

d) The “TOL“ measured species include toluene, ethylbenzene, butylbenzene, isopropylbenzene and propylbenzene.

e) The ”TOL” modeled species includes also other minor monosubstituted aromatics.

f) The “XYL“ measured species includes xylene, trimethylbenzenze and ethyltoluene.

g) The ”XYL” modeled species includes also other minor polysubstituted aromatics.

h) The “α-pinene“ modeled species includes α-pinene and sabinene.

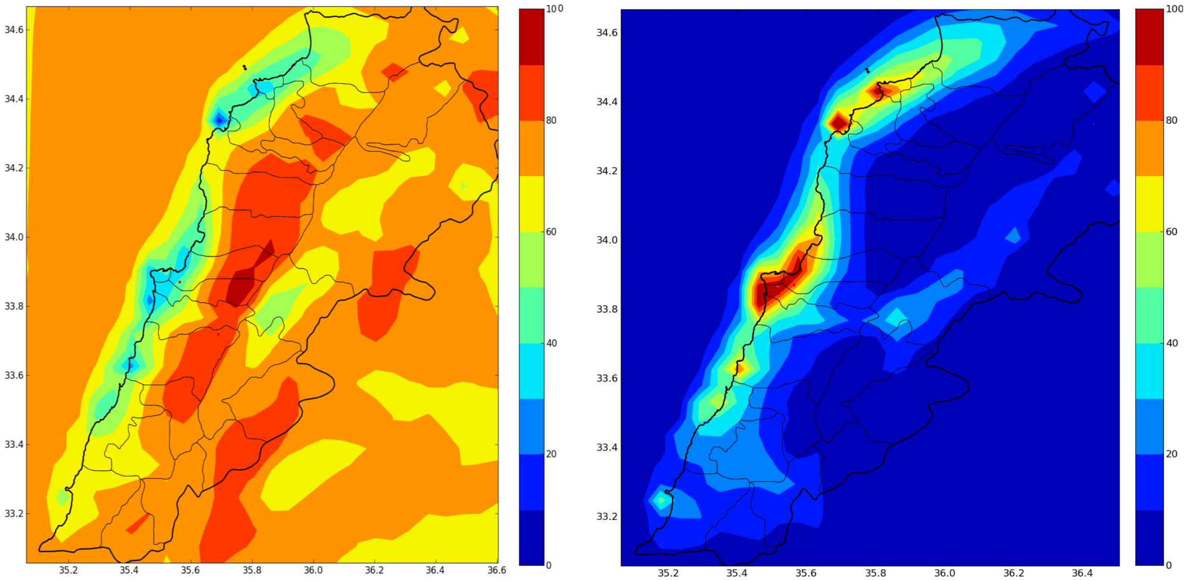

Figure C.3: Modeled average O_3 concentrations (left) and NO_2 concentrations (right) in $\mu g/m^3$ for the outer domain D2 (T = Tripoli ; C = Chekka ; B = Beirut ; J = Jieh).

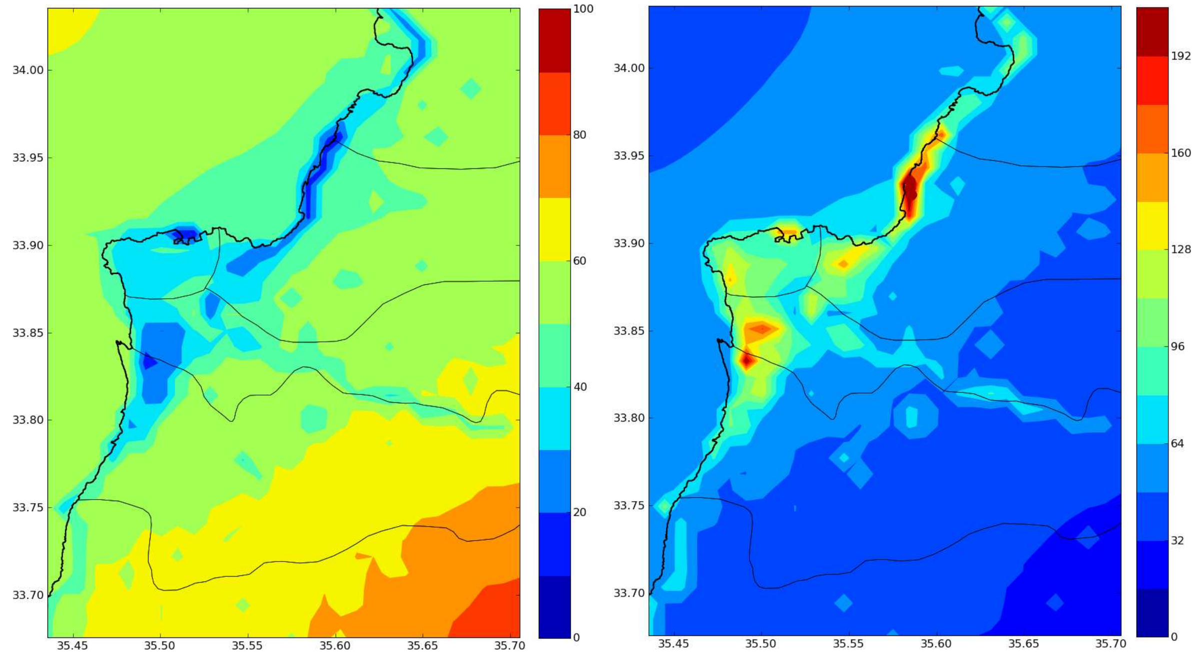

Figure C.4: Modeled average O_3 concentrations (left) and NO_2 concentrations (right) in $\mu g/m^3$ for the inner domain D1.

NO_2 concentrations for D2 and D1 (Figures C.3 and C.4) show lower O_3 concentrations where most NO_x emissions from industries, harbors and road traffic occur and higher values in the mountains. Accordingly, higher concentrations of NO_2 are modeled near the coast in Beirut and its suburbs, in the cities of Tripoli and Chekka in the north and Jieh in the south. Major sources in those areas include dense traffic in urban areas and on highways along the coast, in particular in Beirut and Tripoli, the Zouk power plant located on the coast north of Beirut, the Jieh power plant and the cement plants located in the city of Chekka. Other emissions are generated from the harbors in Beirut and Tripoli and from the international airport located on the coast south of Beirut. Higher O_3 concentrations modeled in the mountains (east of the domain) might be related to a higher VOC/NO_x ratio (Figure C.5), which is more favorable to O_3 formation.

To evaluate the model concentration results at the USJ site, different statistical metrics were calculated for the July 2-18 period, as shown in Table C.4. The model reproduces satisfactorily O_3 concentrations (bias in the range of 9 to 17 %). MNB and MNE values for O_3 of -9 % and 33 %, respectively, are within suggested performance criteria [*Russell and Dennis*, 2000] of 5-15 % for MNB and 30-35 % for MNE. The mean NO_2 concentration is well reproduced by the model but the hourly concentrations show a positive bias. For NO_2, the MNB of 42 % is comparable to the reported value of 35 % obtained during a simulation in the North Sea coastal region in Europe in July 2001 [*Matthias et al.*, 2008] and to the day-time and nigh-time values of -19 % and 31 % reported in Mexico City during the MCMA-2006/MILAGRO field campaign [*Zhang et al.*, 2009]. In addition, a MNB of 74 % for NO_x calculated during this study is in better agreement with observations than the reported value of 101 % for a simulation over Nashville, U.S.A, in July 1999 using the CMAQ model [*Bailey et al.*, 2007]. CO concentrations show an over-prediction by the model on the order of 30 % on average. These results are comparable to those of other studies conducted in Europe, Mexico and the U.S.A [*Matthias et al.*, 2008; *Zhang et al.*, 2009; *Bailey et al.*, 2007]. Biogenic VOC concentrations are small (< 1 $\mu g/m^3$) for both observations and simulations; they show an over-prediction of α-pinene by the model by a factor of two and an under-prediction of isoprene on the order of 30 % on average. However, the α-

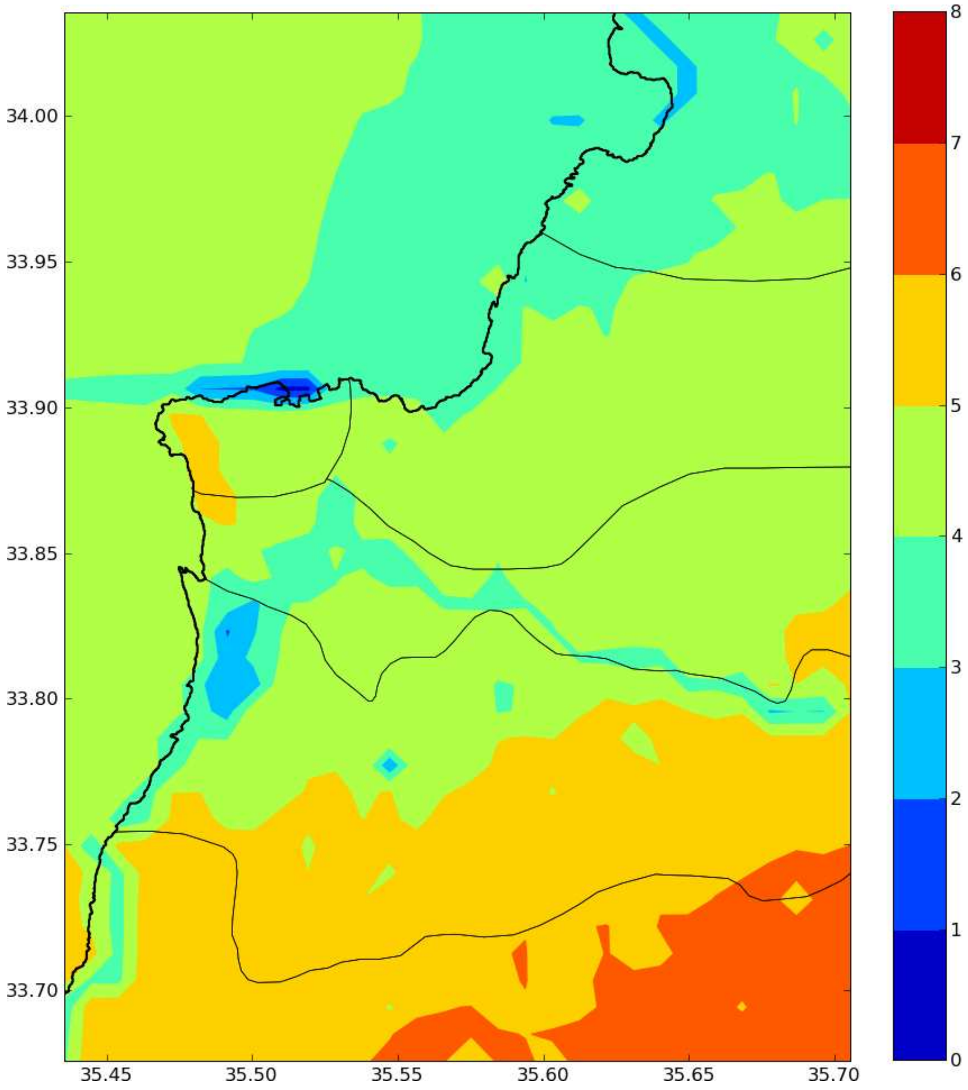

Figure C.5: Modeled average VOC/NO$_x$ ratio for the inner domain D1.

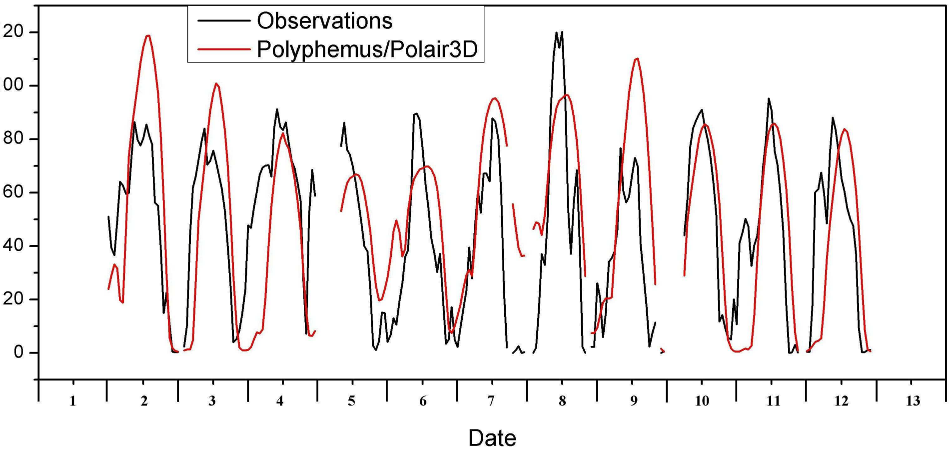

Figure C.6: Temporal variation of observed and modeled O$_3$ concentrations in μg/m^3 from July 2 till July 13, 2011.

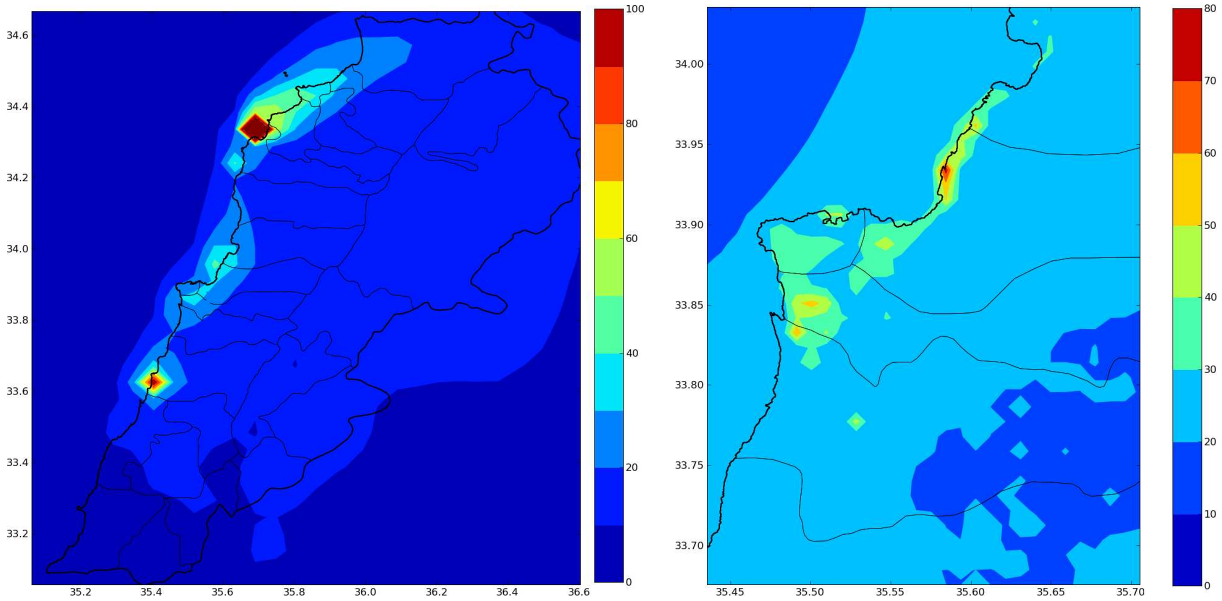

Figure C.7: Modeled average PM2.5 concentrations in μg/m^3 in Lebanon and in the city of Beirut (T = Tripoli ; C = Chekka ; B = Beirut ; S = Sibline).

pinene model species is a surrogate species that includes α-pinene and sabinene. The MNB value of -14 % reported for isoprene is comparable to the reported values of 14 % and -17 % during a simulation in July 2004 using the MOZART-4 CTM [*Horowitz et al.*, 2007]. Anthropogenic VOC such as toluene and xylene are under-estimated by the model by a factor of 2 to 3. Nevertheless, the results obtained are satisfactory because speciated VOC emissions are associated with large uncertainties and modeled VOC concentrations, which are typically not evaluated, are subject to significant bias. Indeed, monoterpene concentrations are underestimated by almost a factor of two in a simulation over the eastern U.S. using the MOZART-4 CTM [*Horowitz et al.*, 2007] due to a significant underestimation in terpene emissions while isoprene emission estimates can differ by more than a factor of 3 for specific times and locations when different driving variables are used in the emissions calculations [*Guenther et al.*, 2006]. Temporal variations for O_3 are shown in Figure C.6 from July 2 till July 13, 2011 (no measurements were recorded after July 13). The model reproduces satisfactorily the diurnal variation of O_3, with a peak O_3 concentration occurring between 12 pm and 1 pm for both observed and modeled values on most days. However, on some days (2, 3, and 9 July), a second O_3 peak is observed between 9 am and 10 am. This second peak is not reproduced by the model.

C.4.2 Particulate pollutants

Modeled $PM_{2.5}$ average surface concentrations (over both land and sea) from July 2 to 18, 2011 are 10 μg/m^3 for Lebanon (D2) and 19 μg/m^3 for Beirut and its suburbs (D1). The spatial distribution of $PM_{2.5}$ concentrations (Figure C.7) shows higher concentrations (> 40 μg/m^3) in the city of Beirut and its northern suburb, Chekka in the north and Sibline in the south. Dense on-road traffic, industrial sources (Zouk plant north of Beirut and the cement plants near the coast of Chekka and Sibline) and Beirut international airport located south of Beirut lead to significant air pollutant emissions [*Waked et al.*, 2012b]. Lower $PM_{2.5}$ concentrations in the eastern part of the domains (< 20 μg/m^3), are related to the fact that anthropogenic sources in these areas are less significant. This suggests that $PM_{2.5}$ concentrations are dominated by anthropogenic sources. Indeed, biogenic modeled SOA account for only 4 % of total $PM_{2.5}$

Table C.5: Statistical performance evaluation for $PM_{2.5}$, OC, EC and particulate sulfate, nitrate and ammonium at USJ

Species	Obs^{a}	Mod^{b}	RMSE(μg/m^{3})	MFB	MFE
$PM_{2.5}$	21.9	20.8	9.75	-6 %	37 %
OC	5.6	3.57	2.93	-49 %	54 %
EC	1.8	1.17	1.05	-33 %	56 %
Sulfate	6.06	7.35	5.35	25 %	61 %
Nitrate	0.32	0.0049	0.39	-189 %	189 %
Ammonium	1.87	0.32	1.9	-114%	128%

a) Observed mean concentrations (μg/m^{3}).
b) Modeled mean concentrations (μg/m^{3}).

modeled concentrations in the inner domain D1 and 8 % in the outer domain D2. Compared to the WHO annual guideline of 10 μg/m^{3} and 24-hour average guideline of 25 μg/m^{3}, $PM_{2.5}$ concentrations exceed these values in large urban agglomerations such as Beirut and Tripoli and in the regions of Chekka and Sibline where several cement plants are located and modeled $PM_{2.5}$ are above 100 μg/m^{3}.

Statistical model performance at the USJ site is presented in Table C.5. The observed value for $PM_{2.5}$ is a reconstructed mass concentration based on the IMPROVE method (IMPROVE, 2011). Overall, the model reproduces satisfactorily $PM_{2.5}$, OC, EC, and sulfate (SO42-) average concentrations. MFB values in the range of -6 to 49 % and MFE values in the range of 37 to 61 % obtained during this study indicate that the model meets the performance criteria (-60 % $\leqslant$ MFB $\leqslant$ + 60 % and MFE $\leqslant$ 75 %) suggested by Boylan and Russel (2006). For nitrate and ammonium, there is a large underestimation of the model. This high underestimation could be related to uncertainties in NH_3 emissions. The MFB and MFE reported values of -49 % and 54 % obtained for OC during this study are in agreement with the values of -37 % and 50 % reported for Europe in another simulation conducted using Polyphemus/Polair3D [*Couvidat et al.*, 2012a]. In a simulation conducted with the CMAQ model over the eastern U.S., MFB values for $PM_{2.5}$, OC and EC were -3 %, 37 % and 14 %, respectively [*Bailey et al.*, 2007]. Those are lower than the values reported here (Table C.4). However, for sulfate a MFB of 25 % reported here is lower in absolute value than the value of -35 % reported by *Bailey et al.* [2007].

C.5 Conclusion

A modeling study of meteorology and air pollution in Beirut was conducted for the period of July 2-18, 2011 using WRF and Polyphemus/Polair3D. WRF reproduces satisfactorily the diurnal variations for temperature, wind speed, relative humidity and atmospheric pressure and agrees relatively well with observation of wind direction especially from July 6 to July 10, 2011. The WRF results show acceptable performance compared to values reported in other studies in Europe and the United States, however, measurements were available for model performance evaluation only at one site. The air quality modeling results in Beirut, show higher NO_2 concentrations near the coast in the city of Beirut and its northern suburb and lower O_3 concentrations within the city limits. Highest values for $PM_{2.5}$, OC, and EC are modeled within the city limits suggesting that the major sources which lead to the formation of $PM_{2.5}$ are anthropogenic sources. The CTM performance evaluation results show that Polyphemus/Polair3D reproduces satisfactorily O_3, $PM_{2.5}$, OC, EC, and sulfate concentrations. Statistical indicators obtained for the major pollutants are in the range of other studies conducted in Europe and the U.S.A. Furthermore, the O_3 diurnal variation is well reproduced by the model. This modeling study is the first one conducted for Beirut. It provides an overview of the pollutant concentrations in the summer of 2011. Future work should focus on the improvement of the input data such as the emission inventory and the meteorology in order to reduce bias and errors between modeled and observed concentrations. Moreover, observational data from more than one site are needed in order to better evaluate the model. A measurement campaign will be conducted in 2013 in a road tunnel in Beirut in order to obtain specific road transport emission factors representative of the Lebanese fleet.

C.6 Supplementary materials

Table C.6: Definitions of the statistical indicators.

Indicators	Definitions
Root mean square error (RMSE)	$\sqrt{\frac{1}{n}\sum_{i=1}^{n}(c_i - o_i)^2}$
Mean fractional bias (MFB) and mean fractional error (MFE)	$\frac{1}{n}\sum_{i=1}^{n}\frac{c_i - o_i}{(c_i + o_i)/2}$ and $\frac{1}{n}\sum_{i=1}^{n}\frac{\mid c_i - o_i \mid}{(c_i + o_i)/2}$
Normalized mean bias (NMB) and normalized mean error (NME)	$\frac{\sum_{i=1}^{n}(c_i - o_i)}{\sum_{i=1}^{n} o_i}$ and $\frac{\sum_{i=1}^{n}(\mid c_i - o_i \mid)}{\sum_{i=1}^{n} o_i}$
Mean normalized bias (MNB) and mean normalized gross error (MNGE)	$\frac{1}{n}\sum_{i=1}^{n}\frac{c_i - o_i}{o_i}$ and $\frac{1}{n}\sum_{i=1}^{n}\frac{\mid c_i - o_i \mid}{o_i}$
Correlation coefficient	$\frac{\sum_{i=1}^{n}(c_i - \overline{c})(o_i - \overline{o})}{\sqrt{\sum_{i=1}^{n}(c_i - \overline{c})2}\sqrt{\sum_{i=1}^{n}(o_i - \overline{o})2}}$ with $\overline{o} = \frac{1}{n}\sum_{i=1}^{n} o_i$ and $\overline{c} = \frac{1}{n}\sum_{i=1}^{n} c_i$

c_i: modeled values, o_i: observed values, n: number of data.

Bibliography

Afif, C., A. Dutot, C. Jambert, M. Abboud, J. Adjizian-Gérard, W. Farah, P. Perros, and T. Rizk (2009), Statistical approach for the characterization of NO_2 concentrations in Beirut, *Air Qual. Atmos. Health*, *2*, 57-67, 10.1007/s11869-009-0034-2.

Airparif (2011), Source apportionment of airborne particles in Ile-de-France - final report, *Tech. Rep.*, Airparif, Paris, France.

Allan, J. D., P. I. Williams, W. T. Morgan, C. L. Martin, M. J. Flynn, J. Lee, E. Nemitz, G. J. Phillips, M. W. Gallagher, and H. Coe (2010), Contributions from transport, solid fuel burning and cooking to primary organic aerosols in two UK cities, *Atmos. Chem. Phys.*, *10*, 647-668, 10.5194/acp-10-647-2010.

Altieri, K., S. P. Seitzinger, A. G. Carlton, B. Turpin, G. C. Klein, and A. G. Marshall (2008), Oligomers formed through in-cloud methylglyoxal reactions: chemical composition, properties, and mechanisms investigated by ultra-high resolution FT-ICR Mass Spectrometry, *Atmos. Environ.*, *42*, 1476-1490, 10.1016/j.atmosenv.2007.11.015.

Aphekom (2011), Health impact assessment of short and long-term exposure to ozone and PM in 25 european cities, *Tech. Rep.*, Aphekom.

Appel, K. W., K. M. Foley, J. O. Bash, R. W. Pinder, R. L. Dennis, D. J. Allen, and K. Pickering (2011), A multi-resolution assessment of the Community Multiscale Air Quality (CMAQ) model v4.7 wet deposition estimates for 2002-2006, *Geosci. Model Dev.*, *4*, 357-371, 10.5194/gmd-4-357-2011.

Arhami, M., T. Kuhn, P. M. Fine, R. J. Delfino, and C. Sioutas (2006), Effects of sampling artifacts and operating parameters on the performance of a semicontinuous particulate elemental carbon/organic carbon monitor, *Environ. Sci. Tech.*, *40*, 945–954, 10.1021/es0510313.

Asa-Awuku, A., M. A. Miracolo, J. H. Kroll, A. L. Robinson, and N. M. Donahue (2009), Mixing and phase partitioning of primary and secondary organic aerosols, *Geophys. Res. Lett.*, *36*, L15827, 10.1029/2009GL039301.

Bae, M.-S., J. J. Schauer, J. T. DeMinter, J. R. Tuner, D. Smith, and R. A. Cary (2004), Validation of a semi-continuous instrument for elemental carbon and organic carbon using a thermal-optical method, *Atmos. Environ.*, *38*, 2885–2893, 10.1016/j.atmosenv.2004.02.027.

Bailey, E. M., L. L. Gautney, J. J. Kelsoe, M. E. Jacobs, Q. Mao, J. W. Condrey, B. Pun, S.-Y. Wu, C. Seigneur, S. Douglas, J. Haney, and N. Kumar (2007), A comparison of the performance of four air quality models for the Southern Oxidants Study episode in July 1999, *J. Geophys. Res.*, *112, D05306*, 10.1029/2007JD008675.

Barley, M. H., and G. McFiggans (2010), The critical assessment of vapour pressure estimation methods for use in modelling the formation of atmospheric organic aerosol, *Atmos. Chem. Phys.*, *10*, 749-767, 10.5194/acp-10-749-2010.

Bessagnet, B., L. Menut, G. Curci, A. Hodzic, B. Guillaume, C. Liousse, S. Moukhtar, B. Pun, C. Seigneur, and M. Schulz (2008), Regional modeling of carbonaceous aerosols over Europe-focus on secondary organic aerosols, *J. Atmos. Chem.*, *61*, 175-202, 10.1007/s10874-009-9129-2.

Bessagnet, B., C. Seigneur, and L. Menut (2010), Impact of dry deposition of semi-volatile organic compounds on secondary organic aerosols, *Atmos. Environ.*, *44*, 1781-1787, 10.1016/j.amtosenv.2010.01.027.

Bianconi, R., S. Galmarini, and R. Bellasio (2004), Web-based system for decision support in case of emergency: ensemble modelling of long-range atmospheric dispersion of radionuclides, *Environmental Modelling and Software*, *19*, 401-411, 10.1016/S1364-8152(03)00139-7.

Borge, R., V. Alexandrov, J. José del Vas, J. Lumbreras, and E. Rodriguez (2008), A comprehensive sensitivity analysis of the WRF model for air quality applications over the iberian peninsula, *Atmos. Environ.*, *42*, 8560-8574, 10.1016/j.atmosenv.2008.08.032.

Boylan, J. W., and A. G. Russell (2006), PM and light extinction model performance metrics, goals, and criteria for three-dimensional air quality models, *Atmos. Environ.*, *40*, 4946-4959, 10.1016/j.atmosenv.2005.09.087.

Byun, D., and K. L. Schere (2009), Review of the governing equations, computational algorithms and other components of the models-3 community multi scale air quality (CMAQ) modeling system, *Appl. Mech. Rev.*, *59*, 51.

Calvert, J. G., R. Atkinson, K. H. Becker, R. M. Kamens, J. H. Seinfeld, T. J. Wallington, and G. Yarwood (2002), *The mechanisms of atmospheric oxidation of the aromatic hydrocarbons*, Oxford University Press.

Calvert, J. G., R. G. Derwent, J. J. Orlando, G. S. Tyndall, and T. J. Wallington (2008), *Mechanisms of atmospheric oxidation of the alkanes*, Oxford University Press.

Carlton, A. G., B. J. Turpin, H.-J. L. Lim, K. E. Altieri, and S. Seitzinger (2006), Link between isoprene and secondary organic aerosol (SOA): Pyruvic acid oxidation yields low volatility organic acids in clouds, *Geophys. Res. Lett.*, *33*, L06822, 10.1029/2005GL025374.

Carlton, A. G., B. J. Turpin, K. E. Altieri, S. Seitzinger, A. Reff, H. J. Lim, and B. Ervens (2007), Atmospheric oxalic acid and SOA production from glyoxal: Results of aqueous photooxidation experiments, *Atmos. Environ.*, *41*, 7588-7602, 10.1016/j.atmosenv.2007.05.035.

Carlton, A. G., B. J. Turpin, K. E. Altieri, S. P. Seitzinger, R. Mathur, S. J. Roselle, and R. J. Weber (2008), CMAQ model performance enhanced when in-cloud secondary organic aerosol is included: comparisons of organic carbon predictions with measurements, *Environ. Sci. Technol.*, *42*, 8798-8802, 10.1021/es801192n.

Carlton, A. G., C. Wiedinmyer, and J. H. Kroll (2009), A review of secondary organic aerosol (SOA) formation from isoprene, *Atmos. Chem. Phys.*, *9*(14), 4987-5005, 10.5194/acp-9-4987-2009.

Carlton, A. G., P. V. Bhave, S. L. Napelenok, E. O. Edney, G. Sarwar, R. W. Pinder, G. A. Pouliot, and M. Houyoux (2010a), Model representation of secondary organic aerosol in CMAQv4.7, *Environ. Sci. Tech.*, *44*(22), 8553-8560, 10.1021/es100636q.

Carlton, A. G., R. W. Pinder, P. V. Bhave, and G. A. Pouliot (2010b), To what extent can biogenic SOA be controlled?, *Environ. Sci. Technol.*, *44*, 3376-3380, 10.1021/es903506b.

Carter, W. P. L., D. R. Cocker III, D. R. Fitz, I. L. Malkina, K. Bumiller, C. G. Sauer, J. T. Pisano, C. Bufalino, and C. Song (2005), A new environmental chamber for evaluation of gas-phase chemical mechanisms and secondary aerosol formation, *Atmos. Environ.*, *39*, 7768-7788, 10.1016/j.atmosenv.2005.08.040.

Carvalho, D., A. Rocha, M. Gomez-Gesteira, and C. Santos (2012), A sensitivity study of WRF model in wind simulation for an area of high wind energy, *Environ. Modell. Softw.*, *33*, 23-34, 10.1016/j.envsoft.2012.01.019.

Cavalli, F., M. Viana, K. E. Yttri, J. Genberg, and J. P. Putaud (2010), Toward a standardised thermal-optical protocol for measuring atmospheric organic and elemental carbon: the EUSAAR protocol, *Atmos. Meas. Tech.*, *3*, 79-89, 10.5194/amt-3-79-2010.

CBDE (2004), Consensus of buildings and establishments report, *Tech. Rep.*, Central Administrate of Statistics, Beirut, Lebanon.

Chan, A. W. H., K. E. Kautzman, P. S. Chhabra, J. D. Surratt, M. N. Chan, J. D. Crounse, A. Kürten, P. O. Wennberg, R. C. Flagan, and J. H. Seinfeld (2009), Secondary organic aerosol formation from photooxidation of naphthalene and alkylnaphthalenes: implications for oxidation of intermediate volatility organic compounds (IVOCs), *Atmos. Chem. Phys.*, *9*, 3049-3060, 10.5194/acp-9-3049-2009.

Chan, A. W. H., M. N. Chan, J. D. Surratt, P. S. Chhabra, C. L. Loza, J. D. Crounsoe, L. D. Yee, R. C. Flagan, P. O. Wennberg, and J. H. Seinfeld (2010a), Role of aldehyde chemistry and NO_X concentrations in secondary organic aerosol formation, *Atmos. Chem. Phys. Discuss.*, *10*, 10219-10269, 10.5194/acpd-10-10219-2010.

Chan, M. N., J. D. Surratt, M. Claeys, E. S. Edgerton, R. L. Tanner, S. L. Shaw, M. Zheng, E. M. Knipping, N. C. Eddingsaas, P. O. Wennberg, and J. H. Seinfeld (2010b), Characterization and quantification of isoprene-derived epoxydiols in ambient aerosol in the southeastern United States, *Environ. Sci. Technol.*, *44*, 4590-4596, 10.1021/es100596b.

Chang, W. L., R. J. Griffin, and D. Dabdub (2010), Partitiong phase preferences for secondary organic aerosol via an urban atmosphere, *Proc. National Academy Sci.*, *107*, 6705-6710, 10.1073/pnas.0911244107.

Chélala, C. (2008), Transport routier et pollution de l'air en NO_2, Ph.D. thesis, Université Saint Joseph, Lebanon.

Chen, J., R. J. Griffin, A. Grini, and P. Tulet (2007), Modeling secondary organic aerosol formation through cloud processing of organic compounds, *Atmos. Chem. Phys.*, *7*, 5343-5355, 10.5194/acp-7-5343-2007.

Chen, W., H. Kuze, A. Uchiyama, Y. Suzuki, and N. Takeuchi (2001), One-year observation of urban mixed layer characteristics at Tsukuba, Japan using a micro pulse lidar, *Atmos. Environ.*, *35*, 4273-4280, 10.1016/S1352-2310(01)00181-9.

Chhabra, P. S., R. C. Flagan, and J. H. Seinfeld (2010), Elemental analysis of chamber organic aerosol using an aerodyne high-resolution aerosol mass spectrometer, *Atmos. Chem. Phys.*, *10*, 4111-4131, 10.5194/acp-10-4111-2010.

Chirico, R., A. S. H. Prevot, P. F. DeCarlo, M. F. Heringa, R. Richter, E. Weingartner, and U. Baltensperger (2011), Aerosol and trace gas vehicle emission factors measured in a tunnel using an aerosol mass spectrometer and other on-line instrumentation, *Atmos. Environ.*, *45*, 2182-2192, 10.1016/j.atmosenv.2011.01.069.

Chou, M.-D., and M. J. Suarez (1994), An efficient thermal infrared radiation parameterization for use in general circulation models.

Claeys, M., B. Graham, G. Vas, W. Wang, R. Vermeylen, V. Pashynska, J. Cafmeyer, P. Guyon, M. O. Andreae, P. Araxo, and W. Maenhaut (2004), Formation of secondary organic aerosols through photooxidation of isoprene, *Science*, *303*, 1173-1176, 10.1126/science.1092805.

Clegg, S. L., P. Beimblecombe, and I. Khan (1996), The Henry's law constant of oxalic acid and its partitioning into the atmospheric aerosol, *Idöjár ás*, *100*, 51-68.

Cocker III, D. R., R. C. Flagan, and J. H. Seinfeld (2001), State-of-the-art chamber facility for studying atmospheric aerosol chemistry, *Environ. Sci. Technol.*, *35*, 2594-2601, 10.1021/es0019169.

Compernolle, S., K. Ceulemans, and J.-F. Müller (2009), Influence of non-ideality on condensation to aerosol, *Atmos. Chem. Phys.*, *9*, 1325-1338, 10.5194/acp-9-1325-2009.

Cooke, W. F., C. Liousse, H. Cachier, and J. Feichter (1999), Construction of a 1°x 1° fossil fuel emission data set for carbonaceous aerosol and implementation and radiative impact in the ECHAM4 model, *J. Geophys. Res.*, *104*, 22137–22162, 10.1029/1999JD900187.

Couvidat, F., and C. Seigneur (2011), Modeling secondary organic aerosol formation from isoprene oxidation under dry and humid conditions, *Atmos. Chem. Phys.*, *11*(2), 893–909, 10.5194/acp-11-893-2011.

Couvidat, F., É. Debry, K. Sartelet, and C. Seigneur (2012a), A Hydrophilic/Hydrophobic Organic (H^2O) model: Model development, evaluation and sensitivity analysis, *J. Geophys. Res.*, *117*, D10304, 10.1029/2011JD017214.

Couvidat, F., Y. Kim, K. Sartelet, C. Seigneur, N. Marchand, and J. Sciare (2012b), Modeling secondary organic aerosol in an urban area: Application to Paris, France, *Submitted to Atmos. Chem. Phys.*

Curci, G., M. Beekmann, R. Vautard, G. Smiatek, R. Steinbrecher, J. Theloke, and R. Friedrich (2009), Modelling study of the impact of isoprene and terpene biogenic emissions on European ozone levels, *Atmos. Environ.*, *43*, 1444-1455, 10.1016/j.atmosenv.2008.02.070.

Darer, I. A., N. C. Cole-Filipiak, A. E. O´Connor, and M. J. Elrod (2011), Formation and stability of atmospheric relevant isoprene-derived organosulfates and organonitrates, *Environ. Sci. Technol.*, *45*, 1895-1902, 10.1021/es103797z.

De Haan, D. O., M. A. Tolbert, and J. L. Jimenez (2009a), Atmospheric condensed-phase reactions of glyoxal with methylamine, *Geophys. Res. Lett.*, *36*, L11819, 10.1029/2009GL037441.

De Haan, D. O., A. L. Corrigan, K. W. Smith, D. R. Stroik, J. J. Turley, F. E. Lee, M. A. Tolbert, J. L. Jimenez, K. E. Cordova, and G. R. Ferrell (2009b), Secondary organic aerosol-forming reactions of glyoxal with amino acids, *Environ. Sci. Technol.*, *43*, 2818–2824, 10.1021/es803534f.

Debry, E., K. Fahey, K. Sartelet, B. Sportisse, and M. Tombette (2007a), Technical note: A new SIze REsolved Aerosol Model (SIREAM), *Atmos. Chem. Phys.*, *7*(6), 1537-1547, 10.5194/acp-7-1537-2007.

Debry, E., C. Seigneur, and K. Sartelet (2007b), Organic aerosols in the air quality platform polyphemus: oxidation pathways, hydrophilic/hydrophobic partitioning and oligomerization, International Aerosol Modeling Algorithms, Davis, USA, 5-7 december 2007.

Deguillaume, L., A. Tilgner, R. Schrödner, R. Wolke, N. Chaumerliac, and H. Herrmann (2009), Towards an operational aqueous phase chemistry mechanism for regional chemistry-transport models: CAPRAM-RED and its application to the COSMO-MUSCAT model, *J. Atmos. Chem.*, *64*, 1-35, 10.1007/s10874-010-9168-8.

Donahue, N. (2011), Implementing the 2d vbs, International Aerosol Modeling Algorithms, Davis, USA, 30 november - 2 december 2011.

Donahue, N. M., A. L. Robinson, C. O. Stanier, and S. N. Pandis (2006), Coupled partitioning, dilution, and chemical aging of semivolatile organics, *Environ. Sci. Technol.*, *40*, 2635–2643, 10.1021/es052297c.

Donahue, N. M., S. A. Epstein, S. N. Pandis, and A. L. Robinson (2011), A two-dimensional volatility basis set: 1. Organic-aerosol mixing thermodynamics, *Atmos. Chem. Phys.*, *11*, 3303-3318, doi:10.5194/acp-11-3303-2011.

Dzepina, K., C. D. Cappa, R. M. Volkamer, S. Madronich, P. F. DeCarlo, R. A. Zaveri, and J. L. Jimenez (2011), Modeling the multiday evolution and aging of secondary organic aerosol during MILAGRO 2006, *Environ. Sci. Technol.*, *45*, 3496–3503, 10.1021/es103186f.

Eddingsaas, N. C., D. G. VanderVelde, and P. O. Wennberg (2010), Kinetics and products of the acid-catalyzed ring-opening of atmospherically relevant butyl epoxy alcohols, *J. Phys. Chem. A*, *114*, 8106-8113, 10.1021/jp103907.

Eddingsaas, N. C., C. L. Loza, L. D. Yee, M. Chan, K. A. Schilling, P. S. Chhabra, J. H. Seinfeld, and P. O. Wennberg (2012), α-pinene photooxidation under controlled chemical conditions – part 2: Soa yield and composition in low- and high-no$_x$ environments, *Atmos. Chem. Phys.*, *12*, 7413-7427, 10.5194/acp-12-7413-2012.

Edney, E. O., T. E. Kleindienst, M. Jaoui, M. Lewabdowski, J. H. Offenberg, W. Wang, and M. Claeys (2005), Formation of 2-methyltetrols and 2-methylglyceric acid in secondary organic aerosol from laboratory irradiated isoprene/NO_X/SO_2/air mixtures and their detection in ambient $PM_{2.5}$ samples collected in the eastern United States, *Atmos. Environ.*, *39*, 5281-5289, 10.1016/j.atmosenv.2005.05.031.

El Haddad, I., Y. Liu, L. Nieto-Gligorovski, V. Michaud, B. Temime-Roussel, E. Quivet, N. Marchand, K. Sellegri, and A. Monod (2009), In-cloud processes of methacrolein under simulated conditions - Part 2: formation of secondary organic aerosol, *Atmos. Chem. Phys.*, *9*, 5107-5117, 10.5194/acp-9-5107-2009.

Emmons, L. K., S. Walters, P. G. Hess, J. F. Lamarque, G. G. Pfister, D. Fillmore, C. Granier, A. Guenther, D. Kinnison, T. Laepple, J. Orlando, X. Tie, G. Tyndall, C. Wiedinmyer, S. L. Baughcum, and S. Kloster (2010), Description and evaluation of the Model for Ozone and Related chemical Tracers, version 4 (MOZART-4), *Geosci. Model Dev.*, *3*, 43-67, 10.5194/gmd-3-43-2010, 2010.

EPRI (1999), Organic aerosol partition module documentation, EPRI, Palo Alto, CA, USA, *Technical Report.*

Ervens, B., and R. Volkamer (2010), Glyoxal processing by aerosol multiphase chemistry: towards a kinetic modeling framework of secondary organic aerosol formation in aqueous particles, *Atmos. Chem. Phys.*, *10*, 8219-8244, 10.5194/acp-10-8219-2010.

Ervens, B., A. G. Carlton, B. J. Turpin, K. E. Altieri, S. M. Kreidenweis, and G. Feingold (2008), Secondary organic aerosol yields from cloud-processing of isoprene oxidation products, *Geophys. Res. Lett.*, *35*, L02816, 10.1029/2007GL031828.

Ervens, B., B. J. Turpin, and R. J. Weber (2011), Secondary organic aerosol formation in cloud droplets and aqueous particles (aqSOA): a review of laboratory, field and model studies, *Atmos. Chem. Phys.*, *11*, 11069-11102, 10.5194/acp-11-11069-2011.

ESCWA (2010), Transport for sustainable development for the arab region: Measures, progress achieved, challenge and policy framework report, *Tech. Rep.*

Fredenslund, A., R. L. Jones, and J. M. Prausnitz (1975), Group-contribution estimation of activity-coefficients in nonideal liquid-mixtures, *AIChE J.*, *21*, 1086-1099.

Froyd, K. D., S. M. Murphy, D. M. Murphy, J. A. de Gouw, N. C. Eddingsaas, and P. O. Wennberg (2010), Contribution of isoprene-derived organosulfates to free tropospheric aerosol mass, *Proc. Natl. Acad. Sci.*, *107*, 21360-21365, 10.1073/pnas.1012561107.

Furukawa, T., and Y. Takahashi (2011), Oxalate metal complexes in aerosol particles: implications for the hygroscopicity of oxalate-containing particles, *Atmos. Chem. Phys.*, *11*, 4289-4301, 10.5194/acp-11-4289-2011.

Gantt, B., N. Meskhidze, and D. Kamykowski (2009), A new physically-based quantification of marine isoprene and primary organic aerosol emissions, *Atmos. Chem. Phys.*, *9*, 4915-4927, 10.5194/acp-9-4915-2009.

Gantt, B., N. Meskhidze, M. C. Facchini, M. Rinaldi, D. Ceburnis, and C. D. O'Dowd (2011), A new physically-based quantification of marine isoprene and primary organic aerosol emissions, *Atmos. Chem. Phys.*, *11*, 8777-8790, 10.5194/acp-11-8777-2011.

Gao, S., N. L. Ng, M. Keywood, V. Varutbangkul, R. Bahreini, A. Nenes, J. He, K. Y. Yoo, J. L. Beauchamp, R. P. Hodyss, R. C. Flagan, and J. H. Seinfeld (2004), Particle phase acidity and oligomer formation in secondary organic aerosol, *Environ. Sci. Technol.*, *38*, 6582-6589, 10.1021/es049125k.

Gaydos, T. M., R. Pinder, B. Koo, K. M. Fahey, G. Yarwood, and S. N. Pandis (2007), Development and application of a three-dimensional aerosol chemical transport model, PMCAMx, *Atmos. Environ.*, *41*(12), 2594-2611, 10.1016/j.atmosenv.2006.11.034.

Gilliam, R. C., C. Hogrefe, and S. Rao (2006), New methods for evaluating meteorological models used in air quality applications, *Atmos. Environ.*, *40*, 5073-5086, 10.1016/j.atmosenv.2006.01.023.

Glasius, M., A. Calogirou, N. R. Jensen, J. Hjorth, and C. J. Nielsen (1997), Kinetic study of gas-phase reactions of pinonaldehyde and structurally related compounds, *Int. J. Chem. Kinet.*, *29*, 527-533, 10.1002/(SICI)1097-4601(1997)29:7<527::AID-KIN7>3.0.CO;2-W.

Goliff, W. S., and W. R. Stockwell (2008), The regional atmospheric chemistry mechanism, version 2, an update, international conference on atmospheric chemical mechanisms, University of California, Davis, CA, USA, available at http://airquality.ucdavis.edu/pages/events/2008/acm/goliff.pdf, last access: 10 august 2010.

Grell, G. A., and D. Devenyi (2002), A generalized approach to parameterizing convection combining ensemble and data assimilation techniques, *Geophys. Res. Lett.*, *29*, 1693, doi:10.1029/2002GL015311.

Grell, G. A., S. E. Peckham, R. Schmitz, S. A. McKeen, G. Frost, W. C. Skamarock, , and B. Eder (2005), Fully coupled online chemistry within the WRF model, *Atmos. Environ.*, *39*, 6957-6975, 10.1016/j.atmosenv.2005.04.027.

Grieshop, A. P., J. M. Logue, N. M. Donahue, and A. L. Robinson (2009), Laboratory investigation of photochemical oxidation if organic aerosol from wood fires. 1: measurement and simulation of organic aerosol evolution, *Atmos. Chem. Phys.*, *9*, 1263-1277, 10.5194/acp-9-1263-2009.

Griffin, R. J., D. Dabdub, M. J. Kleeman, P. Fraser, M., G. R. Cass, and J. H. Seinfeld (2002), Secondary organic aerosol, 3, Urban/regional scale model of size- and composition-resolved aerosols, *J. Geophys. Res.*, *107*, 4334, 10.1029/2001JD000544.

Griffin, R. J., K. Nguyen, D. Dabdub, and J. H. Seinfeld (2003), A coupled hydrophobic-gydrophilic model for predicting secondary organic aerosol formation, *J. Atmos. Chem.*, *44*, 171-190, 10.1023/A:1022436813699.

Guenther, A., N. C. Hewitt, D. Erickson, R. Fall, C. Geron, T. Graedel, P. Harley, L. Klinger, M. Lerdau, W. A. McKay, T. Pierce, B. Scholes, R. Steinbrecher, R. Tallamraju, J. Taylor, and P. A. Zimmerman (1995), A global model of natural volatile organic compounds emissions, *J. Geophys. Res.*, *100*, 8873-8892, 10.1029/94JD02950.

Guenther, A., T. Karl, P. Harley, C. Wiedinmyer, P. I. Palmer, and C. Geron (2006), Estimates of global terrestrial isoprene emissions using MEGAN (Model of Emissions of Gases and Aerosols from Nature), *Atmos. Chem. Phys.*, *6*, 3181-3210, 10.5194/acp-6-3181-2006.

Haeffelin, M., L. Barthès, O. Bock, C. Boitel, S. Bony, D. Bouniol, H. Chepfer, M. Chiriaco, J. Cuesta, J. Delanö, P. Drobinski, J.-L. Dufresne, C. Flamant, M. Grall, A. Hodzic, F. Hourdin, F. Lapouge, Y. Lemaître, A. Mathieu, Y. Morille, C. Naud, V. Noël, W. O´Hirok, J. Pelon, C. Pietras, A. Protat, B. Romand, G. Scialom, and R. Vautard (2005), SIRTA, a ground-based atmospheric observatory for cloud and aerosol research, *Ann. Geophysic.*, *23*, 253-275, 10.5194/angeo-23-253-2005.

Hallquist, M., I. Wängberg, E. Ljungström, I. Barnes, and K.-H. Becher (1999), Aerosol and product yield from NO_3 radical-initiated oxidation of selected monoterpenes, *Environ. Sci. Technol.*, *33*, 553-559, 10.1021/es980292s.

Hallquist, M., J. C. Wenger, U. Baltensperger, Y. Rudich, D. Simpson, M. Claeys, J. Dommen, N. M. Donahue, C. George, A. H. Goldstein, J. F. Hamilton, H. Herrmann, T. Hoffmann,

Y. Iinuma, M. Jang, M. E. Jenkin, J. L. Jimenez, A. Kiendler-Scharr, W. Maenhaut, G. McFiggans, T. F. Mentel, A. Monod, A. S. H. Prévôt, J. H. Seinfeld, J. D. Surratt, R. Szmigielski, and J. Wildt (2009), The formation, properties and impact of secondary organic aerosol: current and emerging issues, *Atmos. Chem. Phys.*, *9*, 5155-5236, 10.5194/acp-9-5155-2009.

Helmig, D., A. Klinger, L. Vierling, P. Zimmerman, and C. Geron (1999a), Biogenic volatile organic compound emissions (BVOCs) I. Identifications from three continental sites in the U.S., *Chemosphere*, *38*, 2163-2187, 10.1016/S0045-6535(98)00425-1.

Helmig, D., A. Klinger, L. Vierling, P. Zimmerman, and C. Geron (1999b), Biogenic volatile organic compound emissions (BVOCs) II. Landscape fluxes potentials from three continental sites in the U.S., *Chemosphere*, *38*, 2189-2204, 10.1016/S0045-6535(98)00424-X.

Henze, D. K., and J. H. Seinfeld (2006), Global secondary organic aerosol from isoprene oxidation, *Geophys. Res. Lett.*, *33*, L09812, 10.1029/2006GL025976.

Henze, D. K., J. H. Seinfeld, N. L. Ng, J. H. Kroll, T.-M. Fu, D. J. Jacob, and C. L. Heald (2008), Global modeling of secondary organic aerosol formation from aromatic hydrocarbons: high- vs. low-yield pathways, *Atmos. Chem. Phys.*, *8*, 2405-2420, 10.5194/acp-8-2405-2008.

Hilal, S. H., S. N. Ayyampalayam, and L. A. Carreira (2008), Air-liquid partition coefficient for a diverse set of organic compounds: Henry's law constant in water and hexadecane, *Environ. Sci. Technol.*, *42*, 9231-9236, 10.1021/es8005783.

Hodzic, A., S. Madronich, B. Bohn, S. Massie, L. Menut, and C. Wiedinmyer (2007), Wildfire particulate matter in Europe during summer 2003: meso-scale modeling of smoke emissions, transport and radiative effects, *Atmos. Chem. Phys.*, *7*, 4043–4064, 10.5194/acp-7-4043-2007.

Hodzic, A., J. L. Jimenez, S. Madronich, M. R. Canagaratna, P. F. DeCarlo, L. Kleinman, and J. Fast (2010), Modeling organic aerosols in a megacity: potential contribution of semi-volatile and intermediate volatility primary organic compounds to secondary organic aerosol formation, *Atmos. Chem. Phys.*, *10*, 5491-5514, 10.5194/acp-10-5491-2010.

Hogrefe, C., S. Isukapalli, X. Tang, P. Georgopoulos, S. He, E. Zalewsky, W. Hao, J. Ku, T. Key, and G. Sistla (2011), Impact of biogenic emission uncertainties on the simulated response of ozone and fine Particulate Matter to anthropogenic emission reductions, *J. Air Waste Manag. Assoc.*, *61*, 92-108, 10.3155/1047-3289.61.1.92.

Hong, S.-Y., Y. Noh, and J. Dudhia (2006), A new vertical diffusion package with an explicit treatment of entrainment processes, *Mon. Wea. Rev.*, *134*, 2318–2341, 10.1175/MWR3199.1.

Horowitz, L. W., S. Walters, D. L. Mauzerall, L. K. Emmons, P. J. Rasch, C. Granier, X. Tie, J. F. Lamarque, M. G. Schultz, G. S. Tyndall, J. J. Orlando, and G. P. Brasseur (2003), A global simulation of tropospheric ozone and related tracers: description and evaluation of MOZART, version 2, *J. Geophys. Res.*, *108*, D24, 4784, 10.1029/2002JD002853.

Horowitz, L. W., A. M. Fiore, G. P. Milly, R. C. Cohen, A. Perring, P. J. Wooldridge, P. G. Hess, L. K. Emmons, and J. F. Lamarque (2007), Observational constraints on the chemistry of isoprene nitrates over the eastern United States, *J. geophys. Res.*, *112*, D12S08, 10.1029/2006JD007747.

Hoyle, C. R., M. Boy, N. M. Donahue, J. L. Fry, M. Glasius, A. Guenther, A. G. Hallar, K. Huff Hartz, M. D. Petters, T. Petäjä, T. Rosenoern, and A. P. Sullivan (2011), A review of the anthropogenic influence on biogenic secondary organic aerosol, *Atmos. Chem. Phys.*, *11*, 321-343, 10.5194/acp-11-321-2011.

IIASA (2012), Average annual anthropogenic heat flux for major capital cities in the world, *Tech. Rep.*

Ion, A. C., R. Vermeylen, I. Kourtchev, J. Cafmeyer, X. Chi, A. Gelencsér, W. Maenhaut, and M. Claeys (2005), Polar organic compounds in rural pm$_{2.5}$ aerosols from K-puszta, Hungary, during a 2003 summer field campaign: Sources and diel variations, *Atmos. Chem. Phys.*, *5*, 1805-1814, 10.5194/acp-5-1805-2005.

Iraci, L. T., B. M. Baker, G. S. Tyndall, and J. J. Orlando (1999), Measurements of the Henry's law coefficients of 2-methyl-3-buten-2-ol, methacrolein and methylvinyl ketone, *J. Atmos. Chem.*, *33*, 321-330, 10.1023/A:1006169029230.

Isaacman, G., K. R. Wilson, W. H. Chan, D. R. Worton, J. R. Kimmel, T. Nah, T. Hohaus, M. Gonin, J. H. Kroll, D. R. Worsnop, and A. H. Goldstein (2012), Improved resolution of hydrocarbon structures and constitutional isomers in complex mixtures using gas chromatography-vacuum ultraviolet-mass spectrometry, *Anal. Chem.*, *84*, 2335-2342, 10.1021/ac2030464.

Jacob, D. J. (1986), Chemistry of OH in remote clouds and its role in the production of formic acid and peroxymonosulfate, *J. Geophys. Res.*, *91*, 9807-9826, 10.1029/JD091iD09p09807.

Jacob, D. J. (2000), Heterogeneous chemistry and tropospheric ozone, *Atmos. Environ.*, *34*, 2131-2159, 10.1016/S1352-2310(99)00462-8.

Jaeglé, L., D. J. Jacob, W. H. Brune, and P. O. Wennberg (2001), Chemistry of HO$_x$ radicals in the upper troposphere, *Atmos. Environ.*, *35*, 469-489, 10.1016/S1352-2310(00)00376-9.

Jang, M., N. M. Czoschke, S. Lee, and R. M. Kamens (2002), Heterogeneous atmospheric aerosol production by acid-catalysed particle-phase reactions, *Science*, *298*, 814-817, 10.1126/science.1075798.

Jang, M., N. M. Czoschke, and A. L. Northcross (2005), Semiempirical model for organic aerosol growth by acid-catalyzed heterogeneous reactions of organic carbonyls, *Environ. Sci. Technol.*, *39*, 164-174, 10.1021/es048977h.

Jardine, K., A. Yañez Serrano, A. Arneth, L. Abrell, A. Jardine, J. van Haren, P. Artaxo, L. V. Rizzo, F. Y. Ishida, T. Karl, J. Kesselmeier, S. Saleska, and T. Huxman (2011), Within-canopy sesquiterpene ozonolysis in Amozonia, *J. Geophys. Res.*, *116*, D19301, 10.1029/2011JD016243.

Jimenez, J. L., M. R. Canagaratna, N. M. Donahue, A. S. H. Prevot, Q. Zhang, J. H. Kroll, P. F. DeCarlo, J. D. Allan, H. Coe, N. L. Ng, A. C. Aiken, K. S. Docherty, I. M. Ulbrich, A. P. Grieshop, A. L. Robinson, J. Duplossy, J. D. Smith, K. R. Wilson, V. A. Lanz, C. Hueglin, Y. L. Sun, J. Tian, A. Laaksonen, T. Raatikainen, J. Rautiainen, P. Vaattovaara, M. Ehn, M. Kulmala, J. M. Tomlinson, D. R. Collins, M. J. Cubison, E. J. Dunlea, J. A. Huffman, T. B. Onash, M. R. Alfarra, P. I. Williams, K. Bower, Y. Kondo, J. Schneider, F. Drewnick, S. Borrmann, S. Weimer, K. Demerjian, D. Salcedo, L. Cottrell, R. Griffin, A. Takami, T. Miyoshi, S. Hatakeyama, A. Shimono, J. Y. Sun, Y. M. Zhang, K. Dzepina, J. R. Kimmel, D. Sueper, J. T. Jayne, S. C. Herndon, A. M. Trimborn, L. R. Williams, E. C. Wood, A. M. Middlebrook, C. E. Kolb, U. Baltensperger, and D. R. Worsnop (2009), Evolution of organic aerosols in the atmosphere, *Science*, *326*, 1525-1529, 10.1126/science.1180353.

Johnson, D., S. R. Utembe, M. E. Jenkin, R. G. Derwent, G. D. Hayman, M. R. Alfarra, H. Coe, and G. McFiggans (2006), Simulating regional scale secondary organic aerosol formation during the TORCH 2003 campaign in the southern UK, *Atmos. Chem. Phys.*, *6*, 403-418, 10.5194/acp-6-403-2006.

Junker, C., and C. Liousse (2008), A global emission inventory of carbonaceous aerosol from historic records of fossil fuel and biofuel consumption for the period 1860-1997, *Atmos. Chem. Phys.*, *8*, 1195-1027, 10.5194/acp-8-1195-2008.

Kamens, R. M., and M. Jaoui (2001), Modeling aerosol formation from α-pinene + NOx in the presence of natural sunlight using gas-phase kinetics and gas-particle partitioning theory, *Environ. Sci. Technol.*, *35*, 1394–1405, 10.1021/es001626s.

Kamens, R. M., M. W. Gery, H. E. Jeffries, M. Jacksons, and E. I. Cole (1982), Ozone-isoprene reactions: product formation and aerosol potential, *Int. J. Chem. Kinet.*, *14*, 955-975.

Kanakidou, M., J. H. Seinfeld, S. N. Pandis, I. Barnes, F. J. Dentener, M. C. Facchini, R. Van Dingenen, B. Ervens, A. Nenes, C. J. Nielsen, E. Swietlicki, J. P. Putaud, Y. Balkanski, S. Fuzzi, J. Horth, G. K. Moortgat, R. Winterhalter, C. E. L. Myhre, K. Tsigaridis, E. Vignati, E. G. Stephanou, and J. Wilson (2005), Organic aerosol and global climate modelling: a review, *Atmos. Chem. Phys.*, *5*, 1053-1123, 10.5194/acp-5-1053-2005.

Karl, M., A. Guenther, R. Köble, and G. Seufert (2009), A new European plant-specific emission inventory of biogenic volatile organic compounds for use in atmospheric transport models, *Biogeosciences*, *6*, 1059-1087, 10.5194/bg-6-1059-2009.

Kautzman, K. E., J. D. Surratt, M. N. Chan, A. W. H. Chan, S. P. Hersey, P. S. Chhabra, N. F. Dalleska, P. O. Wennberg, R. C. Flagan, and J. H. Seinfeld (2010), Chemical composition of gas- and aerosol-phase products from the photooxidation of naphthalene, *J. Phys. Chem. A*, *114*, 913-934, 10.1021/jp908530s.

Keene, W. C., A. A. P. Pszenny, J. R. Maben, E. Stevenson, and A. Wall (2004), Closure evaluation of size-resolved aerosol pH in the New England coastal atmosphere during summer, *J. Geophys. Res.*, *109*, D23307, 10.1029/2004JD004801.

Kessler, E. (1969), On the distribution and continuity of water substance in atmospheric circulation, *Meteorol. Monogr.*, *10*, 88.

Kim, Y. (2011), Modélisation de la qualité de l'air: évaluation des paramétrisations chimiques et météorologiques, Ph.D. thesis, Université Paris-Est.

Kim, Y., K. Sartelet, and C. Seigneur (2009), Comparison of two gas-phase chemical kinetic mechanisms of ozone formation over Europe, *J. Atmos. Chem.*, *62*, 82-119, 10.1007/s10874-009-9142-5.

Kim, Y., F. Couvidat, K. Sartelet, and C. Seigneur (2011a), Comparison of different gas-phase mechanisms and aerosol modules for simulating particulate matter formation, *J. Air Waste Manage. Assoc*, *61*, 1218-1226.

Kim, Y., K. Sartelet, and C. Seigneur (2011b), Formation of secondary aerosols: impact of the gas-phase chemical mechanism, *Atmos. Chem. Phys.*, *11*, 583-598, 10.5194/acp-11-583-2011.

Kleindienst, T. E., M. Lewandowski, J. H. Offenberg, M. Jaoui, and E. O. Edney (2007), Ozone-isoprene reactions: Re-examination of the formation of secondary organic aerosol, *Geophys. Res. Lett.*, *34*, L01805, 10.1029/2006GL027485.

Kleindienst, T. E., M. Lewandowski, J. H. Offenberg, M. Jaoui, and E. O. Edney (2009), The formation of secondary organic aerosols from the isoprene + OH reaction in the absence of NO_X, *Atmos. Chem. Phys.*, *9*, 6541-6558, 10.5194/acp-9-6541-2009.

Koo, B., C. Chien, G. Tonnesen, R. Morris, J. Johnson, T. Sakulyanontvittaya, P. Piyachaturawat, and G. Yarwood (2011), Natural emissions for regional modeling of background ozone and particulate matter and impacts on emissions control strategies, *Atmos. Environ.*, *44*, 2372-2382, 10.1016/j.atmosenv.2010.02.041.

Kourtchev, I., J. Warnke, W. Maenhaut, T. Hoffmann, and M. Claeys (2008a), Polar organic marker compounds in $PM_{2.5}$ aerosol from a mixed forest site in western Germany, *Chemosphere*, *73*, 1308-1314, 10.1016/j.chemosphere.2008.07.011.

Kourtchev, I., T. M. Ruuskanen, P. Keronen, L. Sogacheva, M. Dal Maso, A. Reissell, X. Chi, R. Vermeylen, M. Kulmala, W. Maenhaut, and M. Claeys (2008b), Determination of isoprene and α-/β-pinene oxidation products in boreal forest aerosols from Hyytiälä, Finland: diel variations and possible link with particle formation events., *Plant Biol.*, *10*, 138-149, 10.1055/s-2007-964945.

Kouvarakis, G., K. Tsigaridis, M. Kanakidou, and N. Mihalopoulos (2000), Temporal variations of surface regional background ozone over crete island in the southeast mediterranean, *J. geophys. Res.*, *105*, 4399-4407, 10.1029/1999JD900984.

Kroll, J. H., and J. H. Seinfeld (2008), Chemistry of secondary organic aerosol: Formation and evolution of low-volatility organics in the atmosphere, *Atmos. Environ.*, *42*, 3593-3624, 10.1016/j.atmosenv.2008.01.003.

Kroll, J. H., N. L. Ng, S. M. Murphy, R. C. Flagan, and J. H. Seinfeld (2006), Secondary organic aerosol formation from isoprene photooxidation, *Environ. Sci. Technol.*, *40*, 1869-1877, 10.1021/es0524301.

Kusaka, H., H. Kondo, Y. Kikegawa, and F. Kimura (2001), A simple single-layer urban canopy model for atmospheric models: Comparison with multi-layer and slab models, *Bound.-Lay. Meteorol.*, *101*, 329-358, 10.1023/A:1019207923078.

Lee, J. Y., and D. A. Lane (2009), Unique products from the reaction of naphthalene with the hydroxyl radical, *Atmos. Environ.*, *43*, 4886-4893, 10.1016/j.atmosenv.2009.07.018.

Lee, J. Y., and D. A. Lane (2010), Formation of oxidized products from the reaction of gaseous phenanthrene with the oh radical in a reaction chamber, *Atmos. Environ.*, *44*, 2469-2477, 10.1016/j.atmosenv.2010.03.008.

Lee-Taylor, J., S. Madronich, B. Aumont, A. Baker, M. Camredon, A. Hodzic, G. S. Tyndall, E. Apel, and R. A. Zaveri (2011), Explicit modeling of organic chemistry and secondary organic aerosol partitioning for Mexico City and its outflow plume, *Atmos. Chem. Phys.*, *11*, 13219-13241, 10.5194/acp-11-13219-2011.

Lelieveld, J., H. Berresheim, S. Borrmann, P. J. Crutzen, F. J. Dentener, H. Fischer, J. Feichter, P. J. Flatau, J. Heland, R. Holzinger, R. Korrmann, M. G. Lawrence, Z. Levin, K. M. Markowicz, N. Mihalopoulos, A. Minikin, V. Ramanathan, M. de Reus, G. J. Roelofs, H. A. Scheeren, J. Sciare, H. Schlager, M. Schultz, P. Siegmund, B. Steil, E. G. Stephanou, P. Stier, M. Traub, C. Warneke, J. Williams, and H. Ziereis (2002), Global air pollution crossroads over the mediterranean, *Science*, *298*, 794-799, 10.1126/science.1075457.

Lelieveld, J., P. Hoor, P. Jackel, A. Pozzer, P. Hadjinicolaou, J. P. Cammas, and S. Beirle (2009), Severe ozone air pollution in the persian gulf region, *Atmos. Chem. Phys.*, *9*, 1393-1406, 10.5194/acp-9-1393-2009.

Liggio, J., and S.-M. Li (2006), Organosulfate formation during the uptake of pinonaldehyde on acidic sulfate aerosols, *Geophys. Res. Lett.*, *33*, L13808, 10.1029/2006GL026079.

Liggio, J., S.-M. Li, and R. McLaren (2005), Heterogeneous reactions of glyoxal on particulate matter: Identification of acetals and sulfate esters, *Environ. Sci. Technol.*, *39*, 1532–1541, 10.1021/es048375y.

Lim, B. Y., and P. J. Ziemann (2009a), Chemistry of secondary organic aerosol formation from oh radical-initiated reactions of linear, branched and cyclic alkanes in the presence of NO_x, *Aerosol. Sci. Technol.*, *43*, 604-619, 10.1080/02786820902802567.

Lim, B. Y., and P. J. Ziemann (2009b), Effects of molecular structure on aerosol yields from oh radical-initiated reactions of linear, branched, and cyclic alkanes in the presence of NO_x, *Environ. Sci. Technol.*, *43*, 2328-2334, 10.1021/es803389s.

Lim, H.-J., A. G. Carlton, and B. J. Turpin (2005), Isoprene forms secondary organic aerosol through cloud processing: Model simulations, *Environ. Sci. Technol.*, *39*(12), 4441-4446, 10.1021/es048039h.

Limbeck, A., H. Puxbaum, L. Otter, and M. C. Scholes (2001), Semivolatile behavior of dicarboxylic acids and other polar organic species at a rural background site (Nylsvely, RSA), *Atmos. Environ.*, *35*, 1853-1862, 10.1016/S1352-2310(00)00497-0.

Liousse, C., B. Guillaume, J. M. Grégoire, M. Mallet, C. Galy, V. Pont, A. Akpo, M. Bedou, P. Castéra, L. Dungall, E. Gardrat, C. Granier, A. Konaré, F. Malavelle, A. Mariscal, A. Mieville, R. Rosset, D. Serça, F. Solmon, F. Tummon, E. Assamoi, V. Yoboué, and P. Van Velthoven (2010), Updated African biomass burning emission inventories in the framework of the AMMA-IDAF program, with an evaluation of combustion aerosols, *Atmos. Chem. Phys.*, *10*(19), 9631-9646, 10.5194/acp-10-9631-2010.

Liu, J., D. Jones, J. Worden, D. Noone, M. Parrington, and J. Kar (2009a), Analysis of the summertime buildup of tropospheric ozone abundances over the Middle East and North Africa as observed by the tropospheric emission spectrometer instrument, *J. geophys. Res.*, *114*, D05304, 10.1029/2008JD010993.

Liu, P., and Y. Zhang (2008), A computationally-efficient secondary organic aerosol module for three-dimensional air quality models, *Atmos. Chem. Phys.*, *8*, 3985-3998, 10.5194/acp-8-3985-2008.

Liu, Y., I. El Haddad, M. Scarfogliero, L. Nieto-Gligorovski, B. Temime-Roussel, E. Quivet, N. Marchand, B. Picquet-Varrault, and A. Monod (2009b), In-cloud processes of methacrolein under simulated conditions - Part 1: Aqueous phase photooxidation, *Atmos. Chem. Phys.*, *9*, 5093-5105, 10.5194/acp-9-5093-2009.

Liu, Y., F. Siekmann, P. Renard, A. El Zein, G. Salque, I. El Haddad, B. Temime-Roussel, D. Voisin, R. Thissen, and A. Monod (2012), Oligomer and SOA formation through aqueous phase photooxidation of methacrolein and methyl vinyl ketone, *Atmos. Environ.*, *49*, 123-129, 10.1016/j.atmosenv.2011.12.012.

Louis, J.-F. (1979), A parametric model of vertical eddy fluxes in the atmosphere, *Bound.-Lay. Meteorol.*, *17*, 187-202.

Ludwig, J., and O. Klemm (1990), Acidity of size-fractionated aerosol particles, *Water Air Soil Pollut*, *49*, 35-50, 10.1007/BF00279508.

Luecken, D. J. (2008), Comparison of atmospheric chemical mechanisms for regulatory and research applications, in *Simulation and Assessment of Chemical Processes in a Multiphase Environment*, pp. 95-106, Springer, The Netherlands, 10.1007/978-1-4020-8846-9_8.

Luecken, D. J., S. Phillips, G. Sarwar, and C. Jang (2008), Effects of using the CB05 vs. SAPRC99 vs. CB4 chemical mechanism on model predictions: Ozone and gas-phase photochemical precursor concentrations, *Atmos. Environ.*, *42*, 5805-5820, 10.1016/j.atmosenv.2007.08.056.

Lukács, H., A. Gelencsér, A. Hoffer, G. Kiss, K. Horváth, and Hartyáni (2009), Quantitative assessment of organosulfates in size-segregated rural fine aerosol, *Atmos. Chem. Phys.*, *9*, 231-238, 10.5194/acp-9-231-2009.

Mallet, V., D. Quélo, B. Sportisse, M. Ahmed de Biasi, É. Debry, I. Korsakissok, L. Wu, Y. Roustan, K. Sartelet, M. Tombette, and H. Foudhil (2007), Technical Note: The air quality modeling system Polyphemus, *Atmos. Chem. Phys.*, *7*(20), 5479–5487, 10.5194/acp-7-5479-2007.

Martilli, A., A. Clappier, and M. W. Rotach (2002), An urban surface exchange parameterisation for mesoscale models, *Bound.-Lay. Meteorol.*, *104*, 261-304, 1023/A:1016099921195.

Massoud, R., A. Shihadeh, M. Roumié, M. Youness, J. Gerard, N. Saliba, R. Zaarour, M. Abboud, W. Farah, and N. A. Saliba (2011), Intraurban variability of PM_{10} and $PM_{2.5}$ in an eastern mediterranean city, *Atmos. Res.*, *101*, 893-901, 10.1016/j.atmosres.2011.05.019.

Matthias, V., A. Aulinger, and M. Quante (2008), Adapting CMAQ to investigate air pollution in north sea coastal region, *Environ. Modell. Softw.*, *23*, 356-368, 10.1016/j.envsoft.2007.04.010.

Mauldin III, R., S. Madronich, S. Flocke, and F. Eisele (1997), New insights on oh: Measurements around and in clouds, *Geophys. Res. Lett.*, *24*, 3033-3036.

Mellor, G. L., and T. Yamada (1974), A hierarchy of turbulence closure models for planetary boundary layers, *J. Atmos. Sci.*, *31*, 1791-1806.

Meng, Z., D. Dabdub, and J. H. Seinfeld (1998), Size-resolved and chemically resolved model of atmospheric aerosol, *J. Geophys. Res.*, *103*, 3419–3435, 10.1029/97JD02796.

Menut, L., A. Goussebaile, B. Bessagnet, D. Khvorostiyanov, and A. Ung (2012), Impact of realistic hourly emissions profiles on air pollutants concentrations modelled with CHIMERE, *Atmos. Environ.*, *49*, 233-244, 10.1016/j.atmosenv.2011.11.057.

Meylan, W. M., and P. H. Howard (1991), Bond contribution method for estimating henry's law constants, *Environ. Toxicol. Chem*, *10*, 1283-1293, 10.1002/etc.5620101007.

Meylan, W. M., and P. H. Howard (2000), SRC's EPI suite, v3.20, *Tech. Rep.*, Syracuse Research Corporation.

Michoud, V., A. Kukui, M. Camredon, A. Colomb, A. Borbon, K. Miet, B. Aumont, M. Beekmann, R. Durand-Jolibois, S. Perrier, P. Zapf, G. Siour, W. Ait-Helal, N. Locoge, S. Sauvage, V. Gros, C. Afif, M. Furger, G. Ancellet, and J. F. Doussin (2012), Radical budget analysis in a suburban european site during the MEGAPOLI summer field campaign, *Atmos. Chem. Phys. Discuss.*, *12*, 15883-15943, 10.5194/acpd-12-15883-2012, 2012.

Middleton, P., J. S. Chang, J. C. Del Corral, H. Geiss, and J. M. Rosinski (1988), Comparison of RADM and OSCAR precipitation chemistry data, *Atmos. Environ.*, *22*, 1195-1208, 10.1016/0004-6981(88)90350-2.

Mlawer, E. J., S. J. Taubman, P. D. Brown, M. J. Iacono, and S. A. Clough (1997), Radiative transfer for inhomogeneous atmospheres : RRTM, a validated correlated-k model for the longwave, *J. Geophys. Res.*, *102*, 16663-16682, 10.1029/97JD00237.

MoE (2005), National environmental action plan, *Tech. Rep.*, Ministry of environment, Beirut, Lebanon.

Molders, N. (2008), Suitability of the Weather Research and Forecasting (WRF) model to predict the june 2005 fire weather for interior Alaska, *Weather and Forecasting*, *23*, 953-973, 10.1175/2008WAF2007062.1.

Monahan, E., D. Spiel, and K. Davidson (1986), *Oceanic whitecaps and their role in air-sea exchange processes*, chap. A model of marine aerosol generation via whitecaps and wave disruption, Dordrecht: D. Reidel Pub.

Monod, A., and J. Doussin (2008), Structure-activity relationship for the estimation of oh-oxidation rate constants of aliphatic organic compounds in the aqueous phase: alkanes, alcohols, organic acids and bases, *Atmos. Environ.*, *33*, 7611-7622, 10.1016/j.atmosenv.2008.06.005.

Morris, R. E., B. Koo, A. Guenther, G. Yarwood, D. McNally, T. W. Tesche, G. Tonnesen, J. Boylan, and B. Brewer (2006), Model sensitivity evaluation for organic carbon using two multi-pollutant air quality models that simulate regional haze in the southeastern United States, *Atmos. Environ.*, *40*(26), 4960-4972, 10.1016/j.atmosenv.2005.09.088.

Mueller, S., and J. Mallard (2011), Contributions of natural emissions to Ozone and PM(2.5) as Simulated by the Community Multiscale Air Quality (CMAQ) model, *Environ. Sci. Technol.*, *45*, 4817-4823, 10.1021/es103645m.

Murphy, B. N., and S. N. Pandis (2009), Simulating the formation of semivolatile primary and secondary organic aerosol in a regional chemical transport model, *Environ. Sci. Technol.*, *43*, 4722–4728, 10.1021/es803168a.

Nakanishi, M., and H. Niino (2004), An improved Mellor-Yamada Level-3 model with condensation physics: its design and verification, *Bound.-Lay. Meteorol.*, *112*, 1-31, 10.1023/B:BOUN.0000020164.04146.98.

Nenes, A., S. N. Pandis, and C. Pilinis (1998), ISORROPIA: A new thermodynamic equilibrium model for multiphase multicomponent inorganic aerosols, *Aquat. Geoch.*, *4*, 123-152.

Nenes, A., P. S. N., and C. Pilinis (1999), Continued development and testing of a new thermodynamic aerosol module for urban and regional air quality models, *Atmos. Environ.*, *33*(10), 1553-1560, 10.1016/S1352-2310(98)00352-5.

Ng, N. L., P. S. Chhabra, A. W. H. Chan, J. D. Surratt, J. H. Kroll, A. J. Kwan, D. C. McCabe, P. O. Wennberg, A. Sorooshian, S. M. Murphy, N. F. Dalleska, R. C. Flagan, and J. H. Seinfeld (2007a), Effect of NO_x level on secondary organic aerosol (SOA) formation from the photooxidation of terpenes, *Atmos. Chem. Phys.*, *7*, 5159–5174, 10.5194/acp-7-5159-2007.

Ng, N. L., J. H. Kroll, A. W. H. Chan, P. S. Chhabra, R. C. Flagan, and J. H. Seinfeld (2007b), Secondary organic aerosol formation from m-xylene, toluene, and benzene, *Atmos. Chem. Phys.*, *7*, 3909-3922, 10.5194/acp-7-3909-2007.

Ng, N. L., A. J. Kwan, J. D. Surratt, A. W. H. Chan, P. S. Chhabra, A. Sorooshian, H. O. T. Pye, J. D. Crounse, P. O. Wennberg, R. C. Flagan, and J. H. Seinfeld (2008), Secondary organic aerosol (SOA) formation from reaction of isoprene with nitrate radicals (NO_3), *Atmos. Chem. Phys.*, *8*, 4117-4140, 10.5194/acp-8-4117-2008.

Nguyen, T. B., A. P. Bateman, D. L. Bones, S. A. Nizkorodov, J. Laskin, and A. Laskin (2010), High-resolution mass spectrometry analysis of secondary organic aerosol generated by ozonolysis of isoprene, *Atmos. Environ.*, *44*, 1032-1042, 10.1016/j.atmosenv.2009.12.019.

Odum, J. R., T. Hoffman, F. Bowman, D. Collins, R. C. Flagan, and J. H. Seinfeld (1996a), Gas/particle partitioning and secondary organic aerosol yields, *Environ. Sci. Technol.*, *30*, 2580-2585, 10.1021/es950943+.

Odum, J. R., F. Hoffmann, D. Bowman, D. Collins, R. C. Flagan, and J. H. Seinfeld (1996b), Gas/particle partitioning and secondary organic aerosol yields, *Environ. Sci. Technol.*, *30*, 2580-2585, 10.1021/es950943+.

Offenberg, J. H., M. Lewandowski, E. O. Edney, T. E. Kleindienst, and M. Jaoui (2007), Investigation of a systematic offset in the measurement of organic carbon with a semicontinuous analyzer, *J. Air Waste Manage. Assoc.*, *57*, 596-599.

Ostro, B., and L. Chestnut (1998), Assessing the health benefits of reducing particulate matter air pollution in the United States, *Environ. Res.*, *76*, 94-106, 10.1006/enrs.1997.3799.

Pandis, S. N., S. E. Paulson, J. H. Seinfeld, and R. C. Flagan (1991), Aerosol formation in the photooxidation of isoprene and β-pinene, *Atmos. Environ.*, *25*, 997-1008, 10.1021/es0524301.

Pankow, J. F. (1994a), An absorption model of gas/particle partitioning of organic compounds in the atmosphere, *Atmos. Environ.*, *28A*, 185-188.

Pankow, J. F. (1994b), An absorption model of the gas/aerosol partitioning involved in the formation of secondary organic aerosol, *Atmos. Environ.*, *28A*, 189-193.

Pankow, J. F., and W. E. Asher (2008), SIMPOL.1: a simple group contribution method for predicting vapor pressures and enthalpies of vaporization of multifunctional organic compounds, *Atmos. Chem. Phys.*, *8*, 2773-2796, 10.5194/acp-8-2773-2008.

Paulot, F., J. D. Crounse, H. G. Kjaergaard, A. Kürten, J. St. Clair, J. H. Seinfeld, and P. O. Wennberg (2010), Unexpected epoxide formation in the gas-phase photooxidation of isoprene, *Science*, *325*, 730-733, 10.1126/science.1172910.

Peltier, R. E., R. J. Weber, and A. P. Sullivan (2007), Investigating a liquid-based method for online organic carbon detection in atmospheric particles, *Aerosol. Sci. Technol.*, *41*, 1117-1127, 10.1080/02786820701777465.

Perri, M. J., Y. B. Lim, S. P. Seitzinger, and B. J. Turpin (2010), Organosulfates from glycoladehyde in aqueous aerosols and clouds: Laboratory studies, *Atmos. Environ.*, *44*, 2658-2664, 10.1016/j.atmosenv.2010.03.031.

Polidori, A., B. Turpin, H.-J. Lim, J. C. Cabada, R. Subramanian, S. N. Pandis, and A. L. Robinson (2006), Local and regional secondary organic aerosol : Insights from a year of semi-continuous carbon measurements at Pittsburgh, *Aerosol. Sci. Tech.*, *40*, 861-872, 10.1080/02786820600754649.

Pöschl, U., R. Von Kuhlmann, N. Poisson, and P. J. Crutzen (2000), Development and intercomparison of condensed isoprene oxidation mechanisms for global atmospheric modeling, *J. Atmos. Chem.*, *37*, 29-52, 10.1023/A:1006391009798.

Pouliot, P., H. Denier van der Gon, M. Schaap, M. Moran, and U. Nopmongcol (2012), Comparing emissions inventories and model-ready emissions datasets between Europe and North America for the AQMEII project, *Atmos. Environ.*, *53*, 4-14, 10.1016/j.atmosenv.2011.12.041.

Pozzoli, L., G. Janssens-Maenhout, T. Diehl, I. Bey, M. G. Schultz, J. Feichter, E. Vignati, and F. Dentener (2011), Re-analysis of tropospheric sulfate aerosol and ozone for the period 1980-2005 using the aerosol-chemistry-climate model ECHAM5-HAMMOZ, *Atmos. Chem. Phys.*, *11*, 9563-9594, 10.5194/acp-11-9563-2011.

Presto, A. A., M. A. Miracolo, N. M. Donahue, and A. L. Robinson (2010), Secondary organic aerosol formation from high-NO_x photo-oxidation of low volatility precursors: n-alkanes, *Environ. Sci. Technol.*, *44*, 2029–2034, 10.1021/es903712r.

Prevot, A. S. H., M. Crippa, S. N. Pandis, M. Beekmann, and U. Baltensperger (2011), Organic aerosols and their sources in Paris during the MEGAPOLI campaigns, *Geophysical Research Abstracts*, *13*, EGU2011-4631-2.

Pun, B. K. (2008), Development and initial application of the sesquiversion of MADRID, *J. Geophys. Res.*, *113*, D12212, 10.1029/2008JD009888.

Pun, B. K., and C. Seigneur (2007), Investigative modeling of new pathways for secondary organic aerosol formation, *Atmos. Chem. Phys.*, *7*, 2199-2216, 10.5194/acp-7-2199-2007.

Pun, B. K., and C. Seigneur (2008), Organic aerosol spatial/temporal patterns: Perspectives of measurements and model, *Environ. Sci. Tech.*, *42*(19), 7287-7293, 10.1021/es800500j.

Pun, B. K., C. Seigneur, D. Grosjean, and P. Saxena (2000), Gas-phase formation of water-soluble organic compounds in the atmosphere: A retrosynthetic analysis, *J. Atmos. Chem.*, *35*, 199-223, 10.1023/A:1006261217691.

Pun, B. K., R. J. Griffin, C. Seigneur, and J. H. Seinfeld (2002a), Secondary organic aerosol. 2. Thermodynamic model for gas/particle partitioning of molecular constituents, *J. Geophys. Res.*, *107*, 433, 10.1029/2001JD000542.

Pun, B. K., S.-Y. Wu, and C. Seigneur (2002b), Contribution of biogenic emissions to the formation of ozone and particulate matter in the eastern United States, *Environ. Sci. Technol.*, *36*, 3586-3596, 10.1021/es015872v.

Pun, B. K., S.-Y. Wu, C. Seigneur, J. H. Seinfeld, R. J. Griffin, and S. N. Pandis (2003), Uncertainties in modeling secondary organic aerosols: Three-dimensional modeling studies in Nashville/western Tennessee, *Environ. Sci. Technol.*, *37*, 3647-3661, 10.1021/es0341541.

Pun, B. K., C. Seigneur, and K. Lohman (2006), Modeling secondary organic aerosol formation via multiphase partitioning with molecular data, *Environ. Sci. Technol.*, *40*, 4722-4731, 10.1021/es0522736.

Pye, H. O. T., and J. H. Seinfeld (2010), A global perspective on aerosol from low-volatility organic compounds, *Atmos. Chem. Phys.*, *10*(9), 4377-4401, 10.5194/acp-10-4377-2010.

Rao, S. T., S. Galmarini, and K. Puckett (2011), Air Quality Model Evaluation International Initiative (AQMEII): Advancing the State of the Science in Regional Photochemical Modeling and Its Applications, *Bulletin of the American Meteorological Society*, *92*, 23-30, 10.1175/2010BAMS3069.1.

Raventos-Duran, T., M. Camredon, R. Valorso, and B. Aumont (2010), Structure-activity relationships to estimate the effective henry's law coefficients of organics of atmospheric interest, *Atmos. Chem. Phys. Discuss.*, *10*, 4617-4647, 10.5194/acpd-10-4617-2010.

Real, E., and K. N. Sartelet (2011), Modeling of photolysis rates over europe: impact on chemical gaseous species and aerosols, *Atmos. Chem. Phys.*, *11*, 1711-1727, 10.5194/acp-11-1711-2011.

Robinson, A. L., N. M. Donahue, M. K. Shrivastava, E. A. Weitkamp, A. M. Sage, A. P. Grieshop, T. E. Lane, J. R. Pierce, and S. N. Pandis (2007), Rethinking organic aerosols: Semivolatile emissions and photochemical aging, *Science*, *315*, 1259–1262, 10.1126/science.1133061.

Robinson, N. H., J. F. Hamilton, J. D. Allan, B. Langford, D. E. Oram, Q. Chen, K. Docherty, D. K. Farmer, J. L. Jimenez, M. W. Ward, C. N. Hewitt, M. H. Barley, M. E. Jenkin, A. R. Rickard, S. T. Martin, G. McFiggans, and H. Coe (2011), Evidence for a significant proportion of secondary organic aerosol from isoprene above a maritime tropical forest, *Atmos. Chem. Phys.*, *11*, 1039-1050, 10.5194/acp-11-1039-2011.

Roeckner, E., R. Brokopf, M. Esch, M. Giorgetta, S. Hagemann, L. Kornblüh, L. E. Manzini, U. Schlese, and U. Schulzweida (2006), Sensitivity of simulated climate to horizontal and vertical resolution in the ECHAM5 atmosphere model, *J. Climate*, *19*, 3771-3791, 10.1175/JCLI3824.1.

Rollins, W. A., A. Kiender-Scharr, J. L. Fry, T. Brauers, S. S. Brown, H.-P. Dorn, W. P. Dubé, H. Fuchs, A. Mensah, T. F. Mentel, R. Tillmann, R. Wegener, P. J. Wooldridge, and R. C. Cohen (2009), Isoprene oxidation by nitrate radical: alkyl nitrate and secondary organic aerosol yields, *Atmos. Chem. Phys.*, *9*, 6685-6703, 10.5194/acp-9-6685-2009.

Roustan, Y., K. N. Sartelet, M. Tombette, É. Debry, and B. Sportisse (2010), Simulation of aerosols and gas-phase species over Europe with the Polyphemus system. Part II: Model sensitivity analysis for 2001, *Atmos. Environ.*, *44*, 4219-4229, 10.1016/j.atmosenv.2010.07.005.

Royer, P., P. Chazette, K. Sartelet, Q. J. Zhang, M. Beekmann, and J.-C. Raut (2011), Comparison of lidar-derived pm_{10} with regional modeling and ground-based observations in the frame of MEGAPOLI experiment, *Atmos. Chem. Phys.*, *11*, 10705-10726, 10.5194/acp-11-10705-2011.

Ruppert, L., and K. H. Becker (2000), A product study of the oh radical-initiated oxidation of isoprene: formation of C_5-unsaturated diols, *Atmos. Environ.*, *34*, 1529-1542, 10.1016/S1352-2310(99)00408-2.

Russell, A. G. (2008), EPA Supersites program-related emissions-based particulate matter modeling: initial applications and advances, *J. Air Waste Manage. Assoc.*, *58*, 289-302, 10.3155-1047-3289.58.2.289.

Russell, A. G., and R. Dennis (2000), NARSTO critical review of photochemical models and modeling, *Atmos. Environ.*, *34*, 2283-2324, 10.1016/S1352-2310(99)00468-9.

Russell, M., and D. T. Allen (2005), Predicting secondary organic aerosol formation rates in southeast Texas, *J. Geophys. Res.*, *110*, D07S17, 10.1029/2004JD004722.

Salamanca, F., A. Krpo, A. Martilli, and A. Clappier (2010), A new building energy model coupled with an urban canopy parameterization for urban climate simulations- Part I. formulation, verification, and sensitivity analysis of the model, *Theor. Appl. Climatol.*, *99*, 331-344, 10.1007/s00704-009-0142-9.

Saliba, N. A., S. Moussa, H. Salame, and M. El-Fadel (2006), Variation of selected air quality indicators over the city of Beirut, Lebanon: Assessment of emission sources, *Atmos. Environ.*, *40*, 3263-3268, 10.1016/j.atmosenv.2006.01.054.

Saliba, N. A., H. Kouyoumdjian, and M. Roumié (2007), Effect of local and long-range transport emissions on the elemental composition of $PM_{10-2.5}$ and $PM_{2.5}$ in Beirut, *Atmos. Environ.*, *41*, 6497-6509, 10.1016/j.atmosenv.2007.04.032.

Sartelet, K., E. Debry, K. Fahey, Y. Roustan, M. Tombette, and B. Sportisse (2007), Simulation of aerosols and gas-phase species over Europe with the Polyphemus system. Part I: model-to-data comparison for 2001, *Atmos. Environ.*, *41*, 6116-6131, 10.1016/j.atmosenv.2007.04.024.

Sartelet, K., H. Hayami, and B. Sportisse (2008), MICS Asia Phase II Sensitivity to the aerosol module, *Atmos. Environ.*, *42*(15), 3562-3570, doi:10.1016/j.atmosenv.2007.03.05.

Sartelet, K. N., F. Couvidat, C. Seigneur, and Y. Roustan (2012), Impact of biogenic emissions on air quality over Europe and North America, *Atmos. Environ.*, *53*, 131-141, 10.1016/j.atmosenv.2011.10.046.

Sarwar, G., D. Luecken, G. Yarwood, G. Z. Whitten, and W. P. L. Carter (2008), Impact of an updated carbon bond mechanism on predictions from the CMAQ modeling system: Preliminary assessment, *J. Appl. Meteor. Climatol.*, *47*, 3-14, 10.1175/2007JAMC1393.1.

Saxena, P., L. Hildemann, P. H. McMurry, and J. H. Seinfled (1995), Organics alter hygroscopic behavior of atmospheric particles, *J. Geophys. Res.*, *100*, 18755-18770, 10.1029/95JD01835.

Schauer, J. J., M. J. Kleeman, G. R. Cass, and B. R. T. Simoneit (1999), Measurement of emissions from air pollution sources. 2. C_1 through C_{30} organic compounds from medium duty diesel trucks, *Environ. Sci. Technol.*, *33*, 1578–1587, 10.1021/es980081n.

Schell, B., I. J. Ackermann, H. Hass, F. S. Binkowski, and A. Ebel (2001), Modeling the formation of secondary organic aerosol within a comprehensive air quality model system, *J. Geophys. Res.*, *106*, 28275-28293, 10.1029/2001JD000384.

Sciare, J., O. d'Argouges, Q. J. Zhang, R. Sarda-Estève, C. Gaimoz, V. Gros, M. Beekmann, , and O. Sanchez (2010a), Comparison between simulated and observed chemical composition of fine aerosols in Paris (France) during springtime: contribution of regional versus continental emissions, *Atmos. Chem. Phys.*, *10*, 11987-12004, 10.5194/acp-10-11987-2010.

Sciare, J., O. d'Argouges, Q. J. Zhang, R. Sarda-Estève, C. Gaimoz, V. Gros, M. Beekmann, and O. Sanchez (2010b), Comparison between simulated and observed chemical composition of fine aerosols in Paris (France) during springtime: contribution of regional versus continental emissions, *Atmos. Chem. Phys.*, *10*(24), 11987-12004, 10.5194/acp-10-11987-2010.

Sciare, J., O. D'Argouges, R. Sarda-Estève, C. Gaimoz, C. Dolgorouky, N. Bonnaire, O. Favez, B. Bonsang, and V. Gros (2011), Large contribution of water-insoluble secondary organic aerosols in the region of Paris (France) during wintertime, *J. Geophys. Res.*, *116*, D22203, 10.1029/2011JD015756.

Seigneur, C., and A. M. Wegrecki (1990), Mathematical modeling of cloud chemistry in the Los Angeles basin, *Atmos. Environ.*, *24A*, 989-1006.

Seigneur, C., P. Karamchandani, K. Lohman, K. Vijayaraghavan, and R.-L. Shia (2001), Multiscale modeling of the atmospheric fate and transport of mercury, *J. Geophys. Res.*, *106*, 27795-27809, 10.1029/2000JD000273.

Seinfeld, J. H., and S. N. Pandis (1998), *Atmospheric Chemistry and Physics*, Wiley-interscience.

Shaw, S. L., B. Gantt, and N. Meskhidze (2010), Production and emissions of marine isoprene and monoterpenes: A review, *Advances in Meteorology*, p. 408696, 10.1155/2010/408696.

Shiraiwa, M., M. Ammann, T. Koop, and U. Pöschl (2011), Gas uptake and chemical aging of semisolid organic aerosol particles, *Proc. Natl. Acad. Sci.*, *108*, 11003-11008, 10.1073/pnas.1103045108.

Shrivastava, M., J. Fast, R. Easter, W. I. Gustafson Jr., R. A. Zaveri, J. L. Jimenez, P. Saide, and A. Hodzic (2011), Modeling organic aerosols in a megacity: comparison of simple and complex representations of the volatility basis set approach, *Atmos. Chem. Phys.*, *11*, 6639-6662, 10.5194/acp-11-6639-2011.

Shrivastava, M. K., E. M. Lipsky, C. O. Stanier, and A. L. Robinson (2006), Modeling semivolatile organic aerosol mass emissions from combustion systems, *Environ. Sci. Technol.*, *40*, 2671-2677, 10.1021/es0522231.

Shrivastava, M. K., T. E. Lane, N. M. Donahue, S. N. Pandis, and A. L. Robinson (2008), Effects of gas particle partitioning and aging of primary emissions on urban and regional organic aerosol concentrations, *J. Geophys. Res.*, *113*, D18301, 10.1029/2007JD009735.

Simpson, D., W. Winiwarter, G. Börjesson, S. Cinderby, A. Ferreiro, A. Guenther, C. N. Hewitt, R. Janson, M. A. K. Khalil, S. Owen, T. E. Pierce, H. Puxbaum, M. Shearer, U. Skiba, R. Steinbrecher, L. Tarrason, and M. G. Oquist (1999), Inventorying emissions from nature in Europe, *J. Geophys. Res.*, *104*, 8113-8152, 10.1029/98JD02747.

Simpson, D., K. E. Yttri, Z. Klimont, K. Kupiainen, A. Caseiro, A. Gelencsér, C. Pio, H. Puxbaum, and M. Legrand (2007), Modeling carbonaceous aerosol over Europe: Analysis of the CARBOSOL and EMEP EC/OC campaigns, *J. Geophys. Res.*, *112*, D23S14, 10.1029/2006JD008158.

Skamarock, W. C., J. B. Klemp, J. Dubhia, D. O. Gill, D. M. Barker, M. G. Duda, X. Y. Huang, W. Wang, and J. G. Powers (2008a), A description of the advanced research WRF version 3, *Tech. Rep.*, NCAR Technical note-475+STR available at: `http://www.mmm.ucar.edu/wrf/users/docs/arw_v3.pdf`.

Skamarock, W. C., J. B. Klemp, J. Dudhia, D. O. Gill, D. M. Barker, M. G. Duda, X.-Y. H. W. Wang, and J. G. Powers (2008b), A description of the Advanced Research WRF version 3. NCAR Technical note, -475+STR, *Tech. Rep.*

Smoydzin, L., M. Fnais, and J. Lelieveld (2012), Ozone pollution over the Arabian Gulf: role of meteorological conditions, *Atmos. Chem. Phys. Discuss.*, *12*, 6331-6361, 10.5194/acpd-12-6331-2012.

Song, C., R. A. Zaveri, M. Alexander, J. A. Thornton, S. Madronich, J. V. Ortega, A. Zelenyuk, X.-Y. Yu, A. Laskin, and D. A. Maughan (2007), Effect of hydrophobic primary organic aerosols on secondary organic aerosol formation from ozonolysis of α-pinene, *Geophys. Res. Lett.*, *34*, L20803, 10.1029/2007GL030720.

Spittler, M., I. Barnes, I. Bejan, K. J. Brockmann, B. T., and K. Wirtz (2006), Reactions of NO_3 radicals with limonene and α-pinene: Product and SOA formation, *Atmos. Environ.*, *40*, S116-S127, 10.1016/j.atmosenv.2005.09.093.

Stavrakou, T., J. F. Müller, K. F. Boersma, I. De Smedt, and R. J. van der A (2008), Assessing the distribution and growth rates of NO_x emission sources by inverting a 10-year record of NO_2 satellite columns, *Geophys. Res. Lett.*, *35*, L10801, 10.1029/2008GL033521.

Steinbrecher, R., G. Smiatek, R. Köble, G. Seufert, J. Theloke, K. Hauff, P. Ciccioli, R. Vautard, and G. Curci (2009), Intra- and inter-annual variability of VOC emissions from natural and semi-natural vegetation in europe and neighbouring countries, *Atmos. Environ.*, *43*, 1380-1391, 10.1016/j.atmosenv.2008.09.072.

Stockwell, W. R., F. Kirchner, M. Kuhn, and S. Seefeld (1997), A new mechanism for regional atmospheric chemistry modeling, *J. Geophys. Res.*, *102*(D22), 25847-25879, 10.1029/97JD00849.

Struzewska, J., and J. W. Kaminski (2008), Formation and transport of photooxidants over Europe during the July 2006 heat wave - observations and GEM-AQ model simulations, *Atmos. Chem. Phys.*, *8*, 721-736, 10.5194/acp-8-721-2008.

Stull, R. B. (1988), *An introduction to boundary layer meteorology*, Kluwer Academic Publishers, Dordrecht.

Surratt, J. D., S. M. Murphy, J. H. Kroll, N. L. Ng, L. Hildebrandt, A. Sorooshian, R. Szmigielski, R. Vermeylen, W. Maenhaut, M. Claeys, R. C. Flagan, and J. H. Seinfeld (2006), Chemical composition of secondary organic aerosol formed from the photooxidation of isoprene, *J. Phys. Chem. A*, *110*, 9665-9690, 10.1021/jp061734m.

Surratt, J. D., A. W. H. Chan, N. C. Eddingsaas, M. N. Chan, C. L. Loza, A. J. Kwan, S. P. Hersery, R. C. Flagan, P. O. Wennberg, and J. H. Seinfeld (2010), Reactive intermediates revealed in secondary organic aerosol formation from isoprene, *Proc. Natl. Acad. Sci.*, *107*, 6640-6645, 10.1073/pnas.0911114107.

Suzuki, T., K. Ohtaguchi, and K. Koide (1992), Application of principal components analysis to calculate henry's constant from molecular structure, *Computers Chem.*, *16*, 41-52.

Svendby, T. M., M. Lazaridis, and K. Tørseth (2008), Temperature dependent secondary organic aerosol formation from terpenes and aromatics, *J. Atmos. Chem.*, *59*, 25-46, 10.1007/s10874-007-9093-7.

Szeremeta, E., P. Barzaghi, O. Böge, H. Herrmann, L. Gmachowski, and K. J. Rudzinski (2009), *Atmospheric composition change - Causes and Consequences - Local to Global*, chap. Aqueous-phase reactions of isoprene oxidation products with hydroxyl radicals, Aracne editrice S.r.l.

Szmigielski, R., J. D. Surratt, Y. Gómez-González, P. Van der Veken, I. Kourtchev, R. Vermeylen, F. Blockhuys, M. Jaoui, T. E. Kleindienst, M. Lewandowski, J. H. Offenberg, E. O. Edney, J. H. Seinfeld, W. Maenhaut, and M. Claeys (2007), 3-Methyl-1,2,3-butanetricarboxylic acid: An atmospheric tracer for terpene secondary organic aerosol, *Geophys. Res. Lett.*, *34*, L24811, doi:10.1029/2007GL031338.

Tilgner, A., and H. Herrmann (2010), Radical-drivencarbonyl-to-acid conversion and acid degradation in tropospheric aqueous systems studied by CAPRAM, *Atmos. Environ.*, *44*, 5415-5422, 10.1016/j.atmosenv.2010.07.050.

Troen, I. B., and L. Mahrt (1986), A simple model of the atmospheric boundary layer , sensitivity to surface evaporation, *Bound.-Lay. Meteorol.*, *37*, 129-148.

Tsimpidi, A. P., V. A. Karydis, M. Zavala, W. Lei, N. Bei, L. Molina, and S. N. Pandis (2011), Sources and production of organic aerosol in Mexico City: insights from the combination of a chemical transport model (PMCAMx-2008) and measurements during MILAGRO, *Atmos. Chem. Phys.*, *11*, 5153-5168, 10.5194/acp-11-5153-2011.

Tulet, P., A. Grini, R. J. Griffin, and S. Petitcol (2006), ORILAM-SOA: A computationally efficient model for predicting secondary organic aerosols in three-dimensional atmospheric models, *J. Geophys. Res.*, *111*, D23208, 10.1029/2006JD007152.

Turpin, B. J., and H.-J. Lim (2001), Species contributions to $PM_{2.5}$ mass concentrations: revisiting common assumptions for estimating organic mass, *Aerosol. Sci. Tech.*, *35*, 602-610, 10.1080/02786820119445.

Valorso, R., B. Aumont, M. Camredon, T. Raventos-Duran, C. Mouchel-Vallon, N. L. Ng, J. H. Seinfeld, J. Lee-Taylor, and S. Madronich (2011), Explicit modelling of SOA formation from α-pinene photooxidation: sensitivity to vapour pressure estimation, *Atmos. Chem. Phys.*, *11*, 6895-6910, 10.5194/acp-11-6895-2011.

van Pinxteren, D., A. Plewka, D. Hofmann, K. Müller, H. Kramberger, B. Svrcina, K. Bächmann, W. Jaeschke, S. Mertes, J. L. Collett Jr., and H. Herrmann (2005), Schmücke hill cap cloud and valley stations aerosol characterisation during FEBUKO (II): Organic compounds, *Atmos. Environ.*, *39*, 4305-4320, 10.1016/j.atmosenv.2005.02.014.

Vautard, R., M. D. Moran, E. Solazzo, R. C. Gilliam, V. Matthias, R. Bianconi, C. Chemel, J. Ferreira, B. Geyer, A. B. Hansen, A. Jericevic, M. Prank, A. Segers, J. D. Silver, J. Werhahn, R. Wolke, S. T. Rao, and S. Galmarini (2012), Evaluation of the meteorological forcing used for the Air Quality Model Evaluation International Initiative (AQMEII) air quality simulations, *Atmos. Environ.*, *53*, 15-37, 10.1016/j.atmosenv.2011.10.065.

Verwer, J. G., E. J. Spee, J. G. Bloom, and W. Hundsdorfer (1999), A second-order rosenbrock method applied to photochemical dispersion problems, *SIAM J. Sci. Comput.*, *20*, 1456-1480, 10.1137/S1064827597326651.

Vestreng, V. (2003), Review and revision. emission data reported to CLRTAP Tech. Rep., EMEP MSW-W, *Tech. Rep.*, Norwegian Meteorological Institute, Oslo, Norway.

Vijayaraghavan, K., C. Seigneur, P. Karamchandani, and S.-Y. Chen (2007), Development and application of a multi-pollutant model for atmospheric mercury deposition, *J. Appl. Meteorol. Climatol.*, *46*, 1341-1353, 10.1175/JAM2536.1.

Volkamer, R., P. J. Ziemann, and M. J. Molina (2009), Secondary organic aerosol formation from acetylene (c_2h_2): seed effect on SOA yields due to organic photochemistry in the aerosol aqueous phase, *Atmos. Chem. Phys.*, *9*, 1907-1928, 10.5194/acp-9-1907-2009.

Vutukuru, S., R. J. Griffin, and D. Dabdub (2006), Simulation and analysis of secondary organic aerosol dynamics in the south coast air basin of California, *J. Geophys. Res.*, *111*, D10S12, 10.1029/2005JD006139.

Waked, A., and C. Afif (2012), Emissions of air pollutants from road transport in Lebanon and other countries in the Middle East region, *Atmos. Environ.*, *61*, 446-452, 10.1016/j.atmosenv.2012.07.064.

Waked, A., C. Seigneur, F. Couvidat, Y. Kim, K. Sartelet, C. Afif, A. Borbon, P. Formenti, and S. Sauvage (2012a), Modeling air pollution in Lebanon: evaluation at a suburban site in Beirut, *Submitted to Atmos. Chem. Phys.*

Waked, A., C. Afif, and C. Seigneur (2012b), An atmospheric emission inventory of anthropogenic and biogenic sources for Lebanon, *Atmos. Environ.*, *50*, 88-96, 10.1016/j.atmosenv.2011.12.058.

Wang, L., R. Atkinson, and J. Arey (2007), Formation of 9,10-phenanthrenequinone by atmospheric gas-phase reactions of phenanthrene, *Atmos. Environ.*, *41*, 2025-2035, 10.1016/j.atmosenv.2006.11.008.

Wiedinmyer, C., B. Quayle, C. Geron, A. Belote, D. McKenzie, X. Zhand, S. O'Neill, and K. K. Wynne (2006), Estimating emissions from fires in north america for air quality modeling, *Atmos. Environ.*, *40*, 3419-3432, 10.1016/j.atmosenv.2006.02.010.

WRAP (2008), Western Regional Air Parternship, 2005. Development of 2000-04 baseline period and 2018 projection year emission inventories, Prepared by Air Sciences, Inc. Project No. 178-8, *Tech. Rep.*, Air Sciences, Inc., Golden, CO, USA.

Yarwood, G., S. Rao, M. Yocke, and G. Whitten (2005), Updates to the carbon bond chemical mechanism: CB05 final report to the US EPA, RT-0400675, available at: http://www.camx.com/publ/pdfs/CB05_Final_Report_120805.pdf.

Yasmeen, F., N. Sauret, J.-F. Gal, P.-C. Maria, L. Massi, W. Maenhaut, and M. Claeys (2010), Characterization of oligomers from methylglyoxal under dark conditions: a pathway to produce secondary organic aerosol through cloud processing during nighttime, *atmos. chem. phys.*, *10*, 3803-3812, 10.5194/acp-10-3803-2010.

Yaws, C., and H.-C. Yang (1992), *Henry's law constant for compound in water, in Thermodynamic and Physical Property Data*, C. L. Yaws, ed., Gulf Publishing Company, Houston, TX.

Yu, H., Y. Kaufman, M. Chin, G. Feingold, L. Remer, T. Anderson, Y. Balkanski, N. Bellouin, O. Boucher, S. Christopher, P. DeCola, R. Kahn, D. Koch, N. Loeb, M. Reddy, M. Schulz, T. Takemura, and M. Zhou (2006), A review of measurement-based assessments of the aerosol direct radiative effect and forcing, *Atmos. Chem. Phys.*, *6*, 616-666, 10.5194/acp-6-613-2006.

Yu, S., P. V. Bhave, R. L. Dennis, and R. Marthur (2007), Seasonal and regional variations of primary and secondary organic aerosols over the continental United States: Semi-empirical estimates and model evaluation, *Environ. Sci. Technol.*, *41*, 4690-4697, 10.1021/es061535g.

Zhang, Q., J. L. Jimenez, M. R. Canagaratna, J. D. Allan, H. Coe, I. Ulbrich, M. R. Alfarra, A. Takami, A. M. Middlebrook, Y. L. Sun, K. Dzepina, E. Dunlea, K. Docherty, P. F. De-Carlo, D. Salcedo, T. Onasch, J. T. Jayne, T. Miyoshi, A. Shimono, S. Hatakeyama, N. Takegawa, Y. Kondo, J. Schneider, F. Drewnick, S. Borrmann, S. Weimer, K. Demerjian, P. Williams, K. Bower, R. Bahreini, L. Cottrell, R. J. Griffin, J. Rautiainen, J. Y. Sun, Y. M. Zhang, and D. R. Worsnop (2007a), Ubiquity and dominance of oxygenated species in organic aerosols in anthropogenically-influence northern hemisphere mildlatitudes, *Geophys. Res. Lett.*, *34*, 10.1029/2007GL029979.

Zhang, Y., B. Pun, K. Vijayaraghavan, S.-Y. Wu, C. Seigneur, S. N. Pandis, M. Z. Jacobson, A. Nenes, and J. H. Seinfeld (2004), Development and application of the Model of Aerosol Dynamics, Reaction, Ionization, and Dissolution (MADRID), *J. Geophys. Res.*, *109*, D01202, 10.1029/2003JD003501.

Zhang, Y., P. Liu, B. Pun, and C. Seigneur (2006), A comprehensive performance evaluation of MM5-CMAQ for the summer 1999 southern oxidants study episode. Part I: Evaluation protocols, databases, and meteorological predictions, *Atmos. Environ*, *40*, 4825-4838, 10.1016/j.atmosenv.2005.12.043.

Zhang, Y., J.-P. Huang, D. K. Henze, and J. H. Seinfeld (2007b), Role of isoprene in secondary organic aerosol formation on a regional case, *J. Geophys. Res.*, *112*, D20207, 10.1029/2007JD008675.

Zhang, Y., M. K. Dubey, S. C. Olsen, J. Zheng, and R. Zhang (2009), Comparisons of WRF/Chem simulations in Mexico City with ground-based rama measurements during the 2006-MILAGRO, *Atmos. Chem. Phys.*, *9*, 3777-3798, 10.5194/acp-9-3777-2009.

Zhang, Y., Y. Pan, K. Wang, J. D. Fast, and G. A. Grell (2010a), WRF/Chem-MADRID: Incorporation of an aerosol module into WRF/Chem and its initial application to the TexAQS2000 episode, *J. Geophys. Res.*, *115*, D18202, 10.1029/2009JD013443.

Zhang, Y. Y., L. Müller, R. Winterhalter, G. K. Moortgat, T. Hoffmann, and U. Pöschl (2010b), Seasonal cycle and temperature dependence of pinene oxidation products, dicarboxylic acids and nitrophenols in fine and coarse air particulate matter, *Atmos. Chem. Phys.*, *10*, 7859-7873, 10.5194/acp-10-7859-2010.

Zuend, A., C. Marcolli, T. Peter, and J. H. Seinfeld (2010), Computation of liquid-liquid equilibria and phase stabilities: implications for rh-dependent gas/particle partitioning of organic-inorganic aerosols, *Atmos. Chem. Phys.*, *10*, 7795-7820, doi:10.5194/acpd-10-12497-2010.